NELSON MANDELA UNIVERSITY

COMPARATIVE STUDY OF THE EFFECT OF ILOPROST ON NEUROINFLAMMATORY CHANGES IN C8-B4 MICROGLIAL CELLS AND MURINE MODEL OF TRYPANOSOMIASIS

By

Ashleigh Jacobs (216027438)

A dissertation submitted in fulfilment of the requirements for the degree of *Magister Scientiae* (MSc) in Human Physiology in the Faculty of Science, Nelson Mandela University.

Supervisor: Dr. DC. Ajonijebu

Co-Supervisor: Professor GB Dealtry

April 2024


NELSON MANDELA
UNIVERSITY

ACKNOWLEDGEMENTS

I'd like to give thanks and praise to God my heavenly Father and saviour Jesus Christ, for giving me the strength and wisdom that I needed to complete my master's degree. Through everything I give God all the glory and praise.

I'd like to give a special thanks to both my Supervisor and Co-supervisor, Dr. Chris Ajonijebu and Professor Gill Dealtry, for their continued support, patience, and guidance throughout my research project. It has been an absolute pleasure both learning from you and being taught by you, I'm honored to have been your student. I'd also like to thank the entire Department of Physiology at Nelson Mandela University for creating a warm environment to carry out both my research and education for the past 6 years. Mrs. Megan Fensham, the heart and soul of our laboratory, thank you for going above and beyond for each one of us. I truly appreciate you so much.

I'd like to say a special thanks to Dr. Olaolu and the Nigerian Institute of Trypanosomiasis Research for facilitating and assisting with my animal study. It has been my greatest pleasure collaborating with you.

A very big thank you to Drs Pereira and Fortuin-Seedat. Dr Pereira, particularly for your gentle teaching method when it came to techniques in the cell laboratory, thank you for always being willing to share your knowledge and expertise and always going the extra mile for me. Thank you for making sure I had the necessary tools to start my research when I didn't have much at all. Dr Fortuin-Seedat my saving grace in the lab, thank you for guiding me and taking the time out of your day to help me perfect one of my techniques, thank you for never making me feel like I wasn't capable of doing anything yet providing your knowledge and wisdom without hesitation. You've helped me grow as a student and researcher.

My dear friends Shiraz and Zaphezulu, for the endless hours spent in the laboratory together working, even packing tip boxes for one another when the other was heavily into an experiment. Thank you for sharing the joys and also all the disappointments. Your continued support and encouragement will be something I cherish for the rest of my life.

I’d also like to thank my parents and my sister for being my anchor during the entire duration of my studies, my parents especially for always putting my education first regardless of the circumstances we face as a family. My darling mum who has shared in every emotion I’ve gone through for 2 years and no matter what the requirements were, would always assure me that we would find a way to make it happen. Your prayers have truly carried me through.

To my fiancé Fazloedeen, my absolute best friend in entire world, thank you for always believing in me and pushing me to do my best.

Lastly, I’d like to thank the National Research Fund (NRF) for funding this project and both the Nelson Mandela University’s Post Graduate Research Scholarship and NRF for financial support during my master’s degree course.

TABLE OF CONTENTS

LIST OF FIGURES

LIST OF TABLES

LIST OF ABBREVIATIONS

ARG-1	Arginase-1
ARRIVE	Animal Research Reporting of In Vivo Experiments
BBB	Blood-brain barrier
BDNF	Brain-derived neurotrophic factor
CA	Cornu Ammonis
Ca^{2+}	Calcium
cAMP	Cyclic adenosine monophosphate
CD206	Mannose-receptor
CNS	Central nervous system
COX	Cyclooxygenase
CRE	cAMP response element
CREB	cAMP response element binding protein
CSF	Cerebrospinal fluid
DAPI	4’,6-diamidino-2-phenylindole
DG	Dentate gyrus
DNA	Deoxyribonucleic acid
GABA	Gamma aminobutyric acid
HAT	Human African trypanosomiasis
IL-1 β	Interleukin 1 beta
IL-4	Interleukin 4
IL-3	Interleukin 3
IFN- γ	Interferon-gamma
I.p	Intraperitoneal
IP	Prostacyclin receptor
I.v	Intravenous
iNOS	Inducible Nitric Oxide Synthase

IL-4Rα	Interleukin 4 receptor alpha
LPS	Lipopolysaccharide
MAPK	Mitogen-activated protein kinases
MHC	Major histocompatibility complex
NF-KB	Nuclear factor Kappa-B
NMU	Nelson Mandela University
NITR	Nigerian Institute for Trypanosomiasis Research
NO	Nitric oxide
NVRI	Nigerian Veterinary Research Institute
PAMP	Pathogen-associated molecular pattern
PCD	Programmed cell death
Pi3K	Phosphatidylinositol-3-kinase
PLC-γ	Phospholipase C-gamma
RNA	Ribonucleic acid
ROS	Reactive oxygen species
STAT	Signal transducer and activator of transcription
T.b	*Trypanosoma brucei*
T.h	T-helper
TNF-α	Tumour necrosis factor-alpha
TrkB	Tyrosine kinase B
VSG	Variant surface glycoprotein
WHO	World Health Organization

LIST OF SYMBOLS

^{o}C	Degrees celsius
=	equal
<	Less than
≤	Less than or equal to
%	Percent
Cm^{2}	Square centimeter
$\mu g\ mL^{-1}$	Microgram per milliliter
µL	Microliter
mL	Milliliter
$ng\ mL^{-1}$	Nanogram per milliliter
$ng\ \mu L^{-1}$	Nanogram per microliter

ABSTRACT

Neurodegenerative conditions significantly impact well-being and quality of life in individuals with major symptoms including mood disorders, cognitive decline, and psychiatric disturbances, often resulting from neuroinflammation triggered by immune responses to bacterial or parasitic infections such as gram-negative bacteria or Human African Trypanosomiasis. Microglia play a crucial role in both neurotoxicity and cellular processes involved in restoring the neural health. Exploring the therapeutic potential of prostacyclin and its analogues in regulating microglia responses to inflammatory insult and treating *Trypanosoma brucei* (*T.b*) infection remains an unexplored area. The aim of this study was to assess the potential neuroprotective effects of Iloprost through comparative analysis of neuroinflammatory responses in both microglial cells exposed to lipopolysaccharide (LPS) and mouse brains infected with *T.b brucei*.

In phase I of this study both resting and LPS treated C8-B4 microglial cells were exposed to varying concentrations of Iloprost. The effects of Iloprost on LPS-induced inflammation were analysed using immunofluorescence to detect microglial activation and differentiate between pro and anti-inflammatory phenotypes. Furthermore, pro and anti-inflammatory cytokine secretion was determined using an ELISA, in addition gene expression analysis was carried out using quantitative polymerase chain reaction (qPCR). Also, DNA methylation status of C8-B4 cells exposed to LPS challenge alone or in combination with various concentrations of Iloprost were determined using bisulfite sequencing technique followed by qPCR. In phase II of the study, a total of twenty-four Albino Swiss male mice (8-10 weeks old) were divided into four treatment groups with 6 mice in each group. All treatment groups except the non-infected control were inoculated with the *T.b brucei* parasite. One group received a single intraperitoneal injection of Diminazene aceturate (4 mg kg^{-1}) while the remaining group received repeated intraperitoneal injections of Iloprost (200 µg kg^{-1}). On day ten of the study, mouse brains were removed on ice using forceps. The hippocampal tissues were dissected out and processed for quantification of gene expression changes in pro and anti-inflammatory cytokines.

Overall, the findings of this study indicate that LPS-induced pro-inflammatory cytokine, TNF-α and IL-1β, secretion and gene expression is down-regulated in C8-B4

microglial cells treated with Iloprost. Furthermore, there was a significant up-regulation in the expression of anti-inflammatory genes, particularly ARG-1, CD206, BDNF and CREB in response to Iloprost treatment following LPS-induced inflammation. This study is also the first to confirm M2 microglial polarization with Iloprost treatment in both resting and LPS treated cells. However, hypermethylation at CREB and BDNF promoter regions was observed 24 hours after Iloprost treatment. Additionally, Iloprost reversed hypomethylation at the BDNF promoter region that had been induced by LPS treatment. The rodent model also indicated a downregulation in the pro-inflammatory cytokine, IL-1β, expression and upregulation of BDNF transcription in *T.b brucei* infected mice treated with repeated doses of Iloprost. In conclusion, determining the immunomodulatory roles of Iloprost in both *in vitro* and *in vivo* models of neuroinflammation could assist in the development of alternative therapy for neurodegenerative disease.

Keywords: brain infection, DNA methylation, Iloprost, microglial polarization, neuroinflammation, trypanosome.

CHAPTER ONE

INTRODUCTION

1.1 Neuroinflammatory diseases

Neurodegeneration is a common hallmark of many neuroinflammatory diseases (Chen *et al*., 2016). This phenomenon occurs in the central nervous system (CNS) and is characterized by loss of neuronal structure and function. Neurodegeneration is observed following viral or protozoan insult as seen in multiple sclerosis and Human African trypanosomiasis (HAT) (Chiara *et al*., 2012, Tesoriero *et al*., 2018). Neuroinflammation is one of the main defense mechanisms used to protect the brain by removing or inhibiting the spread of pathogens. Microglia and astrocytes are two key regulators of the inflammatory processes in the CNS where they are categorized as either neurotoxic or neuroprotective (Kwon and Koh, 2020). Microglia-mediated neurotoxicity is a result of activation through pattern recognition receptors when there is an excessive immune response, this activation leads to the production of pro-inflammatory cytokines that have the ability to damage neuronal tissue (Block *et al*., 2007). In contrast, microglia can adopt a neuroprotective role by undergoing phenotype switching to alternatively activated microglia, inhibiting pro-inflammatory cytokine production, and downregulating the immune response (Giunti *et al*., 2014). However, the relationship between activated glial cells is complex and their phenotypic profile may change based on the progression of the neurodegenerative disease (Afridi *et al*., 2020). Therefore, investigating and understanding their roles and the regulation of their phenotypic profile in response to disease is essential for developing effective therapies.

1.2 Impact of neuroinflammatory disease

One of the major risk factors for developing neurodegenerative diseases is age (Hou *et al*., 2019). Literature states that systemic inflammation levels are increased in elderly people and coupled with this is neurodegeneration (Kumar, 2018). The impact of neuroinflammatory diseases ranges from mild cognitive impairment characterized by amnesia to more severe symptoms such as depression and meningoencephalitis

(Baglio *et al*., 2013). Previously, research models have been developed to study dementia and Alzheimer's as common neurodegenerative diseases associated with neuroinflammation (Nazem *et al*., 2015, Slanzi *et al*., 2002). This model of neurodegenerative disease, however, differs slightly from infectious disease. The key challenge in infectious diseases, such as HAT, is to eradicate the causative agent with as little damage to the host as possible. Previous treatments have been known to cure the infected individual yet later lead to death due to the side effects of the administered treatment (Steverding, 2010).

1.3 Long-term effects of neuroinflammatory disease on the quality of life

Neurodegenerative diseases, whether age-related or infectious, impact the quality of life of affected individuals. The most prominent symptoms that affect the quality of life in individuals suffering from neurodegenerative diseases are depression, psychiatric disturbances, and loss of cognitive function (Batista and Pereira, 2015). In certain documented cases attempts to treat the primary infection have led to complete paralysis of the patient as a side effect of therapy (Braakman *et al*., 2006). These diseases also cause irreversible demyelination and loss of axons. Individuals affected by this subset of diseases often suffer from behavioral changes and spend the remainder of their lives in frail care or in mental institutions unable to lead a normal life (Low and Ho, 2017, Giordano *et al*., 2022). In the case of HAT infections, morbidity can occur in as little as two weeks (Dunn *et al*., 2022).

1.4 Human African trypanosomiasis

Since its first documented case, HAT reportedly has an annual incidence of 300,000 cases in the affected regions and of this estimated amount only 992 and 663 cases were reported for 2019 and 2020, respectively (Franco *et al*., 2022). Detection of the disease largely relies on microscopy and visualization of the trypanosome in blood samples of infected animals or humans, however a study determined that prevalence rates can be underestimated using this technique (Mulenga *et al*., 2021). Throughout the 20th century the disease, although lethal, was neglected and transmission soared through the late 1990s (Büscher *et al*., 2018). The World Health Organization (WHO) has since put measures in place to eradicate the disease. The WHO classifies a

disease as eradicated upon a zero incidence of infection or once the causative agent is no longer present (Corona, 2020). The control measures include continuous testing of people at risk and controlling tsetse fly populations. Since these measures have been implemented, WHO has validated Uganda for having eliminated the gambiense HAT however, Uganda remains an endemic region for rhodesiense HAT. Since testing for the disease decreased over the 2020 period due to COVID-19, both the rural communities and travelers in affected areas remain at risk of contracting the fatal disease (Mwiinde *et al*., 2022).

CHAPTER TWO

LITERATURE REVIEW

2.1 Background of the study

Human African trypanosomiasis (HAT) also known as sleeping sickness, is caused by the protozoan species *Trypanosoma brucei* (*T.b*) and is transmitted through the bite of a tsetse fly (Fig. 1) (Stitch *et al*., 2002). The disease commonly presents itself in two forms caused by infection with the *T.b gambiense* which originates from West Africa or *T.b rhodesiense* which is of East African origin (Kennedy, 2019). *T.b gambiense* infection is known to persist for months or years, while the *T.b rhodesiense* infection is known to be acute, rapidly progressing, and is also associated with severe symptoms at the three-week mark (Kennedy, 2019, Mbaya *et al*., 2012).

The disease is characterized by two stages namely stage 1 or the hemolytic phase and stage 2 known as the encephalitic phase (Bouteille and Buguet, 2012). According to the most recent statistics (Rodgers *et al*., 2017), an estimated 65-70 million individuals are at risk of contracting the disease, however, documented cases are less than 1000 (Rodgers *et al*., 2017, Kuriakose *et al*., 2016). During the hemolytic phase of the disease, the protozoan enters the peripheral circulation where replication of the organism takes place, while the phenotypic expression is characterized by anemia (Mbaya *et al.*, 2012). In the second stage of the disease, the trypanosome invades the CNS where it is responsible for observed effects such as altered mental state, and in the absence of treatment, results in the affected individual displaying neurological deficits and eventually death (Bouteille and Buguet, 2012). Neurological symptoms include memory impairment, tremors, and nerve neuropathy (Maclean *et al*., 2012).

Progression from stage 1 to stage 2 occurs when the trypanosome penetrates the host blood-brain barrier (BBB) and later embeds itself into the parenchyma of the brain tissue (Laperchia *et al*., 2016). This stage of the infection is associated with the development of neuroinflammation and is characterized by the presence of inflammatory cells, infiltration of the meninges and choroid, followed by inflammation of the parenchymal vessels, and eventually the development of encephalitis (Rodgers

et al., 2017). Literature states that once the disease reaches this stage of the infection, the parasite is shielded from many trypanocidal drugs (Frevert *et al*., 2017). This emphasizes the need for investigating the pharmacological trafficking of drugs across the BBB and whether it could ease the parasitic burden or reverse any neuroinflammatory damage. A major effort to alleviate parasite-elicited pathology lies in activating type 2 immune responses to induce alternative activation of macrophages or microglia with anti-inflammatory properties (Stijlemans *et al*., 2007).

To date, the treatment of this disease is limited, and existing drugs have been shown to have a certain level of toxicity (Baral, 2010). Prostacyclin, which is a member of the prostaglandin family, has recently been shown to have a therapeutic role in inflammatory disease (Stitham *et al*., 2011). Previous studies have shown that prostacyclin and its analogues can selectively inhibit the production of pro-inflammatory cytokines from activated peripheral mononuclear blood cells (Luttmann *et al*., 1999). However, these regulatory roles have not been investigated in a neuronal cell line or CNS disease pathology involving trypanosome infection. The pharmacological trafficking of potential curative products through the blood-CNS barrier to suppress parasite burden and enhance the reversal of cognitive dysfunction also remains poorly understood. Previous studies link dysregulation of the cytokine network, excessive production of inflammatory cytokines, and the release of inflammatory mediators as the major cause of death in infected humans and animals (Uzonna *et al*., 1998, Shi *et al*., 2003). This further supports the need to investigate methods of alleviating parasite-elicited pathology and subsequent treatment.

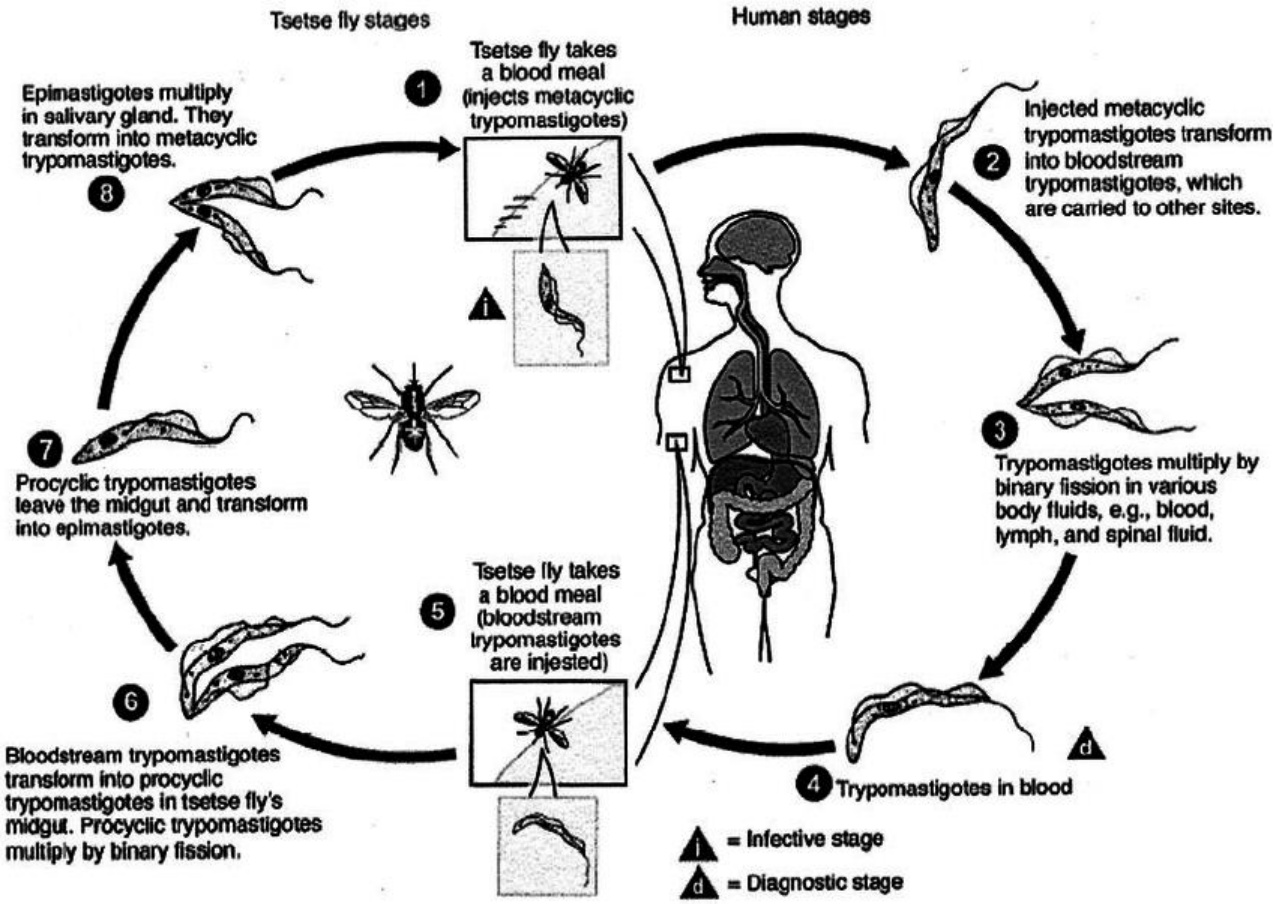

Fig. 1: *Life cycle of Trypanosoma brucei (source: Chappius et al., 2005)*

2.2 Trypanosoma brucei

Trypanosomes are single-celled protozoa with an array of subspecies, each described as causing very different diseases (Morrison, 2011).

The parasite is restricted to sub-Saharan Africa through its vector and the species is divided into three subspecies based on geographical origin (Franco *et al*., 2014). Previously, the Gambian form of the disease was seen as the primary human infection as its host is restricted to humans (table 1). However, the disease caused by *T.b rhodesiense* is zoonotic and can also infect humans (Dunn *et al*., 2022). Lastly, the third subspecies *T.b. brucei*, restricted to animals, is known to cause a disease characterized by wasting of the infected organism and is usually referred to as nagana.

Table 1: *Subspecies of Trypanosomes and host of infection (adapted from Balmer et al., 2011)*

Subspecies	***Host***
T. brucei gambiense	Human
T. brucei rhodesiense	Animal/Human
T brucei brucei	Animal

The trypanosome life cycle begins with the tsetse fly depositing an inoculum of trypomastigotes into the skin when taking a blood meal. The parasite then differentiates into long slender trypomastigotes that are proliferative and able to establish infections within the host (Alfituri *et al*., 2020). The proliferative parasites then travel from the site of infection to the lymph nodes via afferent lymphatic vessels before spreading systemically and establishing an infection in the bloodstream (Alfituri *et al*., 2020). The trypanosomes are able to establish colonies in various tissues such as the skin, adipose tissue, or CNS, where they become well adapted to thrive and persist.

2.3 Pathophysiology of Trypanosoma brucei infection

The symptoms of the HAT disease include skin lesions, intermittent fever, headaches, rigors, transient edema, generalized lymphadenopathy, and meningoencephalitis (Pearson, 2020). Both subspecies penetrate the central nervous system, however, the key difference between *T.b gambiense* and *T.b rhodesiense* is the amount of time taken by the parasite to reach the CNS. In the case of *T.b rhodesiense*, CNS manifestation of the species could occur within weeks. The observed effects of the disease include dysesthesia, extrapyramidal motor disturbances, sleep disorders, and neuropsychiatric changes (Kristensson and Bentivoglio, 1999). The Trypanosome species make use of the host immune system cytokines to facilitate their growth and have excellent evasion mechanisms in place to survive within the host environment.

2.4 Host Immune response to infection and evasion mechanisms of Trypanosoma brucei.

The host immune systems' two key responses comprise the innate and adaptive immune responses. During infection, the innate immune system serves as the first line of defense against the *T.b* parasite, it responds in the same manner to all foreign material as it is nonspecific (Marshall *et al*., 2018). The innate immune system relies on myeloid cells which engulf and destroy pathogens. These cells include macrophages and dendritic cells which also present antigens to the cells of the adaptive immune system (Beutler, 2004). These mononuclear cells play an essential role in the innate immune response to infectious agents, they induce the production of proteins that form part of the complement system, acute-phase reaction to infection and also produce many cytokines that affect various cellular responses (Gordon and Plüddemann, 2017).

Macrophages are highly specialized immune cells that display phenotypic heterogeneity, this allows them to react to different biological stimuli and further modify their phenotype based on the type of infection or microorganism at hand (Hirayama *et al*., 2018). These immune cells are involved in tissue homeostasis, repair, defense, and inflammation (Gordon and Plüddemann, 2017). They can also undergo phenotype switching between M1 macrophages which produce pro-inflammatory cytokines and mediators resulting in inflammation, and M2 macrophages which produce anti-inflammatory cytokines and mediate wound healing (Mantovani *et al*., 2012). In the inflammatory response to infection, macrophages secrete pro-inflammatory cytokines that are involved in up-regulating inflammatory reactions in an attempt to rid the host body of the invading agent (Chen *et al*., 2018). Cytokines are small, secreted proteins and each cytokine has a defined effect on the interactions between specific cells, they also form important biochemical messengers and illicit various signaling pathways (Zhang and An, 2007).

Tumour necrosis factor-α (TNF-α) plays a role in the regulation of macrophage function and is released after exposure to infection or trauma (Kato *et al*., 2016). The cytokine is one of the most frequent mediators in inflammatory tissue and plays an important role in integrating the production of a pro-inflammatory cytokine cascade

(Parameswaran and Patial, 2010). TNF-α has been documented to be trypanolytic for the *T.b* species, unlike other pro-inflammatory cytokines which the protozoan uses to its advantage (Magez *et al*.,1999). The role of TNF-α in HAT infection is predominantly to control the growth of the parasite, however, the resulting inflammatory response can induce severe tissue pathogenicity which causes chronic inflammation that is damaging to both peripheral and CNS tissues (Vanwalleghem *et al*., 2017).

Interleukin-1 (IL-1) is known as a key regulator of inflammation through its control of an array of innate immune system processes, it exists in two individual forms namely IL-1α and IL-1β (Kaneko *et al*., 2019). The cytokine is commonly associated with trypanosomiasis as it is secreted by macrophages, microglia, and astrocytes during the infection (Kato *et al*., 2016). CNS immune cells also secrete TNFα and IL-1β to alleviate the effects of potentially harmful agents. Previous literature suggests that overproduction of TNFα, IL-1β along with other pro-inflammatory cytokines is the main cause of death in mouse models of trypanosomiasis (*Shi et al*., 2002). TNFα and IL-1β also have been associated with a negative impact on cognitive function (Derecki *et al*., 2009).

The resident cells of the immune system recognize the pathogen-associated molecular pattern (PAMP) molecule of the *T.b* which is a glycosylphosphatidylinositol residue on the outer membrane of the microorganism. This protein is shed in the bloodstream of infected individuals and is bound to the variant surface glycoprotein (VSG) molecules of the *T.b* (Moreno *et al*., 2019, Hong and Kinoshita, 2009). PAMP recognition then stimulates the inflammatory response by macrophages and dendritic cells, which secrete cytokines that promote the recruitment of adaptive immune cells. In the adaptive immune system, evidence suggests that the *T.b* activates both T-helper (Th) cell-independent and Th-cell-dependent B-cell responses to the VSG. This activates antibody responses to the antigen and a highly polarized type 1 cytokine response (Mansfield and Paulnock, 2005). Type 1 cytokines favor strong cellular immune responses and consist of mediators such as interleukins, TNF-α and interferon-γ (IFN- γ). The main mechanism of parasite clearance from resistant animal species is through B-cell antibody production with specific antibodies targeted at parasitic infections (Onyilagha and Uzonna, 2019).

2.5 Adaptive immune response

For Trypanosomes to survive inside a host, they need to successfully evade the host's immune mechanisms. One major characteristic that the species makes use of is antigenic shifting through its VSG (Levison, 2016). The trypanosome species contain up to 10^7 VSG molecules on its membrane surface, the VSG is continuously changing during replication, and this prevents trypanosome lysis by the complement alternative pathway (Baral, 2010). The VSG also induces autoantibodies (Fig. 2), production of TNF α and triggers IFN- γ production by T cells (Vincendeau and Bouteille, 2005).

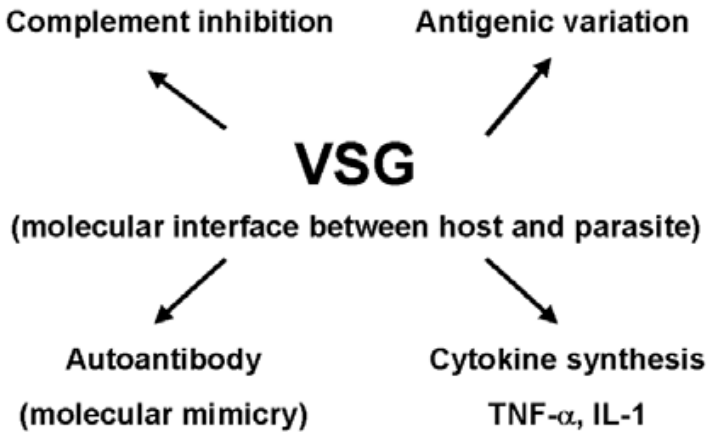

Fig. 2: *Variable surface glycoprotein functions (Source : Vincendeau and Bouteille, 2005)*

Increased antibody titer in response to specific VSG will destroy most of the parasitic population; however, any remaining parasite with an altered VSG evades the host immune responses (Fig. 3). This manipulation of the host immune system has been linked to chronic *T.b* infection which lasts for years (Aitcheson *et al*., 2005).

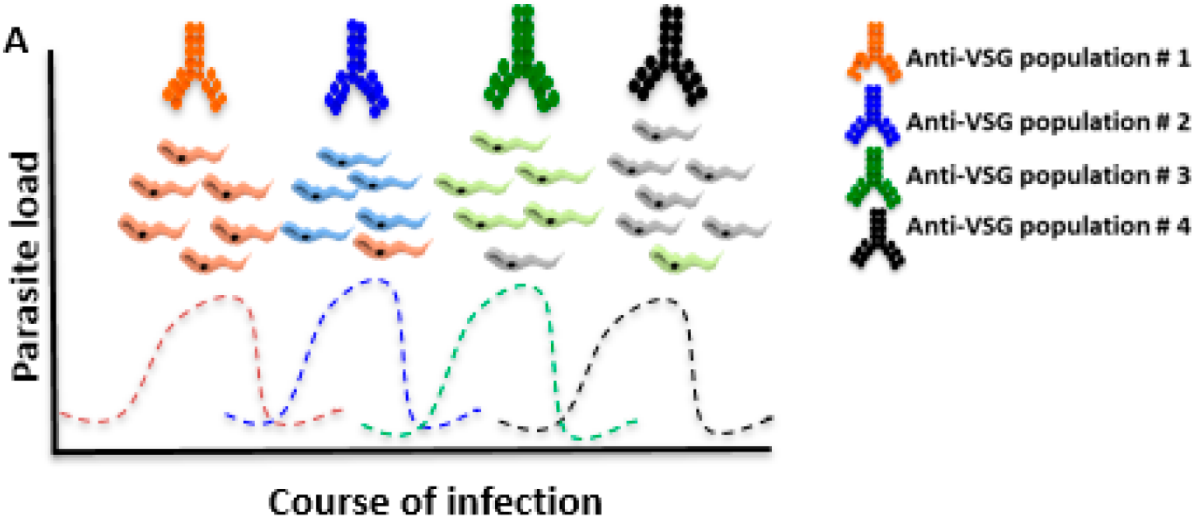

***Fig. 3**: Host immunosuppression by VSG shifting in T.b (Source: Moreno et al., 2019)*

Circulating endotoxins in the host peripheral circulation also play a role in the adverse effects of the disease (Levison, 2016). As previously stated, resident macrophages secrete cytokines that promote inflammation and recruitment of T-cells and B-cells that display a highly antigen-specific response to irradicate the parasite. However, once antigenic shift takes place the immune cells no longer destroy the pathogen, and the infection persists. The *T.b* then invades the host CNS using mechanisms proposed to be similar to leukocyte extravasation (Masocha *et al*., 2007).

In the CNS the *T.b* species initially accumulate in the stroma of the choroid plexus, between a layer of fenestrated endothelium and a layer of epithelia that produces cerebrospinal fluid (CSF) (Frevert *et al*., 2017). This results in an inflammatory response that spreads from the plexus into the parenchyma. It has been documented that *T.b* invades the parenchyma only at the final stages of the disease, defined as when meningoencephalitis is fully established (Philip *et al*., 1994, Pentreath *et al*., 1995). CNS infection triggers astrocyte activation along with microglia hyperplasia which leads to the accumulation of macrophages and activated T cells and B cells in the white matter of the brain (Rock *et al*., 2004). It is important to note that the BBB restricts access of peripheral leukocytes such as T cells, B cells, and macrophages to the brain parenchyma (Gemechu and Bentivoglio, 2021). These immune cells can amplify inflammation and cause neuronal dysfunction and damage.

2.6 Immune cells of the CNS

The CNS is a tightly regulated environment with own resident immune cells. In the CNS lymphocytes reside mostly in the meninges and choroid plexus; however, a few lymphocytes are also found in the brain parenchyma, specifically in the fimbria of the dorsal hippocampus (Morimoto and Nakajima, 2019). Another immune cell that plays a key role in the modulation of the immune response and a variety of physiological functions within the brain is the astrocyte. Astrocytes are involved in the maintenance of the BBB, modulation of synaptic plasticity, and regulation of energy homeostasis, all of which affect cognition, sleep, and circadian rhythm (Priego and Valiente, 2019). The foot processes of astrocytes extend onto the basement membrane of all brain capillaries and signal the formation of tight junctions by endothelial cells that constitute the BBB (Giovannoni and Quintana, 2020). They control both the entry and restriction of leukocytes across the BBB. The immune cells collectively act to continuously monitor the environment of the CNS for pathogens.

Microglia, which are specialized macrophages in the CNS, constitute the bulk of the immune cells, and their function is to remove damaged neurons and infectious agents (Wake and Douglas, 2011). Their morphology consists of a small soma with fine cellular processes (Kettenmann *et al*., 2019), this is known to be their 'resting' state (M0) where they actively survey the microenvironment. Microglial cells exhibit an M0 phenotype under healthy conditions (Wei and Li, 2022). Characterization of their M0 phenotype is by functional dormancy, absent expression of activation molecules along with no antigen-presenting cell phenotype (Lier *et al*., 2021).

2.6.1 Astrocytes

Astrocytes become activated in areas with an incomplete BBB such as in the choroid plexus and it has been suggested that astrocyte activation in response to the *T.b* infection is one of the first CNS responses to invasion (Gichuki,1994). Astrocytes become stimulated by a variety of signals to release TNF-α, IL-1β, and IFN- γ which are involved in the recruitment of leukocytes to the site of infection (Fig. 4) (Giovannoni and Quintana, 2020). Furthermore IFN- γ induces the production of the chemokine

CXCL10 that facilitates parasite and peripheral T-cell accumulation in the brain (Amin *et al*., 2009).

Astrocytes alter the permeability of the BBB to peripheral leukocytes during infection. However, in the case of *T.b* infection, the parasites' constant antigenic shifting causes recurrent bouts of inflammation and thus, the immune response persists. Although the protozoan species causes neuroinflammation, little is known about the mechanisms and how it contributes to the cognitive responses observed.

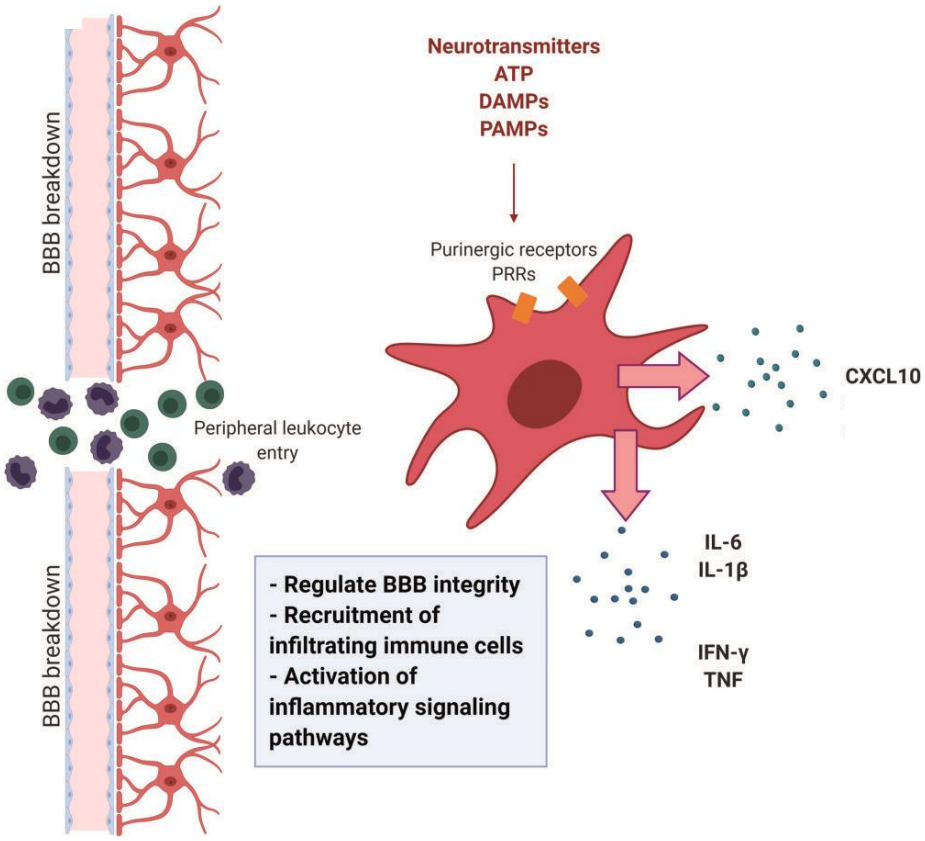

Fig. 4: *Astrocyte activation and responses to PAMP (Adapted from Soung and Klein, 2020)*

2.6.2 Microglia

Microglia constitute about 10% of the total cell population in an adult brain (Shao *et al*., 2022). This subtype of immune cells originates from the yolk sac during

embryogenesis and migrates into the CNS (Ginhoux *et al*., 2010). They can be found in the dentate gyrus of the hippocampus, substantia nigra, and prefrontal cortex (Bachiller *et al*., 2018, Kongsui *et al*.,2014). They are not uniformly distributed across the brain and will be observed in the highest numbers in the hippocampal dentate gyrus, substantia nigra and parts of the basal ganglia (Tan *et al*., 2020, Lawson *et al*., 1990).

The number of microglia is regulated by the microenvironment in the brain, this can change in response to infection where these immune cells possess the same morphological heterogeneity as macrophages (Bachiller *et al*., 2018). Microglia proliferate under specific conditions that include stress, aging and infectious disease (Mander *et al*., 2006, Schramm and Waismain, 2022). Microglia can modify their proliferation, phagocytic activity, and antigen presentation as well as release inflammatory cytokines in response to infection. They can be characterized in three phenotypic classes namely, resting/surveilling, pro-inflammatory and anti-inflammatory microglia. These immune cells also take part in synaptic remodeling, pruning, vessel patterning, and angiogenesis promotion (Jurga *et al*., 2020). Because microglia are one of the first lines of defense against pathogens, their activation is key for protecting the brain tissue. However, a persistent infection coupled with inflammation affects neuronal plasticity, impairs memory, and is also responsible for the extensive tissue damage observed in neurodegenerative disease (Muzio *et al*., 2021).

Resting microglia continuously extend and retract their processes to monitor the microenvironment for any signs of infection or homeostasis-perturbing events (Wei and Li, 2022). When their fine processes become stimulated by exogenous or endogenous ligands, they assume an activated state which can be determined with the use of Ionized calcium binding adaptor molecule 1 (IBA-1) (Ohsawa *et al*., 2004). IBA-1 is known to participate in membrane ruffling and phagocytosis in activated microglia (M1 microglia) that are adapted to quickly resolve any damage and return the environment to a state of homeostasis (Wei and Li, 2022).

2.6.3 Classically activated microglia (M1)

Classically activated microglia (M1) are pro-inflammatory in nature. The hallmark of pro-inflammatory phenotype is secretion of pro-inflammatory cytokines, TNF-α and IL-1β (Fig. 5). Like macrophage activation, microglial M1 activation relies on pro-inflammatory cytokine production (Orihuela *et al*., 2016).

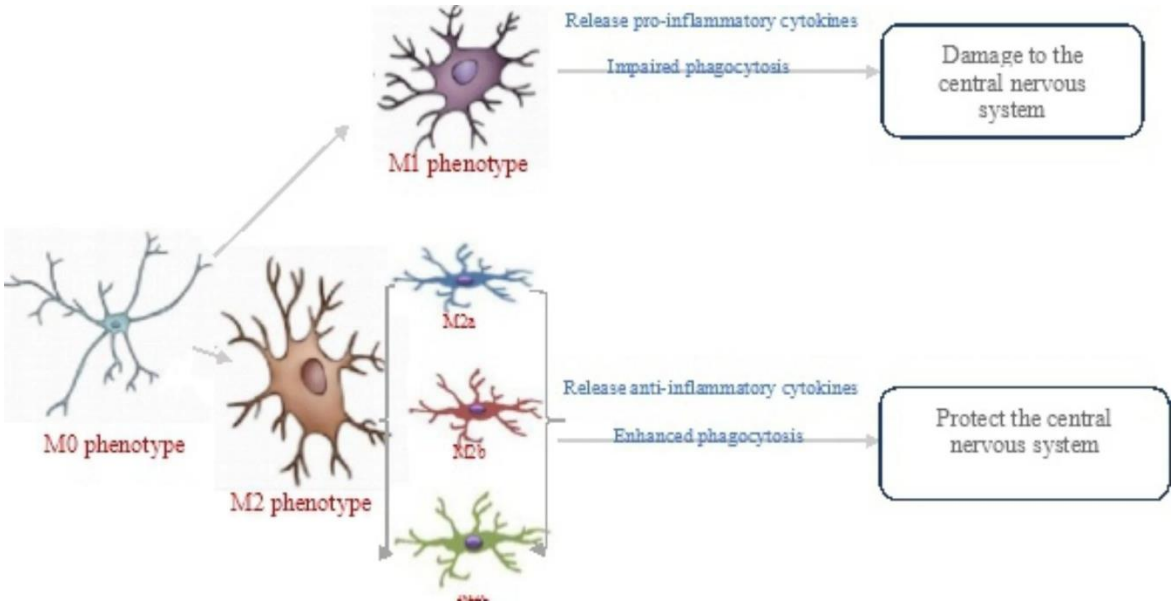

Fig. 5*: Microglial phenotypes and functions (Source: Wei and Li, 2022)*

Polarization from the M0 to M1 phenotype can be achieved through lipopolysaccharide (LPS) or IFN- γ stimulation. LPS is a bacterial endotoxin and a ligand of the Toll-like Receptors (TLR), specifically TLR4 which become activated upon LPS binding to the LPS-binding protein and starting the pro-inflammatory signalling cascade (Guo *et al*., 2022). Downstream effectors of this pathway include activation of two major pro-inflammatory pathways, nuclear factor kappa-B (NF- κB) and mitogen-activated protein kinases (MAPK) signalling pathways. The specific effectors are phosphorylation of Signal Transducer and Activator of Transcription (STAT) , with STAT1 and 3 mediating M1 polarization (Guo *et al*., 2022). These pathways result in the pro-inflammatory genes. Similar to peripheral macrophages, microglia respond to various pro-inflammatory cytokines, redox molecules such as inducible nitric oxide (iNOS) and nicotinamide adenine dinucleotide phosphate (NADPH) oxidase, co-stimulatory proteins, and major histocompatibility complex II (MHC-II) (Ta *et al*., 2019, Guo *et al*., 2022). Literature states that under the M1 phenotype phagocytosis is

temporarily halted and the outcome of an M1 polarizing event is dependent on iNOS production or the activation of NOD-like receptor family pyrin domain-containing 3 (NLRP3) inflammasome complex (Orihuela *et al*., 2016). The inflammasome complex further facilitates the production of IL-1β from precursor proteins (Netea *et al*., 2014).

2.7 Brain structures and chemicals affected by Trypanosoma brucei infection

The brain comprises several different structures within its cerebral cortex. These structures are responsible for cognition, mental imagery, and the ability to produce and understand language (Ackerman, 1992). The areas of interest that are particularly affected by *T.b* infection include the choroid plexus, meninges, brain parenchyma and Hippocampus. The hippocampus is an important region of the brain that is involved with learning and memory (Anand and Dhikav, 2012). Previous studies have demonstrated how hippocampal dysfunction is associated with impaired memory (Wible, 2013).

2.7.1 Hippocampus

Structurally the hippocampus is embedded deep within the temporal lobe of the cerebral cortex (Vago *et al*., 2014). It is particularly vulnerable to damage in injury, infection, stress, or psychiatric disorders (Anand and Dhikav, 2012). The hippocampus forms part of the limbic system that is concerned with hunger, motivation, mood, pain, and pleasure.

Anatomically the hippocampus contains three parts namely, the Cornu ammonis (CA), dentate gyrus (DG) and the subiculum (Fig. 6) (Rajmohan and Mohandas, 2007, Chauhan *et al*., 2021). The CA and DG are separated by the hippocampal sulcus and below the sulcus lies the subiculum, followed by the entorhinal area (EC). The Cornu ammonis is further divided into CA1, CA2, CA3, and CA4 regions. The CA1 region of the hippocampus is composed of pyramidal neurons with triangular soma while the CA2-4 region is composed of pyramidal neurons with an ovoid soma (Graves *et al*., 2012, Duvernoy *et al*., 2013).

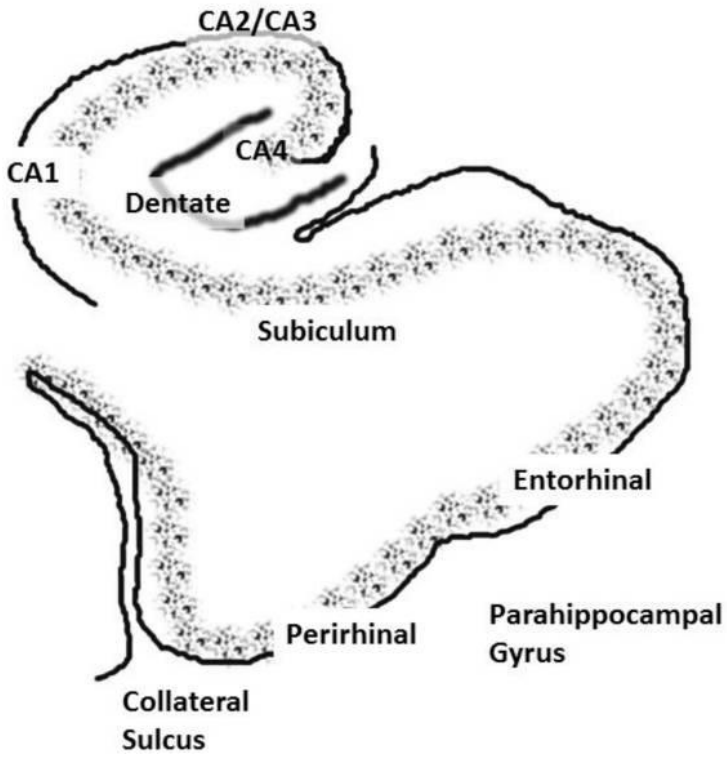

Fig. 6: *A coronal slice depicting regions of the hippocampus and associated structures (Source: Wible, 2013)*

Long-term potentiation was first discovered in this region of the brain. The hippocampus is one of the regions in the brain where neurogenesis continues even in adults (Catlow *et al*., 2016). While this structure is important in learning and memory, it also functions in spatial navigation, emotional behavior, and regulation of hypothalamic functions (Maguire *et al*., 2006, Rubin *et al*., 2014).

Learning and memory comprise of two prominent pathways: the polysynaptic and direct pathway. The two pathways differ in that the polysynaptic pathway is important in semantic memory and the direct pathway is important in episodic and spatial memory (Anand and Dhikav, 2012). Hippocampal projections contain norepinephrine, serotonergic, and dopaminergic neurons. It also contains an important cholinergic and GABAergic projection that originates from the medial septal area and innervates all parts of the hippocampus (Khakpai *et al*., 2013). The consequence of destruction of this projection can lead to severe impairment of memory (Terry and Buccafusco, 2003, Maurer and Williams, 2017).

Previous studies have linked LPS-induced neuroinflammation to changes within the hippocampus which include a reduction of the receptors involved in spatial memory (Rosi *et al*., 2004). A previous study modelling neurogenesis in the hippocampus,

determined that cell proliferation in the dentate gyrus is increased when IL-1β and TNF-α receptors are diminished or inhibited (Valero *et al*.,2017). In fact, inflammation compromises the survival of hippocampal neuroprecursor cells, as evidenced by the induction of cell death in these progenitor cells following intraperitoneal administration of LPS (Sierra *et al*., 2010).

2.7.2 Implications of neuroinflammation on memory formation and learning structures of the brain

Neurodegeneration is a key feature in the late stage of the *T.b* infection. Previous studies have linked hypothalamic lesions with memory deficits (Thompson and Kim, 1996, Vercruysee *et al*., 2018). Neuronal damage has mostly been studied in terms of sleep disturbances associated with *T.b* infection where atrophy, as well as structural and functional changes, have been observed in infected rats (Laperchia *et al*., 2018). Cognitive impairments observed in sleeping sickness include learning and memory impairment as well as difficulty concentrating (Mudji *et al*.,2020). However, the mechanisms by which the infection causes these effects remain poorly understood. DNA methylation in neuronal cells has been linked to mediating memory acquisition and storage by altering the expression of key molecules such as brain-derived neurotrophic factor (BDNF) (Hwang *et al*, 2017, Day and Sweatt, 2010), which is involved in learning and memory by enhancing synaptic transmission across nerve cells (Jovanovic *et al*., 2000).

2.7.3 Brain-Derived Neurotrophic Factor.

BDNF is a member of the neurotrophin family and is known for its neuroprotective functions mediating the survival and differentiation of neurons in the brain. It also plays a role in the regulation of synaptic strength (Yamada *et al*., 2002). BDNF gene translation first begins with the production of pro-BDNF which is then cleaved by endoproteases to produce mature BDNF (m-BDNF) in the presynaptic neurons. m-BDNF then binds to the tyrosine kinase B (TrkB) receptor on the postsynaptic neuron that triggers signaling cascades including the Ras-mitogen-activated protein kinase (MAPK), the phosphatidylinositol-3-kinase (PI3K), and the phospholipase Cγ (PLC-γ) pathways (Ibrahim *et al*., 2022). These pathways increase the influx of calcium^{2+} (Ca^{2+})

leading to activation of transcription factors by phosphorylation and thereby increasing BDNF expression (Fig. 7)

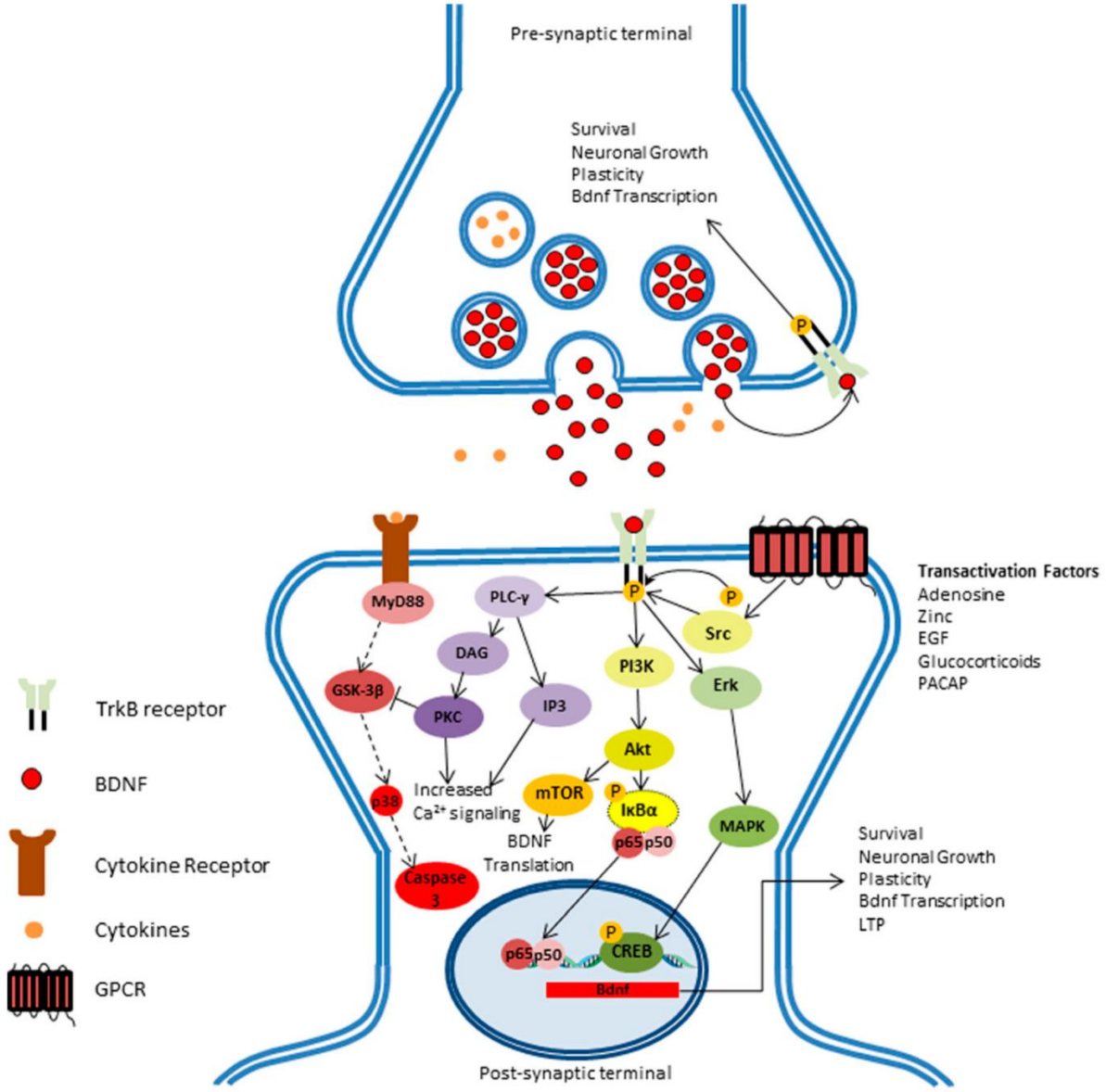

Fig. 7*: Pathways by which BDNF modulates neuronal cell survival, growth, and plasticity. The binding of BDNF to the TrkB receptor activates 3 different signalling pathways: the first pathway being the activation of the PLC-γ leading to an increased level of* Ca^{2+} *that will terminate the apoptosis caused by inflammatory mediators. The second pathway is through activation of PI3K resulting in the transcription of BDNF mRNA and downstream gene regulation through NF-κB. Lastly, activation of the third pathway causes induction of Erk that further plays a role in gene regulation through MAPK and subsequently CREB. (Source: Ibrahim et al., 2022)*

BDNF modulates the growth and complexity of dendrites, and an increase in BDNF in the hippocampus is associated with spatial learning (McAllister *et al*., 1995). BDNF is also essential for memory storage. A previous study demonstrated inhibition of BDNF expression caused a deficit in memory persistence, whilst intra-hippocampal infusion of BDNF reversed this deficit in memory persistence (Bekinschtein *et al*., 2007). Another study also depicted how mice lacking BDNF showed impaired long-term potentiation and how these changes can be restored by the re-expression of BDNF (Ernfors *et al*., 1994). Furthermore, methylation of the plasticity-promoting gene, BDNF, decreased its expression which has been associated with impaired memory and depression (Ferrer *et al*., 2019, Poon *et al*., 2020). Neural plasticity is the ability of the brain to rewire its structure in response to either internal or external stimuli (Nayak *et al*., 2022), DNA demethylation and methylation of specific genes form part of the epigenetic mechanisms of neuronal plasticity.

2.7.4 cAMP response element binding protein

cAMP response element binding protein (CREB) is a transcription factor located in the nucleus and cytosol of cells. The activity of CREB impacts processes such as proliferation, differentiation, survival of nerve cells, neurogenesis, neuronal plasticity, and long-term potentiation in the CNS (Wang *et al*., 2018). It elicits its effects once phosphorylated by kinases, which subsequently allows the transcription factor to bind to the cAMP response element (CRE) (Lonze and Ginty, 2002). Previous studies demonstrate that knockout of CREB results in neuronal apathy which becomes more apparent when coupled with an absence of cAMP-responsive element modulator (CREM) (Kida, 2012, Yu *et al*., 2018). CREB in its active state is also known to promote the synthesis of proteins that are involved in neuronal plasticity. CREB has been found to influence spatial learning and cued information with increases in the phosphorylation of the protein associated with learning and inversely, decreases in CREB phosphorylation are associated with interference of memory (Brightwell *et al*., 2007). Previous studies also demonstrated that treatment with CREB enhanced long-term memory as well as learning capabilities (Barco *et al*., 2003, Brightwell *et al*. 2007, Liu *et al*., 2011). However, its role in trypanosomiasis remains poorly understood (Sakamoto *et al*., 2013). Furthermore, the epigenetic changes associated with the expression of CREB and BDNF in trypanosomiasis have not been investigated.

2.8 Epigenetic changes associated with memory formation and learning

Memory formation and learning can be broadly characterized as lasting alterations of behavioral output produced in response to a transient environmental input (Zovkic *et al*., 2013). To induce these lasting alterations, cells need to undergo a complex set of stimulus-specific cellular and molecular changes to consolidate a memory into an everlasting trace (Zovkic *et al*., 2013). Over the past 50 years, researchers have recognized the importance of gene transcription and protein synthesis in memory formation. However, the relatively short half-life of proteins raised an important question of how memories can be consolidated for a lifetime. Epigenetics and its roles in preserving transcriptional changes in response to short-lived proteins that will result in lasting memory formation have gained interest (Puckett and Lubin, 2011). This has led to the development of the field of Neuroepigenetics, which encompasses the unique mechanisms and processes allowing dynamic experience-dependent regulation of the epigenome in nondividing cells of the nervous system.

2.9 Epigenetic mechanisms

Epigenetic mechanisms are made up of key regulators of DNA compaction and transcription. A variety of DNA modifications exist that alter gene expression. They do so by altering DNA accessibility and chromatin structure to regulate gene expression (Handy *et al*.,2012). These mechanisms can be divided into three classes namely, DNA methylation, histone modification, and non-coding RNA (Loscalzo and handy, 2014). However, very few of these have been studied about learning and memory (Puckett and Lubin, 2011). Two of the epigenetic mechanisms that are known to play a role in learning and memory are histone modifications and DNA methylation (Branco *et al*., 2011, Peixoto and Abel, 2013).

Histone modification occurs through acetylation or deacetylation by acetyltransferases or deacetylases (Bannister and Kouzarides, 2011). It can also occur through histone phosphorylation at serines, threonines and tyrosines in the N-terminal histone tails (Bannister and Kouzarides, 2011). Histone phosphorylation and acetylation are usually associated with transcriptional activation (Ellenbroek and Youn, 2016,

Tirupapuliyur, 2011). Lastly, histone modifications can also occur through methylation of side chains of lysine and arginine. (Bannister and Kouzarides, 2011, Alam *et al*., 2015). Histone methylation regulates gene expression through the recruitment of transcription factors as opposed to directly altering chromatin structure, in this manner the transcription factors will either promote or silence gene expression (Fallah *et al*., 2021).

DNA methylation is characterized by the covalent attachment of a methyl group to the C5 position of cytosine by enzymes known as DNA methyltransferases (DNMTs). This primarily occurs in CpG dinucleotide containing regions and often in regulatory sequences that suppress gene expression (Loscalzo and handy, 2014). The methylated cytosine can suppress transcription by preventing the binding of transcription factors or promote the binding of transcription repressors.
Recent studies have also found DNA methylation to be key in synaptic plasticity and neuronal stem cell differentiation (Juliandi *et al*., 2010, Heyward and Sweatt, 2015). However, the methylation status of specific proteins, BDNF and CREB, that are important for memory and synaptic plasticity has yet to be characterized in HAT.

2.10 Protective mechanisms of the host immune system to infection.

The host immune response to invasion is both damaging to the infectious agent and the host tissues itself, because of this the immune system also has to carry out wound healing processes characterized by anti-inflammatory pathways from specialized cells. In the peripheral immune system, these cells consist of reparative M2 phenotype macrophages. These macrophages secrete cytokines such as IL-10 and express cell surface markers such as mannose receptor (CD206) and IBA-1 (Bethea and Fischer, 2021, Yunna *et al*., 2020). The immune response has a natural switch from the pro-inflammatory state to the anti-inflammatory state once an infectious agent has been removed. This means that the anti-inflammatory pathway closely follows the inflammatory response post-infection. However, with chronic inflammation the pro-inflammatory response shifts from short-to-long lived and results in an imbalance in this sensitive system (Lee and Choi, 2015, Furman *et al*., 2019).

The anti-inflammatory cytokines secreted by immune cells will essentially block the expression of pro-inflammatory cytokines and therefore ease inflammation and any subsequent inflammatory damage (Murray, 2006, Opal *et al*., 2000). The main observation with endogenous cytokines in trypanosomiasis is the over-expression of pro-inflammatory cytokines. Studies have been carried out to alleviate tissue pathogenicity and chronic infection by stimulating the anti-inflammatory pathways (Stiljemans *et al*., 2007, Bhattacharjee *et al*., 2012).

2.11 Protective mechanisms of the host immune system in the CNS

The CNS possesses similar anti-inflammatory mechanisms to those found in the peripheral immune system to undergo wound healing in response to inflammation, although wound healing in the CNS is more limited. Neuronal tissue is known to have a low regenerative potential and regeneration often results in scar formation that impedes function in that region. This is due to the fact that neurons themselves do not have reparative capabilities, especially in cases where demyelination is observed (Radtke *et al*., 2007).

During the wound healing process anti-inflammatory cytokines are released from specialized cells such as alternatively activated astrocytes, Th-17 cells, and M2 microglia (Dumont *et al*., 2015). The key cytokines involved in the anti-inflammatory process are Interleukin 10 (IL-10), Arginase-1 (ARG-1), Interleukin 13 (IL-13) and Interleukin 4 (IL-4) (Lobo-Silva *et al*., 2016).

IL-10 is a critical cytokine in the peripheral immune system where it functions to resolve peripheral inflammation. A previous study demonstrated that microglia and astrocytes produce IL-10 in a delayed manner, with cytokine production occurring 8 hours after the activation of TLR or LPS stimulation (Burmeister and Marriot, 2018). ARG-1 is a well-characterized modulator of tissue repair. The cytosolic enzyme catalyzes the hydrolysis of L-arginine into L-ornithine and urea (Morris, 2007). The products of this reaction are used to generate polyamines that have pro-repair properties. The enzyme also competes with iNOS for L-arginine thereby reducing the production of nitric oxide (NO), a free radical with inflammatory actions (Greenhalgh *et al*., 2016).

IL-4 and IL-13 possess the capability of suppressing inflammatory mediators (Hutchins *et al*., 2012). These cytokines both make use of the signaling receptor IL-4Rα and they induce the differentiation of naïve T cells into type 2 T-helper and T follicular helper cells (Heeb *et al*., 2020). They also stimulate antibody production by B cells, isotype switching to immunoglobulin E, expansion of basophil and eosinophil populations, mast cell activation, and promote the change of macrophages towards the alternatively activated macrophages or M2 macrophages (Gadani *et al*., 2012).

2.12 Alternative microglial activation and differentiation

M2 microglia or alternatively activated microglia are associated with anti-inflammatory pathways via the cytokines IL-4 and IL-13, which signal through IL-4Rα. This action induces a host of downstream processes that lead to potent anti-inflammatory functions (Cherry *et al*., 2014). Under normal immune responses, once the pathogen is removed using pro-inflammatory pathways, the anti-inflammatory response is favored and characterized by debris clearance and tissue repair (Mantovani *et al*., 2012).

M2 microglia also express cell surface markers CD206 and IBA-1 (Hopperton *et al*., 2017).

However, in the case of *T.b* infection, the persisting pathogen results in a prolonged pro-inflammatory response and thus causes further damage to brain tissue. A previous study demonstrated that mice lacking or deficient in M2 microglia showed an increase in lesion size post-brain injury and that a lack of M2 microglia also meant lower levels of neuroprotective factors (Varin and Gordin, 2009, Cherry *et al*., 2014).

2.13 The history of Human African Trypanosomiasis treatment

Trypanosoma brucei was first discovered in 1894 amongst cattle where it decimated livestock in the KwaZulu Natal province in South Africa (Baker, 1995). David Bruce discovered that the protozoan species isolated from the blood of the infected cattle, was responsible for the death of the livestock, and that the tsetse fly was the disease presenting agent in humans (Bruce, 1915). Previously, the disease was thought to occur by separate causes.

Africa experienced its first epidemic of the disease in 1896 which lasted through to 1906, affecting Uganda and Congo with between 300 000 – 500 000 casualties (Steverding, 2010). The first treatment reported by Charles Lavern and Félix Mesnil in 1902, used sodium arsenite as an effective treatment for laboratory animals (Cox FEG, 2004). Two years later Harold Thomas and Anton Breinl published a paper suggesting an arsenical drug called atoxyl as a potential treatment in animals (Winkle, 2005). This drug caused atrophy of the optic nerve and complete blindness in 22 patients treated for the infection (Winkle, 2005). In December 1909, a 26-year-old Englishman infected with the trypanosome was admitted to a hospital under the care of Dr. Ronald Ross (Baker, 1995, Ross and Thompson 1910). As there were no available treatments for the infection, Dr. Ross attempted therapy by treatments including but not limited to atoxyl, quinine, succinimide of mercury, and vaccines prepared by his own trypanosomes grown and extracted from rats (Ross and Thompson, 1911). The patient, unfortunately, died a mere seven months after being admitted to the Doctors' care.

In 1918 the chemist Walter Jacobs and the immunologist, Michael Heidelberger discovered an organo-arsenical tryparsamide which was used to treat the late stage of the disease (Jacobs and Heidelberger, 1919). The following year Wilhelm Roehl developed the first effective drug called Suramin, which was either used on its own or in conjunction with tryparsamide for both human and animal infections (Vickerman,1997). The side effects of Suramin include nephrotoxicity, peripheral neuropathy, and bone marrow toxicity (Weidemar *et al*.,2020).

Arthur Ewins went on to develop the third drug called pentamidine for treating the early stages of infection (Steverding, 2008). By 1949 melarsoprol, another arsenical drug, was being used to treat late-stage trypanosomiasis specifically caused by *T.b rhodesiense* (Lutje *et al*., 2013). Melarsoprol is liposoluble and can cross the BBB. Following the 1950s, several chemotherapy drugs became available to treat animal trypanosome infections, including the aromatic diamidine Diminazene aceturate (Berenil) (Kinabo, 1993).

2.14 Diminazene aceturate as a current therapy for trypanosomiasis

Diminazene aceturate has been used for the treatment of trypanosomiasis in animals since 1955 (Giordani *et al*., 2016). The drug acts by interfering with the protozoan's ability to undergo DNA replication by binding to the kinetoplast DNA as well as inducing heterochromatin condensation during the G2 phase of the parasite's cell cycle (Kuriakose and Uzonna, 2014). The key challenge with the use of Diminazene aceturate for the treatment of trypanosomiasis is the cost of the drug, as well as a concern for disease relapse (Jennings and Gray, 1983, Anene *et al*., 2005). A previous study assessing the efficacy of Diminazene aceturate in the treatment of trypanosomiasis in rats reported that disease relapse occurred even in groups receiving more than two doses of the drug (Ezeh *et al*., 2016). Another important challenge with the use of Diminazene aceturate is drug resistance, where administering sub-therapeutic doses is the main cause for concern (Assefa and Shibeshi, 2018). Thus, there is a need for alternative and more effective treatment.

2.15 Prostacyclin analogue as a novel treatment for trypanosome infection

Prostacyclin (PGI_2) is a member of the prostaglandin (PGI) family. Its roles in the cardiovascular and respiratory system are as a potent vasodilator and inhibitor of platelet aggregation (Stitham *et al*., 2011). However, the bioactive lipid compound and its analogues have become better known for their therapeutic capabilities in inflammatory-related diseases. PGIs are formed when arachidonic acid is released from the plasma membrane by phospholipase enzymes and metabolized by the actions of prostaglandin synthase or cyclooxygenase (COX) 1 and 2 (Ricciotti and FitzGerald, 2011)

Previous studies have shown that prostacyclin and its synthetic analogues can decrease the production of inflammatory cytokines such as TNF-α and induce the production of cytokines such as Interleukin10 (IL-10) which further plays a role in regulating and inhibiting the production of IL-1β (Eisenhut *et al*, 1993; Luttmann *et al*, 1999, Ipseiz *et al*., 2020). These findings suggest that the compound can actively control inflammation. However, its therapeutic potential in treating trypanosomiasis is yet to be characterized. PGI and its metabolites have been shown to reduce cellular proliferation of *T.b*. A previous study suggests a potential mechanism of PGI

analogues as a treatment for *T.b* infection involves programmed cell death (PCD). The bloodstream form of the parasite undergoes apoptosis-like PCD upon binding of PGI or its metabolites to its cell surface receptors (Figarella *et al*., 2005).

A previous study demonstrating the effect of prostacyclin analogues determined that this class of drugs acts by up-regulating the expression of intracellular signaling molecules for anti-inflammatory cytokines. They elicit this effect in dendritic cells, while also downregulating the activity of intracellular signals for pro-inflammatory cytokines (Zhou *et al*., 2007). The potential control of inflammation means that the compound could potentially act synergistically with existing anti-inflammatory cytokines and pathways in the CNS to treat the *T.b* infection.

2.15.1 Prostacyclin regulation of the Immune system

PGI_2 and its analogues regulate both the innate and adaptive immune response, where their effects are known to be anti-inflammatory or immunosuppressive (Dorris and Peebles, 2012). PGI's form part of the lipid mediators that are released under type 2 inflammatory responses (Oyebola *et al*., 2021). Four primary bioactive PGI's are generated *in vivo* namely, prostaglandin E_2 (PGE_2), prostacyclin (PGI_2), prostaglandin D_2 (PGD_2), and prostaglandin $F_{2\alpha}$ ($PGF_{2\alpha}$) (Idborg and Pawelzik, 2022). These derivates of PGI act as autocrine and paracrine mediators to maintain local homeostasis within the body. The amount of PGI production increases in acute inflammation before the recruitment of leukocytes and infiltration of immune cells (Ricciotti and FitzGerald, 2011). Production of PGIs also depends on the activity of COX-1 and 2, where COX-2 activity is induced by inflammatory stimuli, hormones and growth factors and is the more important source of PGIs in inflammatory processes (Smith *et al*., 2000). COX-2 appears to have a dual role in the inflammatory process by initially contributing to the onset of inflammation and later helping to resolve it (Ricciotti and FitzGerald, 2011). COX-2 immunoreactivity can be found in neuronal populations in the cerebral cortex and hippocampus (Minghetti, 2004).

2.15.2 Iloprost structure and mechanism of action

The prostacyclin analogue that was used to carry out this study is Iloprost. Iloprost (fig. 8) is a second-generation structural analogue of Prostacyclin. The chemical compound has a ten-fold greater potency than its first-generation stable analogues and exerts its mechanism of action by binding to a class of receptors belonging to the G-protein coupled receptors termed prostaglandin receptors (IP) (Ruan *et al*., 2010, Dorris and Peebles, 2012).

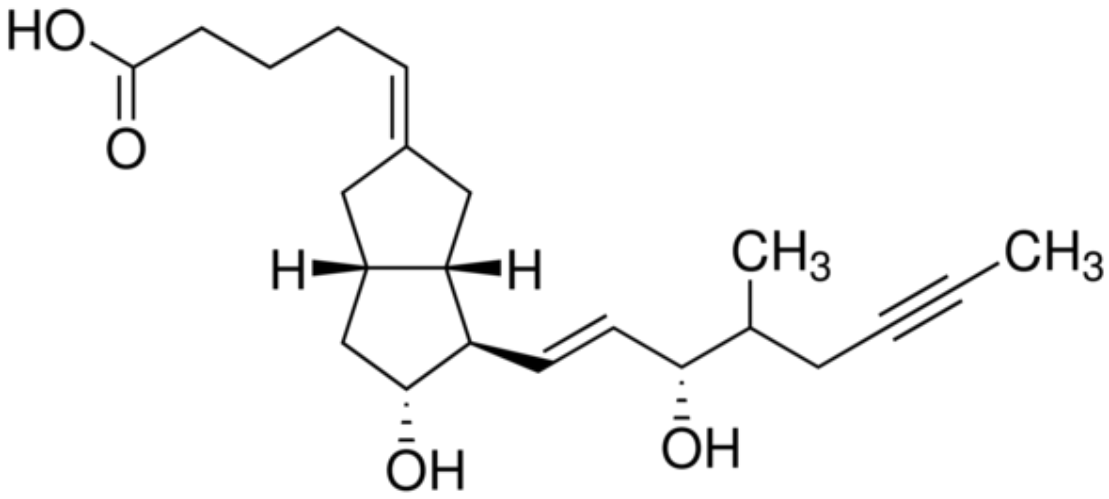

Fig. 8*: Iloprost chemical structure (Source: Sigma-Aldrich)*

Upon binding to the receptor, it triggers the activation of the G-protein and subsequently raises intracellular levels of cAMP (fig. 9). An increase in levels of cAMP then activates protein kinase A (Midgett *et al*., 2011). In the peripheral system, this leads to the inhibition of platelet aggregation, relaxation of smooth muscle, and vasodilation of pulmonary arteries. More specifically, mouse IP receptors have been found to occur on neurons while human IP receptors occur also on macrophages, T regulatory cells, and activated T cells (Dorris and Peebles., 2012)

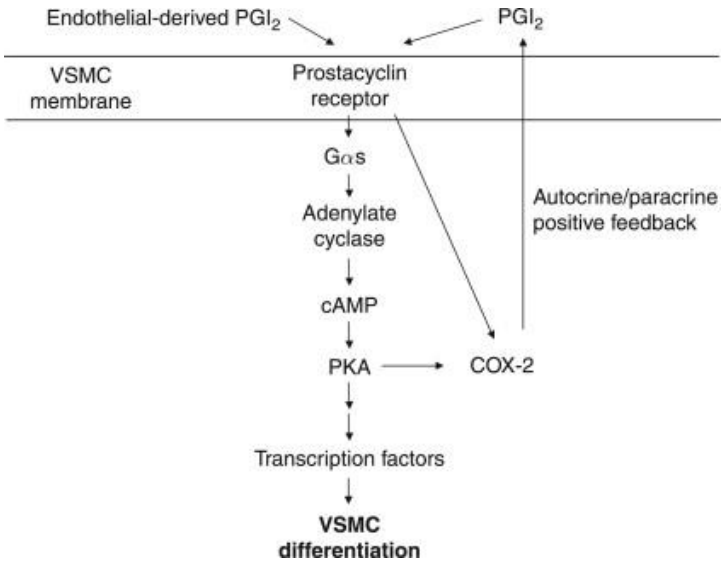

***Fig. 9**: Iloprost mechanism of action (Source: Martin et al., 2010)*

2.16 PROBLEM STATEMENT

Most of the approved medications to treat trypanosomiasis are costly and the risk of disease relapse remains high (Ezeh *et al*., 2016). Another important challenge is drug resistance, as administering sub-therapeutic doses is a contributing factor to the development of resistance (Solomon and Workineh, 2018). Previous studies have shown that prostacyclin and its synthetic analogues exert regulatory roles in neurodegenerative diseases by promoting anti-inflammatory cytokine expression while decreasing endogenous production of proinflammatory cytokines (Eisenhut *et al*, 1993; Luttmann *et al*, 1999, Ipseiz *et al*., 2020). Despite this knowledge, the roles of prostacyclin in microglial activation and differentiation as well as its therapeutic potential against CNS trypanosome infection is yet to be characterized.

2.17 Aims and Objectives of the Study

The aim of this study was to assess the potential neuroprotective effects of Iloprost through comparative analysis of neuroinflammatory responses in both microglial cells exposed to LPS and mouse brains infected with trypanosomes.

The following objectives have been formulated for this research:

1. To determine the generalized effects of LPS and Iloprost treatments on the viability of C8-B4 microglial cells and assess the potential occurrence of cytotoxic effects.
2. To investigate microglial activation and phenotypic switching associated with LPS-induced inflammatory changes in single cells via immunofluorescence detection of specific surface markers.
3. To investigate epigenetic changes associated with microglial response to LPS challenge and Iloprost treatment via assessment of CREB and BDNF DNA methylation profiling.
4. To identify and compare gene expression changes associated with inflammatory challenge influenced by acute exposure of microglia to LPS and trypanosome infection in mouse hippocampal brain tissue.
5. To determine the effective therapeutic dose of Iloprost and explore its potential neuroprotective roles against toxic and inflammatory changes induced by LPS and trypanosome infection.

2.18 Potential Benefits of the Study

The potential benefits of this study include broadening of the knowledge surrounding neuroinflammatory disease and the use of Iloprost as an anti-inflammatory drug. Characterising the ability of Iloprost to induce microglial polarization towards M2/anti-inflammatory microglia which mediate wound healing and debris clearance. Increased knowledge and understanding of the neuroprotective capabilities of prostacyclin class drugs. Providing crucial information in the use of Iloprost as a therapy for *T.b* infection in a mouse model and lastly, providing more information on the epigenetic effects of Iloprost on neuroprotective factor, BDNF, which enables neuronal survival and neurogenesis.

CHAPTER THREE

MATERIALS AND METHODS

This study was conducted in two phases using both cell line and animal-based models.

3.1 Phase I (*in vitro* study)

All cell line-based work was carried out in the tissue culture laboratory situated in the Department of Human Physiology, Nelson Mandela University, South Africa, using C8-B4 microglial cells. Briefly, the therapeutic potential of Iloprost was tested against LPS-induced inflammation in the microglial cells as indicated in the flow diagram below (Fig.10).

3.1.1 Murine C8-B4 Cell line

C8-B4 cells are an immortal cell line that was derived originally from the C57BL/6 mouse cerebellum, and generally express the cell surface markers MAC1, and CD4 (Alliot *et al*., 1996). The cells also produce NO and a number of cytokines (Alliot *et al*., 1996). The C8-B4 cells have been passaged in culture for more than 100 doublings with a doubling time of 48-72 hours (Alliot *et al*., 1996). Ideally, primary mouse microglial cells more closely resemble the responses *in vivo* however, this cell line is said to somewhat mimic a primary cell culture (Figuera-Losada *et al*., 2014). During culture, some C8-B4 cells take up a ramified microglial morphology, whilst other cells, in the same culture, take up a rounder appearance with the presence or absence of branching processes (Alliot *et al*., 1996). They are not immunoreactive to specific antibodies for oligodendrocytes or astrocytes. Therefore, the cell line is thought to be derived from a monocyte-macrophage precursor (Timmerman *et al*., 2018). For this reason, the current study made use of the C8-B4 cell line in a model of LPS-induced neuroinflammation.

3.1.2 Cell culture

C8-B4 cells were purchased from Cellonex (South Africa) and maintained in a complete medium comprised of high glucose Dulbecco's Modified Eagle Medium

(DMEM) supplemented with 10% Fetal bovine serum (BioWest, Celtic, South Africa). The cells were incubated at 37ºC in 5% CO_2 in a humidified atmosphere (Heal Force Incubator, Spellbound, South Africa). Cells were initially cultured in 75 cm^2 culture-treated flasks for adherent cells (Celtic, South Africa) followed by maintenance in 25 cm^2 culture-treated flasks. The medium was changed every 3-4 days, followed by passaging the cells upon reaching 70-80% confluence which was achieved every 5-7 days.

To passage the cells complete medium was aspirated from the flask and the cells were then washed with sterile phosphate buffered saline (PBS) (Celtic, South Africa) at least twice. 1 mL 1X Trypsin was then added to the flask and incubated for 5-10 min at 37ºC. The flask was then observed for detachment of the cells before proceeding with inactivation of the trypsin with 1 mL prewarmed complete medium. The cell suspension was then transferred into a 15 mL tube containing 8 mL complete medium and centrifuged (Sigma 2-6, Lasec, South Africa) at 1300 rpm for 5 min. After centrifugation the supernatant was removed, and the cell pellet was resuspended in 1 mL complete medium. The cells were then counted using trypan blue (BioWest, Celtic South Africa), 50 µL trypan blue was added to an Eppendorf tube and an equivalent volume of the cell suspension was added to the trypan blue. The cell suspension with trypan blue was thoroughly mixed and 10 µL of the mixture was added to a cell counting chamber. The chamber was then inserted into the automated cell counter (Countess II, Thermo-Fischer Scientific, South Africa) which determined the number of cells and the viability of the cells. Cells were maintained at densities of 5×10^5 and 1×10^6 cells in T25 flasks with a total volume of 5 mL.

Cell cultures were selected for treatments based on the confluence and health of the cells. Generally, cells were used at a passage of between 7-9. Cells exhibiting more than ninety percent viability were selected for all experiments before seeding. For experiments requiring a large cell number (RNA extraction and ELISA Assay), the C8-B4 cells were grown and seeded in 10 cm^2 cell culture plates. For each experiment requiring RNA and DNA extractions 1×10^6 cells were seeded in 10 cm^2 plates with a total volume of 10 mL, each treatment plate was prepared in duplicate, and cells were pooled together at the cell harvesting point of the extraction method.

3.1.3 Inducing inflammation and M1 microglial polarization

C8-B4 microglial cells were treated with 100 ng mL^{-1} LPS (Sigma-Aldrich, South Africa), for 24 hours to induce inflammation. A high dose of LPS (100 ng mL^{-1}) was used for this study as it was previously reported to sufficiently provoke inflammatory changes in single cells as compared to a low dose (1 ng mL^{-1}) that often exhibits neuroprotective effects (Mizobuchi *et al*., 2020). The LPS was received as a lyophilized powder that was diluted in sterile PBS to a stock concentration of 1 mg mL^{-1}. A working stock solution of 10 µg mL^{-1} diluted in sterile PBS was then used to make a master mix of 100 ng mL^{-1} LPS treatment in culture media. 96 well microplates were used for cell viability assays with a total volume of 100 µL in each well. The number of wells needed for LPS treatment was determined for the total amount of master mix. The master mix was then prepared in sterile 15 mL tubes and thoroughly mixed to homogenize LPS in the culture media. The media was aspirated 24 hours after seeding and 100 µL of the master mix was then added to each well. The cells were then incubated for 24 hours before Iloprost treatment was introduced.

3.1.4 Iloprost treatment

To investigate the therapeutic effects of Iloprost on LPS-induced inflammatory changes in C8-B4 microglial cells, LPS treated and untreated cells were exposed to three different concentrations of Iloprost at 10,100 and 1000 ng mL^{-1} as shown in Fig. below. Iloprost (Sigma-Aldrich, South Africa) was obtained in lyophilized form and dissolved in 100% dimethyl sulfoxide (DMSO) to a concentration of 1mg mL^{-1}. To test the compound's effect on resting and M1 polarized microglia and its efficacy on LPS-induced inflammation, cells were treated in the presence or absence of LPS and 10, 100, and 1000 ng mL^{-1} Iloprost. A fresh stock concentration of 10 µg mL^{-1} was prepared from the 1 mg mL^{-1} stock in a sterile 2 mL Eppendorf tube on each treatment day. Two control groups were used for this study, these consisted of an untreated control and a vehicle control. The vehicle control consisted of 0.1% DMSO in complete medium as it served as the solvent for Iloprost. All treatments were prepared in fresh complete medium on each treatment day.

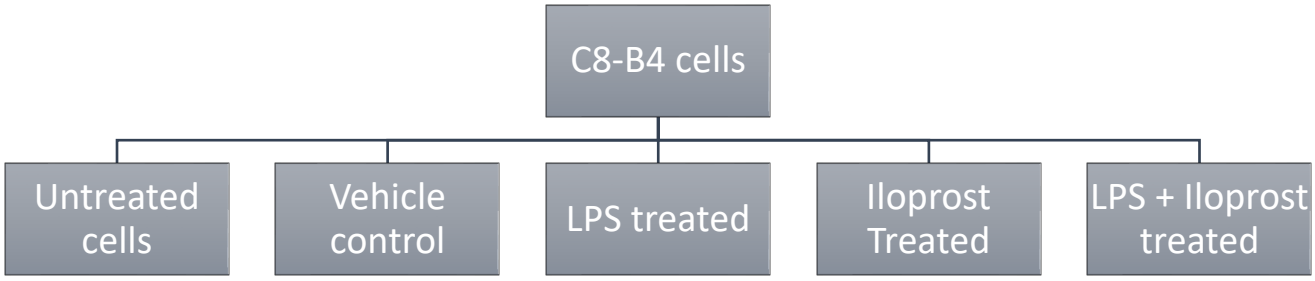

Fig. 10: *Showing cell grouping and treatments.*

3.1.5 Cell viability assay

In this study, the WST-1 assay technique was used to measure cell viability spectrophotometrically. The protocol allows for the analysis of cytotoxic effects and cell proliferation in response to various treatments. The assay makes use of the cleavage of the tetrazolium salt to formazan by cellular mitochondrial dehydrogenase (Fig 11). The amount of formazan dye formed is then directly proportional to the number of viable cells due to the activity of mitochondrial dehydrogenases (Yin *et al*., 2013).

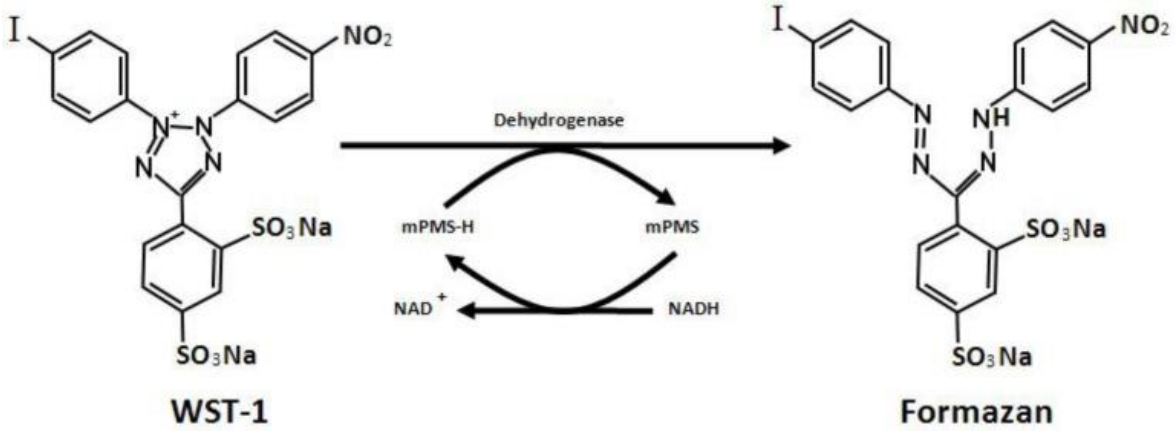

Fig. 11*: Mechanism of WST-1 reduction to formazan product by cellular dehydrogenase. Intermediate electron acceptors include 1-methoxy-5-methyl-phenazium methyl sulphate (mMPMS). Abbreviation: NADH: Nicotinamide adenine dinucleotide (Source: Wang et al., 2012).*

Cells were harvested once 80% confluence was reached. This was achieved by aspirating the culture medium from each flask, the cells were then rinsed thrice with 1 mL sterile PBS, followed by trypsinization and cell counting. Thereafter, the cells were seeded at 1 x 10^4 cells per well in 100 µL complete medium in a 96-well culture-treated plate. The cells were incubated for 24 hr followed by treatments with varying concentrations of Iloprost (10,100 and 1000 ng mL^{-1}), LPS, or LPS + Iloprost. One row of cells received the vehicle alone (DMSO) at a concentration of 0.1% while the negative control group received fresh medium only. The cells were incubated at 37ºC for 24 hours after which 10µL WST-1 reagent (Sigma-Aldrich, USA) was added to each well in the 96-well plate. The plate was incubated for 30 min and shaken for 1 min before the absorbance was measured at 440 nm in a microplate reader on precision reading settings (Multiskan Go, Thermo-Fischer Scientific, South Africa). Thereafter, percentage cell viability was calculated as shown below:

$$\textbf{\% Cell Viability} = \frac{Sample\ (OD) - Blank\ (OD)}{Vehicle\ control\ (OD) - Blank\ (OD)} \times 100$$

3.1.6 Immunofluorescence staining

Immunofluorescence is a technique that enables the detection and localization of various antigens displayed either on the cell surface or intracellularly in both tissues and cells (Im *et al*., 2020). To identify the phenotypic changes of microglia, in response to treatments, all treatment groups were subjected to immunofluorescent staining for cell surface markers with appropriate antibodies; anti-IBA-1, anti-CD86, and anti-CD206 (Table 2). To examine the M1 polarization associated with LPS-induced inflammation, fluorescence intensity was quantified for all treatment groups.

Cells were harvested and seeded in a 96-well plate at a concentration of 1 x 10^4 cells/well in a total volume of 100 µL per well. Following treatment, the cells were rinsed with a pre-warmed culture medium and fixed using absolute methanol for 5 minutes at -20º C. The cells were permeabilized and then fixed with 4% Paraformaldehyde (PF) containing Triton X-100 in Phosphate buffered saline (PBS) for 5 minutes (min) at room temperature (RT). After PF fixation the cells were washed with PBS and incubated in a blocking solution that contained 1% Bovine Serum Albumin (BSA) in PBS with 0.1% Triton X-100 for 1 hr at RT. The blocking solution

reduces any non-specific staining (Buchwalow *et al*., 2011). Where unconjugated primary antibodies were used cells were incubated with the appropriate primary antibody (Table 2 and 3) diluted in blocking solution for 1 hr at 37^{o}C. Where a conjugated primary antibody (CD86-AF488) was used, cultures were incubated with the conjugated primary antibody as prescribed for the primary antibody. Following a wash step with wash buffer containing 1% BSA in PBS, cultures were then incubated with a Alexa Fluor 488-conjugated secondary antibody (where unconjugated primary antibodies were used) for 90 min at RT. The cells were washed with PBS after the 90 min incubation and counterstained with Hoechst33342 (Invitrogen, South Africa) at a final concentration of 0.5 µg mL^{-1} in PBS for 10 min. Hoechst is a non-intercalating dye that is able to stain DNA in fixed cells, the dye specifically binds to adenine-thymine rich regions (Bucevicius *et al*., 2018). Hoechst has an excitation wavelength of 352nm and an emission wavelength of 454nm. An advantage of using Hoechst as a counterstain is that the dye is more membrane permeable than other DNA dyes such as DAPI.

After counterstaining, the cells were again washed with PBS, and 100µL of PBS was added into each well in the 96-well plate before viewing the fluorescence on a Zeiss microscope (Axio Imager.A2, Carl Zeiss, Department of Biochemistry). Image analysis was carried out using Zen Lite software version 3.8.

***Table 2**: Antibody specifications for Immunofluorescence analysis*

Antibody	**Manufacturer**	**Catalogue Number**	**Concentration/ Dilution**
IBA1	Abcam	Ab178846	1µg mL^{-1}
CD206	Novus Biologicals	NBP-1-90020	2µg mL^{-1}
CD86-AF488	Novus Biologicals	NBP-2-34569AF488	2µg mL^{-1}
Goat anti-rabbit IgG AF488	Elabscience	E-AB-1055	1:100

3.1.7 Enzyme-Linked Immunosorbent Assay

An Enzyme-linked Immunosorbent Assay (ELISA) is a method of target molecule detection and quantification using an enzyme reaction with its substrate (Crowther, 1995). An enzyme-labelled antibody specific to the target molecule is employed and enzyme activity is measured colorimetrically (Alhajj and Farhana, 2021). To quantify the levels of pro-inflammatory cytokines IL-1β and TNF-α and neuroprotective cytokine BDNF, in response to treatments, we used ELISA kits (Elabscience, Biocom, South Africa) containing plates that were pre-coated with antibodies specific for each target cytokine.

Cells were seeded in 10 cm^2 culture-treated plates (Celtic, South Africa) at a density of 1 x 10^6 cells per plate and incubated for 24 hours. After exposing the cells to various treatments for 24 hours, culture supernatants were collected and centrifuged at 10,000 x g for 5 min using Prism microcentrifuge (WhiteSci, South Africa) and then stored at -20^{o}C. Once all the biological replicates were collected the ELISA was carried out according to the manufacturer's instructions.

Briefly, 100µL of the standards and samples were pipetted into the appropriate wells. The cytokine in each sample, in this case, IL-1β, TNF-α, or BDNF, was bound by the immobilized antibody. The sample and antibody were then incubated for 90 min at 37^{o}C. Following incubation, 100 µL of biotinylated detection antibody was added and incubated for 1 hr. at 37^{o}C. Three wash steps were carried out to remove any unbound biotinylated antibody followed by the addition of 100µL of Horse-radish peroxidase (HRP)- conjugated working solution to each well and, incubated for 30 min. Thereafter, the plates were then washed five times before 90µL of substrate reagent was added to each well. The plate was sealed and protected from light while incubated for 15 min. 50µL of stop solution was then added to each well and the OD was read at 450nm in a microplate reader on precision reading settings (Multiskan Go, Thermo-Fischer Scientific, South Africa).

3.1.8 Quantitative Reverse Transcriptase Polymerase Chain Reaction (RT-qPCR)

To accurately determine LPS-induced changes in gene expression and the potential roles of Iloprost, the RT-qPCR technique was used to detect and quantify the levels of IL-1β, TNFα, BDNF, CREB, CD206 and ARG-1 mRNA transcripts. RT-qPCR allows for specific, sensitive, and reproducible detection of nucleic acids (Arya *et al*., 2005). It involves the amplification and detection of target cDNA produced from mRNA gene expression, and the amount of a particular nucleic acid or gene sequence is directly proportional to the amount of template before the start of the procedure (Wong and Medrano, 2005).

3.1.8.1 Sample preparation and RNA extraction

For gene expression analysis, C8-B4 cells were harvested from routinely maintained culture flasks when a confluency of 80% was reached. The cells were seeded into 10 cm^2 cultured treated dishes (Corning, USA) at a density of 5 x 10^5 cells. mL^{-1} in 10 mL of complete media. Each treatment was added to a final concentration with the vehicle control plate receiving 0.1% DMSO and the untreated control group receiving fresh complete medium. Each treatment plate was set up in duplicate for 3 separate experiments.

Aurum™ Total RNA-Mini Kit (Biorad, Lasec, South Africa) was used to extract RNA from the samples to ensure high quality yield. Briefly, after treatment, the medium was removed, and the cells were washed twice with 1 mL PBS to remove any dead cells. The cells were harvested using a cell scraper (Biofil, Lasec, South Africa) and transferred into a 15mL centrifuge tube. The cell suspension was then centrifuged (Prism Microcentrifuge, WhiteSci, South Africa) at maximum speed (21 000 x g) for 5 min and the supernatant was decanted. Thereafter, 350 µL lysis buffer supplemented with 1% β-mercaptoethanol was then added to each tube. The content of the tube was then mixed approximately 30 times by pipetting the solution up and down in the centrifuge tube. Once the cells were lysed, an equivalent volume of 70% ethanol was added and mixed as previously described. This mixture was transferred to an RNA binding column in a microcentrifuge tube and centrifuged (Prism Microcentrifuge,

WhiteSci, South Africa) for 30 sec at maximum speed. Once centrifugation was completed, the filtrate was discarded and 700 µL low-stringency wash buffer was added to the column. The column was centrifuged as previously described with the filtrate being discarded before adding 80 µL DNAse I followed by incubating the column for 15 min at RT. 700 µL high-stringency wash solution was added to the column and centrifuged for 30 sec. Following the centrifugation, the filtrate was discarded, and an equivalent volume of low-stringency buffer was added. The column was centrifuged as before for an additional 2 min before being transferred to a capped microcentrifuge tube. 30 µL elution buffer preheated at 70^{o}C was added to the membrane and subsequently incubated in the column for 1 min, after which the RNA was eluted from the column through centrifugation at a maximum speed for 2 min.

The purity and yield of the extracted RNA was determined photometrically using a µDrop plate (Thermo Fischer Scientific, South Africa). The µDrop plate was sterilized by wiping down its base with 70% ethanol and RNase Zap solution (Ambion) before adding 2 µL each of the RNA sample onto the 2 x 8 matric channels on the microplate. RNA was selected based on purity assessed by the µDrop and was considered pure if the absorbance ratio at 260/280nm was between 1.9 and 2.0 (Wilfinger *et al*., 2018). The second parameter for purity was the absorbance at 260/230 nm which was considered pure if the ratio was in the range of 2.0-2.2 (Wilfinger *et al*., 2018). To determine the concentration of RNA in the sample the Beer-Lambert law was used with the absorbance at 260 nm.

$$A = \varepsilon C I$$

Where A = absorbance at 260nm, C = concentration, Ɛ = extinction coefficient of RNA (0.25) and I = the pathlength of the µDrop (0.05). The equation was rearranged to yield the concentration in µg.mL^{-1} which was simplified to ng µL^{-1}.

$$C = \frac{A260nm}{(0.25\ x\ 0.05\ cm)}$$

$$= \mu g\ mL^{-1} / 1000$$

$$= ng\ \mu L^{-1}$$

The extracted RNA was stored at -80^{o}C until cDNA synthesis was carried out.

3.1.8.2 Complementary DNA (cDNA) synthesis

Total RNA was reverse transcribed using iScript™ cDNA synthesis kit (Biorad Laboratory (Pty) Ltd, USA) according to the manufacturer's protocol.

Briefly, to synthesize 1µg cDNA, 1µg RNA was added to an Eppendorf tube containing 4 µL 5x iScript Reaction Mix, 1 µL iScript Reverse Transcriptase, and topped up to 20 µL with nuclease-free water. Each reaction mixture was then incubated in a thermal cycler (Inqaba Biotech, South Africa) for 5 min at 25^{o}C to prime the sample. After priming the mixture was then further incubated for 20 min at 46^{o}C where the reverse transcriptase (RT) is enzymatically active. To inactivate the RT the samples were incubated for 1 min at 95^{o}C and stored at -20^{o}C until PCR analysis was carried out.

3.1.8.3 Primer Selection and Validation

As shown in tables 4 and 5, the specific oligonucleotide sequence for the target genes were extracted from relevant literature and validated using the Primer-Basic Local Alignment Search Tool (BLAST) program from the National Library of Medicine database. This software screens for the target specificity of the primer pair and potential alternative primers and targets (Ye *et al*., 2012). After validation, the biological sequences were sent to Inqaba Biotech (South Africa) for synthesizing primers that are specific to the PCR template. The synthesized primers were centrifuged before use and reconstituted in molecular-grade nuclease-free water (BioConcept, Inqaba Biotec, South Africa) to prepare a 100 µM stock solution. The primers were diluted before each PCR run to a concentration of 10 µM for both forward and reverse primers with Nuclease free water, for use at a final concentration of 250 nM of each primer in the PCR reaction.

Table 3 *: Reference gene primer pairs selected and validated using Primer-BLAST*

HOUSEKEEPING GENES	ACCESSION NUMBER	PRIMER	PRIMER SEQUENCE	LENGTH	ANNEALING TEMP	GC%	Reference paper
ACTIN	NM_001313923.1	*Forward*	ATCTGGCACCACACCTTCTACAATGAGCTGCG	32	66^{o}C	53	Sundby *et al*., 2022
		Reverse	CGTCATACTCCTGCTTGCTGATCCACATCTGC	32		53	
GAPDH	NM_001411843.1	*Forward*	GTGGCAAAGTGGAGATTGTTG	21	60^{o}C	47	Argarwal *et al*., 2020
		Reverse	ACCAGTAGACTCCACGACATA	21		47	

***Table 4**: Target gene primer pairs selected and validated using Primer-BLAST*

TARGET GENES	ACCESSION NUMBER	PRIMER	PRIMER SEQUENCE	LENGTH	ANNEALING TEMP	GC%	Reference paper
TNFα	NM_013693.3	*Forward*	GCCTCTTCTCATTCCTGCTTGTGGCAG	27	60^{o}C	55	Horiuchi *et al*., 2010
		Reverse	GACGTGGGCTACAGGCTTGTCACTCG	26		61	
IL-1β	NM_008361.4	*Forward*	CCTGTCCTGTGTAATGAAAGACGG	24	60^{o}C	50	
		Reverse	TGTCCTGACCACTGTTGTTTCCC	23		52	Minns *et al*., 2023
BDNF	NM_001316310.1	*Forward*	TGCCGCAAACATGTCTATGACG	22	60^{o}C	50	
		Reverse	GCTGTGACCCACTCGCTAATAC	22		54	Aid *et al*., 2007
CREB	NM_009952.2	*Forward*	ACCAGCAGAGTGGAGATGCT	20		55	
		Reverse	ATGGCAATGTACTGCCCACT	20		50	Barton *et al*., 1992
CD206	NM_008625.2	*Forward*	CCACTCTATCCACCTTCACTGATG	24	60^{o}C	50	
		Reverse	CCTGCTCGTCCACAGTCCACCG	22		68	Siret *et al*., 2022
ARG-1	NM_007482.3	*Forward*	GCAGCAGCCGCTGGAACCCAG	21	60^{o}C	71	
		Reverse	GTCCCCGTGGTCTCTCACGTC	21		66	Louis *et al*., 1999

3.1.8.4 Quantification of mRNA using RT-qPCR

After 24 hr cell exposure to LPS and Iloprost treatments, changes in the mRNA expression of pro and anti-inflammatory genes were determined by qPCR. Gene expression was calculated as a fold change using $2^{-\Delta\Delta Ct}$ method (Schmittgen and Livak, 2008) in LPS treated, Iloprost treated, or combined treatments with both LPS and Iloprost, relative to untreated control cells, after normalizing with one reference gene.

All samples were prepared with filtered tips, sterile PCR tubes and solutions made using nuclease-free water (Inqaba Biotec, South Africa). PCR amplification was performed on QuantStudio 3 Applied Biosystems (ThermoFischer Scientific, South Africa) using 20 µL total reaction volume that consisted of 10 µL iTaq Universal SYBR Green Supermix (Lasec, South Africa), 0.5 µL each of forward and reverse primer (Tables 4 and 5), 8 µL nuclease-free water, and 1 µL cDNA template. For the No template control (NTC) molecular grade water was used instead of cDNA template.

The following PCR cycling conditions were used; an initial denaturation at 95^{o}C for 2 min. This was followed by denaturation at 95^{o}C for 15 sec, annealing at 60^{o}C for 60 sec and extension at 72^{o}C for 60 sec for 40 cycles. All samples were assayed in duplicates and in each run, water blanks were included as negative controls. The PCR was analysed using the comparative Cq method, as previously described, to determine fold changes with each treatment (Schmittgen and Livak, 2008). To normalize the data, the housekeeping gene GAPDH was used. All primers were also validated using the Primer-BLAST software available from the National Library of Medicine Database

3.1.9 Gel electrophoresis of PCR products

To confirm whether the PCR reaction yielded a single product, gel electrophoresis was carried out on each treatment sample for the housekeeping gene GAPDH and ARG-1 target gene. 0.5 g agarose powder was added to a conical flask and 50 mL TAE buffer was added to the powder. The agarose was then dissolved by heating the flask in a microwave for approximately 3 min and swirling the flask every 30 sec. The gel was then cooled before adding 2.5 µL PRONASAFE Nucleic acid Staining solution

(Condalab). The flask was gently mixed and poured into a gel mold before inserting the comb. The gel was then left to set, and the samples were prepared by adding 4 µL PCR reaction mix to 2 µL loading dye (Biolabs) in an Eppendorf tube. A DNA ladder was prepared by adding 2 µL Kappa Universal DNA ladder to 4 µL loading dye (Biolabs). The loading dye containing the sample was then gently mixed and given a quick centrifugation for 15 sec (Palm Mini centrifuge, DOT labs). The samples were loaded into the wells of the gel placed in the chamber of the electrode assembling (Lasec, South Africa) and the gel was run for approximately 25 minutes at 100 volts.

3.1.10 DNA methylation protocol

3.1.9.1 DNA extraction

ZR Quick-DNA MiniPrep Plus Kit (Inqaba Biotec, South Africa) was used to extract DNA from the cells according to the manufacturer's protocol. After exposing the microglial cells to various treatments for 24 hr, the medium was removed, and the cells were washed twice with 1 mL PBS to remove any dead cells. The cells were harvested using a cell scraper (Biofil, Lasec, South Africa) with PBS (BioWest, Celtic, South Africa). 200 µL of the cell suspension was added to a microcentrifuge tube and an equal volume of BioFluid and Cell Buffer (supplied by the kit) was added to the cell suspension. 20 µL Proteinase K was then added to the tube containing the harvested cells and buffer mixture and vortexed for 10-15 sec, followed by a 10 min incubation at 55^{o}C. After cell lysis and Proteinase K digestion 420 µL Genomic Binding Buffer was added to the microcentrifuge tube and the sample was vortexed again for 10-15 sec. The mixture was then transferred to a Zymo-Spin^{TM} IIC-XLR Column and the column was placed in a collection tube supplied by the kit. The column with the collection tube was centrifuged at 12,000 x g for 1 min and the flow through was discarded. The spin column was then placed in a new collection tube and 400 µL DNA Pre-wash Buffer was added before an additional centrifugation at 12,000 x g for 1 min. After centrifugation the collection tube was emptied and 700 µL g-DNA Wash Buffer was added to the spin column, this was followed by an additional centrifugation as previously described. A further wash step was carried out using 200 µL g-DNA Wash Buffer before the spin column was transferred into a clean microcentrifuge tube for DNA elution. DNA elution was carried out by applying 50 µL DNA Elution Buffer directly onto the matrix of the column and incubating the column for 5 min at room temperature.

After the incubation period the column was centrifuged using Prism microcentrifuge (WhiteSci, South Africa) at maximum speed (21 000 x g) for 1 min to elute the DNA. An additional centrifugation step was carried out in a new microcentrifuge tube to ensure maximum elution of the extracted DNA. The purity and yield of the extracted DNA was spectrophotometrically determined using a µDrop plate (Thermo Fischer Scientific, South Africa) as previously described. DNA was considered pure if the absorbance ratio at 260/280 nm was 1.8 (Lucena *et al*., 2016). The second parameter for purity was the absorbance at 260/230 nm which was considered pure if the ratio was greater than 1.5 (Lucena *et al*., 2016). The extracted DNA was stored at -20^{o}C overnight until bisulfite conversion was carried out.

3.1.9.2 Gel electrophoresis of DNA extracts

Gel electrophoresis allows for the separation of molecules based on size with smaller molecules travelling more rapidly than larger molecules. The gel was prepared according to the protocol stipulated in section 3.1.9.1. The gel was then left to set, and the samples were prepared by adding 4 µL extracted DNA to 2 µL loading dye (Biolabs) in an Eppendorf tube. A DNA ladder was prepared by adding 2 µL Kappa Universal DNA ladder to 4 µL loading dye (Biolabs). The loading dye containing the sample was then gently mixed and given a quick centrifuge for 15 sec. 1 X TAE buffer was used as the running buffer. The samples were loaded into the wells of the gel and the gel was run for approximately 25 minutes at 100 volts in MS MiniDuo (Lasec, South Africa). Once the run was completed, the gel was viewed on a microDOC and WiseUV (Lasec, South Africa) to visualize DNA bands.

3.1.9.3 Bisulfite conversion

DNA extracts were treated and processed for Bisulfite conversion using the EZ DNA Methylation Kit (Zymo Research, USA) following the manufacturer's instructions. With this protocol, unmethylated cytosines in DNA samples are converted into uracil residues and recognized as thymine in the proceeding PCR reaction, while 5-methylcytosine remains unchanged (Li and Tollefsbol, 2011).

All reagents used for this protocol were prepared before removing the DNA samples from -20^{o}C storage. A volume of DNA extracted at a starting concentration of 500 ng

was used for the bisulfite treatment and CT conversion because larger starting quantities might lead to incomplete CT conversion that would affect downstream applications. The volume of DNA was first added to a microcentrifuge tube and 5 µL of M-Dilution Buffer was then added to the sample and the volume was adjusted to 50 µL with molecular grade water (Celtic, South Africa). The sample containing buffer and water was incubated at 37^{o}C for 15 min before adding 100 µL CT Conversion Reagent into each tube. The samples were then incubated in the dark at 50^{o}C for 12 hr followed by another incubation at 4^{o}C for 10 min. A Zymo-Spin^{TM} IC Column for each treatment group was placed into a collection tube and a volume of 400 µL M-Binding Buffer was loaded into the spin column. After this, the sample containing CT reagent was applied to the spin column and inverted several times after sealing the cap of the column. The collection tube containing the spin column was centrifuged at a maximum (21 000 x g) speed for 30 sec and the flow through was discarded. A wash step was then carried out using 100 µL M-Wash Buffer and centrifugation was carried out as previously described (21 000 x g). Thereafter, 200 µL M-Desulphonation Buffer was applied to the column and an incubation step was carried out at room temperature for 15 min. The column was then centrifuged for 30 sec followed by two additional wash steps with equal volumes of M-Wash Buffer. Lastly, the column was placed in a clean microcentrifuge tube and 10 µL M-Elution Buffer was added directly to the matrix. The tube containing the column was then centrifuged at maximum speed for 30 sec to elute the DNA. The converted DNA was stored at -80^{o}C until PCR analysis was performed.

3.1.9.4 Evaluation of DNA methylation status by qPCR

The DNA methylation status of BDNF and CREB genes in treated and untreated microglial cells were determined by qPCR. Gene expression was calculated as a fold change in LPS treated, Iloprost treated, or a combination treatment of both LPS and Iloprost, relative to untreated and 0.1% DMSO control C8-B4 microglial cells, after normalization with one reference gene. Primers used to detect the specific promoter regions of the target genes or reference genes in the methylated DNA samples have been listed in tables 4 and 5. As previously described, the PCR amplification was also performed on QuantStudio 3 Applied Biosystems (ThermoFischer Scientific. South Africa) with a total reaction volume of 20 µL. Each PCR reaction mix was analyzed in

duplicate and consisted of 10µL iTaq Universal SYBR Green Supermix (Lasec, South Africa), 0.5µL each of a 10 µM stock of forward and reverse primers, 7 µL nuclease-free water, and 2 µL methylated DNA template.

PCR cycling conditions were as follows: 30 sec polymerase activation at 95^{o}C followed by 40 cycles at 95^{o}C for 15 sec, and 60^{o}C for 60 sec. To analyze the data, the Cq values of treated and untreated samples were compared and normalized to GAPDH, while fold changes were comparatively calculated using $2^{-\Delta\Delta Cq}$ as previously described (Schmittgen and Livak, 2008).

3.1.9.5 Gel electrophoresis of PCR products

To confirm if the PCR reaction yielded a single product, gel electrophoresis was carried out on each treatment sample for the housekeeping gene GAPDH and BDNF target gene. 0.5 g agarose powder was added to a conical flask and 50 mL TAE buffer was added to the powder. The agarose was then dissolved by heating the flask in a microwave for approximately 3 min and swirling the flask every 30 sec. The gel was then cooled before adding 2.5 µL PRONASAFE Nucleic acid Staining solution (Condalab). The flask contents were gently mixed and poured into a gel mold before inserting the comb. The gel was then left to set, and the samples were prepared by adding 4 µL PCR reaction mix to 2 µL loading dye (Biolabs) in an Eppendorf tube. A DNA ladder was prepared by adding 2 µL Kappa Universal DNA ladder to 4 µL loading dye (Biolabs). The loading dye containing the sample was then gently mixed and given a quick centrifuge for 15 sec. 1 X TAE buffer was used as the running buffer and poured over the set gel. The samples were loaded into the wells of the gel and the gel was run for approximately 25 minutes at 100 volts MS MiniDuo (Lasec, South Africa). Once the run was completed, the gel was viewed on a microDOC and WiseUV (Lasec, South Africa) to visualize PCR product bands.

3.2 Phase II (*in vivo* study)

In this part of the study, a rodent model of trypanosomiasis was used to investigate the neuroprotective roles of Iloprost against trypanosome-induced inflammatory changes in the brain (Fig. 12). This is part of a collaborative study involving research colleagues situated at the Nigerian Institute for Trypanosomiasis Research (NITR) and

the National Veterinary Research Institute (NVRI), Vom, Nigeria. All animal-based work and data collection were performed by our collaborators at these institutes, whereas data analysis and interpretation were conducted by the research student at Nelson Mandela University.

3.2.1 Animals and treatments

All animal procedures complied with Animal Research Reporting of In Vivo Experiments (ARRIVE) guidelines and were approved by the Animal Ethics Committee at NVRI (*Ethical Clearance*, *AEC/02/102/21*) in Nigeria and Research Ethics Committee (Animal) (*Ethical Clearance, A20-SCI-PHY-001*) of Nelson Mandela University in South Africa, in accordance with National Institute of Health guidelines for the care and use of laboratory animals.

A total of twenty-four Albino Swiss male mice (8-10 weeks old) were used for this study. The animals were obtained and housed within the research animal facility of NITR (Vom, Nigeria). The animals had unrestricted access to food and water *ad libitum*. They were maintained in temperature (21-23^{o}C) and light controlled (lights on from 06h00 to 18h00) rooms throughout the experiment. After one week acclimatization the mice were randomly selected and divided into four groups (n=6 per group), of which one group received phosphate-buffered saline (PBS) and served as non-infected control, whereas the remaining three groups were infected with *T.b brucei* at the start of the experiment (Fig.12).

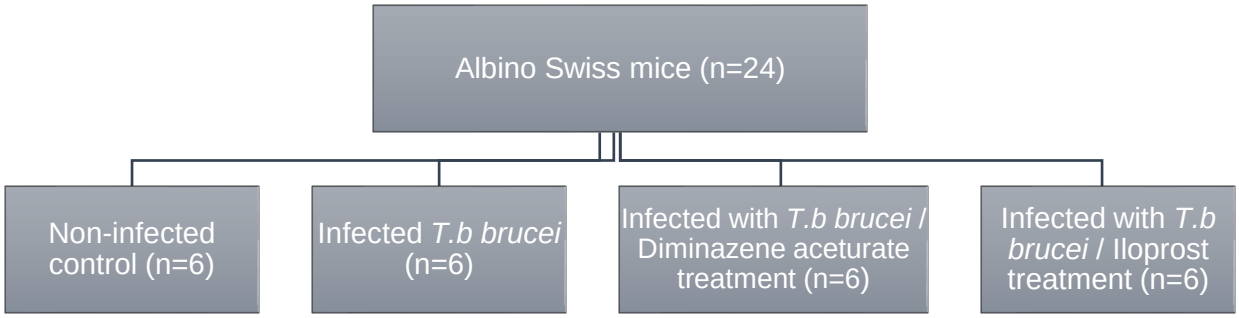

***Fig. 12**: Diagram showing treatment groups and sample size.*

As shown in Fig.13, the infected mice received subcutaneous injections of 5000 inoculum of *T.b brucei* parasite in 0.2 mL of saline. On day 4, one of the infected groups of mice received a single dose of intraperitoneal injection (i.p) of 4 mg kg^{-1} Diminazene aceturate (Kepro, Holland) and another group i.p injections of 200 µg kg^{-1} Iloprost (Celtic, South Africa) daily for four days. Previous study protocols have shown that a single dose of Diminazene aceturate is effective in treating *T.b* infection in rodent models due to the drugs long-acting effect (Eckersall *et al*., 2000, Ezeh *et al*., 2016,). However, due to the short half-life of Iloprost its anti-inflammatory effects are better observed with multiple doses (Uchiyama-Tsuyuki *et al*., 1995).

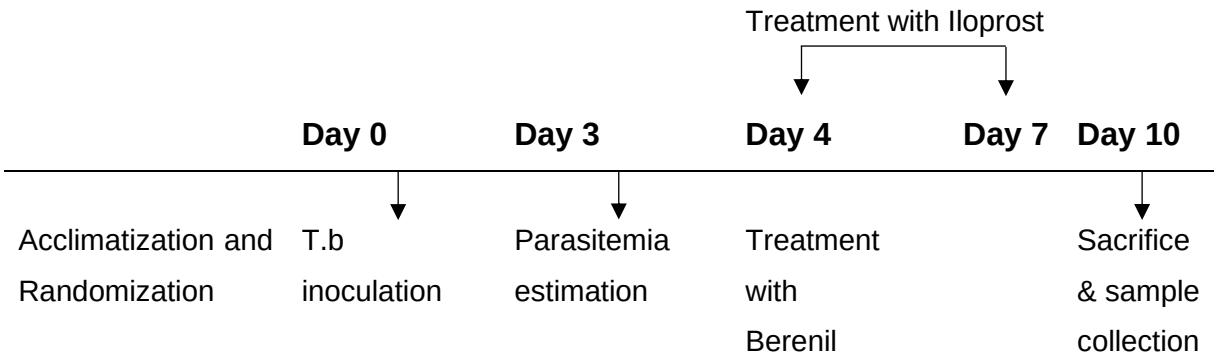

Fig. 13*:The experimental timeline of mice infected with T.b and treated with a single dose of Berenil or repeated doses of Iloprost.*

3.2.2 Visualization of parasitemia in blood and parasite estimation

On day 3 of the experiment, parasitemia load was determined by observing blood samples of infected mice via microscopic examination of a blood smear. Blood samples were collected from the tail vein of mice in all treatment groups and a drop of blood was placed and spread on a slide. The film of blood was dried, and the slide was mounted with a coverslip. Visualization of the parasite was carried out using the 40x objective of the microscope (Nikon, Labophot, Japan).

3.2.3 Euthanasia, Tissue Extraction and Sample Preparation

On day 10 of the experiment, the animals were euthanized using 5% isoflurane in a closed chamber followed by cervical dislocation. The mouse brains were removed

using bone forceps while the hippocampi were dissected out on ice and placed in labelled Eppendorf tubes, snap frozen in liquid nitrogen and stored at -80^{o}C until needed.

3.2.4 Quantitative Reverse Transcriptase Polymerase Chain Reaction (qPCR)

To determine the effect of Iloprost treatment on neuroinflammation induced by trypanosome infection, the expression of pro-inflammatory cytokines, TNF-α and IL1-β along with neuroprotective cytokines BDNF and CREB was assessed by qPCR. qPCR analysis was carried out on hippocampal extracts from each treatment group (n=6) obtained from mice 10 days post *T.b brucei* infection and subsequent treatment.

3.2.5 RNA extraction from hippocampal tissue

Total RNA was isolated from the hippocampal tissue samples the Norgen Biotek Total RNA purification Micro Kit (Lasec, South Africa) and performed according to the manufacturer's protocol. To prepare the lysate, the hippocampal tissue was transferred to a mortar containing liquid nitrogen. The tissue was then ground thoroughly using a pestle after which the liquid nitrogen was allowed to evaporate without thawing the tissue. 300 µL Buffer RL (supplied by kit) was added to the hippocampal tissue which was further ground until the sample was homogenized. The lysate was then transferred to an RNase-free microcentrifuge tube and 20 µL reconstituted Proteinase K (Zymo Research, Inqaba Biotec, South Africa) was added to the tube. The lysate containing Proteinase K was incubated at 55^{o}C for 15 min and vortexed occasionally during the incubation. The lysate was then centrifuged (Eppendorf 5425R, NITR) at 14,000 x g for 2 min to pellet any cell debris. The supernatant was transferred to a new microcentrifuge tube and 450 µL 100% ethanol was added to the lysate and vortexed to mix.

A micro spin-column was assembled in a collection tube provided by the kit, and 600 µL of the lysate containing ethanol was applied onto the column and centrifuged for 1 min at 3,500 x g. Where the entire lysate failed to pass through the column, an additional centrifugation step was carried out at 14,000 x g for 1 min. The flowthrough was discarded, and the spin column was reassembled with its collection tube. 400 µL Wash Solution A was then added to the column and the column was centrifuged at

14,000 x g for 1 min. After centrifugation, the flowthrough was discarded, and the wash step was carried out a second and third time. After three wash steps, the column was centrifuged at 14,000 x g for 2 min to dry the resin and the collection tube was discarded.

The spin column was added into a fresh 1.7 mL elution tube also provided by the kit. To elute the RNA the Elution Solution A was pre-heated to 70^{o}C before addition to the spin column. Initially, 20 µL of the pre-heated Elution Solution A was added to the spin column, and the spin column was incubated for 1 min followed by gently vortexing the column. To elute the RNA, the column was centrifuged for 2 min at 200 x g followed by an additional centrifugation for 1 min at 14,000 x g. To maximize the RNA eluted from the column a second elution was performed with 20 µL Elution Solution A. The RNA extracts were stored at -80^{o}C.

The yield and purity of the extracted RNA was spectrophotometrically determined using Nanodrop One (Thermo Fischer Scientific, USA) at the African Centre of Excellence in Phytomedicine Research. Briefly, 1 µL of the RNA sample was applied onto the Nanodrop pedestal, and the concentration and purity were determined with absorbance readings at 230, 260 and 280 nm. RNA was considered pure if the ratio of the absorbance at 260/280nm was between 1.9 and 2 (Wilfinger et al., 2018). A secondary purity reading was considered at 260/230nm with pure RNA having a value between 2 and 2.2 (Wilfinger et al., 2018).

3.2.6 cDNA Synthesis

Total RNA was reverse transcribed to cDNA using iScript^{TM} cDNA synthesis kit (Bio-Rad Laboratory (Pty) Ltd. USA) according to the manufacturer's instructions. To synthesize 1 µg cDNA, 1 µg RNA was added to an Eppendorf tube with 4 µL 5x iScript Reaction Mix, 1µL iScript Reverse Transcriptase, and topped up to 20 µL with nuclease-free water. Each reaction mixture was then incubated in a thermal cycler (GeneAmp PCR system 9700, USA) for 5 min at 25^{o}C to prime the sample. After priming the mixture was then further incubated for 20 min at 46^{o}C where the reverse transcriptase is enzymatically active. To inactivate the reverse transcriptase the samples were incubated for 1 min at 95^{o}C and stored at -20^{o}C until PCR analysis was carried out.

***Table 5**: Reference gene primer pairs selected and validated using Primer-BLAST*

HOUSEKEEPING GENES	ACCESSION NUMBER	PRIMER	PRIMER SEQUENCE	LENGTH	ANNEALING TEMP	GC%	Reference papers
GAPDH	NM_001411843.1	*Forward*	GTGGCAAAGTGGAGATTGTTG	21	60ºC	47	Argarwal *et al*., 2020
		Reverse	ACCAGTAGACTCCACGACATA	21		47	

***Table 6**:Target gene primer pairs selected and validated using Primer-BLAST*

TARGET GENES	ACCESSION NUMBER	PRIMER	PRIMER SEQUENCE	LENGTH	ANNEALING TEMP	GC%	Reference papers
TNFα	NM_001278601.1	*Forward*	GCCTCTTCTCATTCCTGCTTG	21	60ºC	52	Horiuchi *et al*., 2010
		Reverse	CTGATGAGAGGGAGGCCATT	20		55	
IL-1β	NM_008361.4	*Forward*	CCTTCCAGGATGAGGACATGA	21	60ºC	52	Minns *et al*., 2023
		Reverse	TGAGTCACAGAGGATGGGCTC	21		57	
BDNF	NM_001316310.1	*Forward*	TCACAGCGGCAGATAAAAAG	20	60ºC	50	Aid *et a*l., 2007
		Reverse	TCAGTTGGCCTTTGGATACC	20		45	

CREB	NM_009952.2	*Forward* *Reverse*	ACCAGCAGAGTGGAGATGCT ATGGCAATGTACTGCCCACT	20 20	60ºC	55 50	Barton *et al*., 1992

3.2.6 RT- qPCR

The gene expression of both pro and anti-inflammatory cytokines was determined by quantification in all treatment groups 10 days post *T.b brucei* inoculation and subsequent treatment with Diminazene aceturate or Iloprost relative to the saline control after normalization with one reference gene.

PCR amplification was performed on CFX-96 Real-Time PCR Detection system (Bio-Rad, USA) using a total of 20 µL reaction volume that consisted of 10 µL iTaq Universal SYBR Green Supermix (Lasec, South Africa), 1 µL of each corresponding primer (table 5 and 6), 7 µL nuclease-free water, and 1 µL cDNA. Prepared samples were subjected to the following PCR conditions; an initial denaturation at 95^{o}C for 2 min. This was followed by denaturation at 95^{o}C for 15 sec, annealing at 60^{o}C for 60 sec and extension at 72^{o}C for 60 sec for 40 cycles. To normalize the data, the housekeeping gene GAPDH was used. Each PCR run for the genes of interest was run with the housekeeping gene and fold changes calculated using the comparative Cq method, $2^{-\Delta\Delta Cq}$, as previously described (Schmittgen and Livak, 2008). All primers were also validated using the Primer-BLAST software available from the National Library of Medicine Database

3.3 Data Processing and Statistical Analysis

Statistical analysis was carried out using GraphPad prism 9.0 software (USA) and the data were reported as mean ± standard error of mean. For experiments including cells, a minimum of three independent experiments were carried out with each treatment condition conducted in triplicate (n=3). For the experiment including animals, a sample size of 24 was used with n=6 for each treatment group. The data was checked for normality using the Shapiro-Wilk normality test before it was analysed using either a one-way ANOVA or mixed ANOVA where applicable, followed by Bonferroni's post hoc test with the criteria for significance set at $p \leq 0.05$.

CHAPTER FOUR

RESULTS

4.1 Effects of LPS and Iloprost treatments on cell viability

Before investigating any new treatment, it is important to determine whether the investigative compound has a toxic effect on the cell line and if the concentrations to be tested have any effect on the viability of the cells. Any agent acting on the cells could impact their metabolism and health to varying degrees.

After 24 hours of exposure to LPS and varying concentrations of Iloprost a WST-1 assay was carried out to determine the percentage of viable cells in each treatment group. Exposure to 100 ng mL^{-1} of LPS alone significantly reduced ($p<0,0001$) the percentage of viable cells compared to both untreated and DMSO control groups ($p<0,0001$, Fig 14). It was further observed that subsequent treatment of LPS-exposed cells with high doses of Iloprost (100 and 1000 ng mL^{-1}) significantly improved cell viability when compared to groups exposed to only LPS ($p<0,0001$), and in a manner that was comparable to percentage viability in the control groups (Fig.14). Whereas LPS-exposed cells treated with 10 ng mL^{-1} Iloprost exhibited significant decrease in percentage viability compared to untreated and DMSO controls and cultures treated with higher doses of Iloprost ($p<0,0001$, Fig.14). These results suggest that treatment with higher concentrations of Iloprost may be more effective at improving cell viability and thus protect the cells against the cytotoxic effects of LPS.

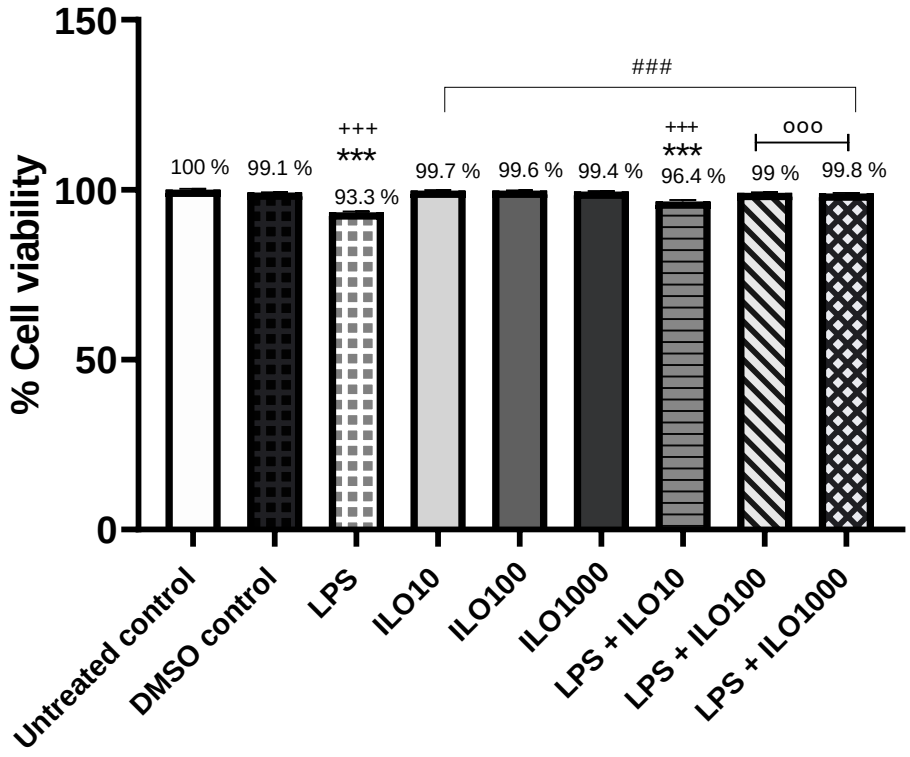

Fig. 14*: The effect of LPS and Iloprost on C8-B4 microglial cell viability 24-hours post treatment. Data are represented as the mean ± SEM from three independent experiments. Statistical significance was determined using One-Way ANOVA with Bonferroni's post hoc test.* $F_{(8,26)} = 84.90$; $^{***}p<0,0001$ *compared to untreated control.* $^{+++}p \leq 0.0001$ *compared to DMSO control.* $^{\#\#\#}p \leq 0.0001$ *compared to LPS treated.* $^{ooo}p \leq 0.0001$ *compared to LPS + 10 ng.mL*$^{-1}$ *Iloprost.*

4.2 Confirmation of M1 polarization in microglia exposed to LPS.

To trigger inflammation an immunogenic stimulus is required. Also, it has been established that pro inflammatory cytokines need to be present in high concentrations for microglia to become classically activated (Cherry *et al*., 2014). A previous study demonstrated that 100 ng mL^{-1} LPS caused M1 polarization in C8-B4 cells (Mizobuchi *et al*.,2020). To confirm whether LPS treatment with 100 ng mL^{-1} E. coli derived endotoxin successfully caused polarization of microglial cells to M1 conformation or inflammatory state, C8-B4 cells were incubated with 100 ng mL^{-1} of LPS for 24 hours followed by fixation labelling with anti-IBA1 and anti-CD86.

As shown in fig.15 A-C, cell exposure to 100 ng. mL^{-1} of LPS for approximately 24 hours provoked microglial activation as evidenced by an observed increase in the IBA-

1^+ cell population. Morphologically, microglia appear amoeboid in structure and exhibit either mono or bipolar processes. In general, IBA-1 expression is increased in activated microglia and thus serves as a preliminary marker for the confirmation of microglial activation in response to inflammatory changes, meanwhile this is not enough to distinguish between proinflammatory M1 and anti-inflammatory M2 phenotypes (Shi *et al*., 2021).

To further confirm M1 polarization, the expression of CD86 antigen in the cells was used as a second marker that is specific to M1 microglia. CD86 forms part of the membrane proteins displayed during microglial M1 activation (Jurga *et al*., 2020). It functions as a membrane co-stimulatory receptor, stimulating cytokine production that will mobilize immune cells to the inflammatory site (Jurga *et al*., 2020). Our results show that CD86 fluorescence was increased 24 hours post LPS treatment (Fig 15 D-F), which confirms that LPS challenge certainly induced M1 polarization in the exposed microglia cells.

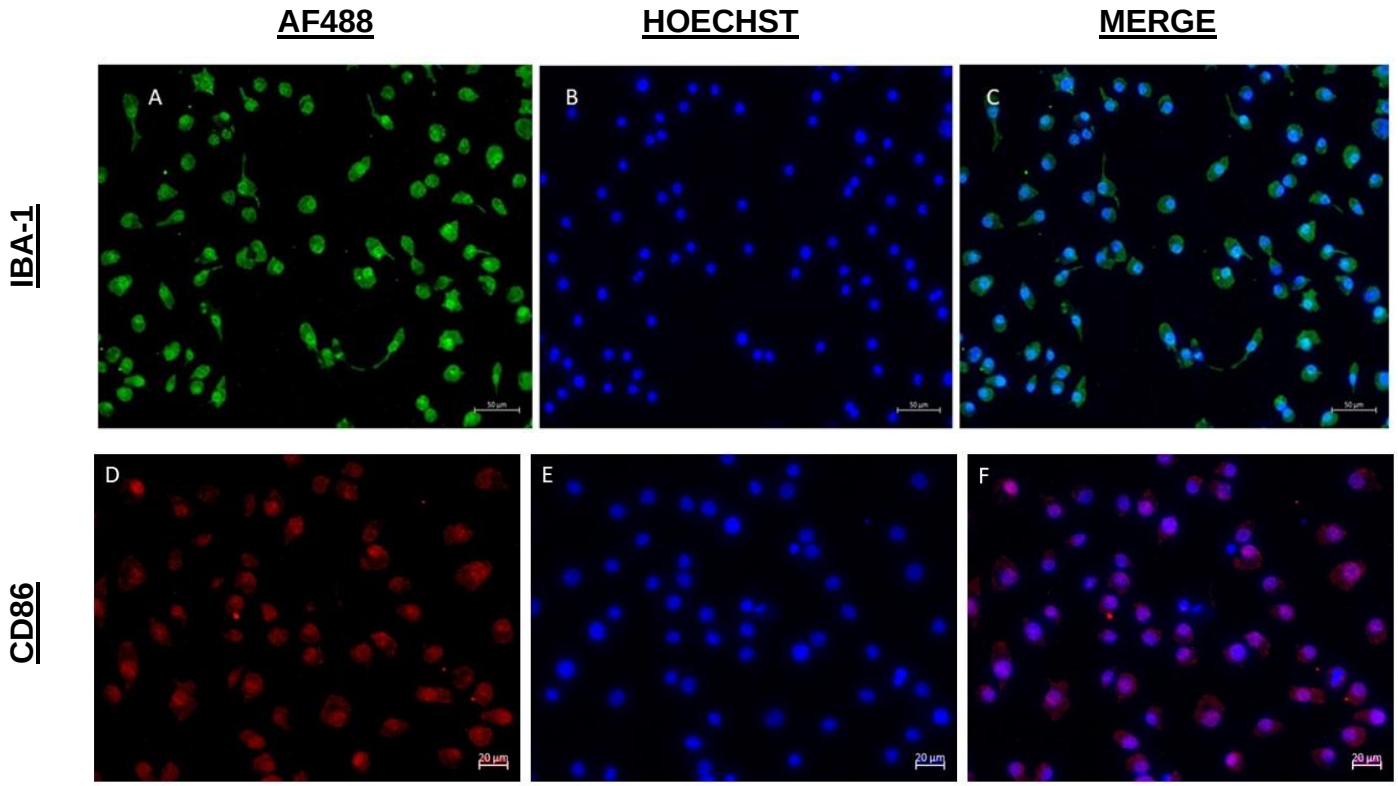

Fig. 15: *IBA-1 localisation in C8-B4 microglial cells treated with 100 ng mL^{-1} LPS for 24 hrs (**A**). Hoechst staining of nuclear material (**B**) and (**C**) showing merged image obtained using Zeiss fluorescent microscope Axio-A2. Cells were fixed 24 hours post treatment. Scale bar = 50µm. CD86 cell surface marker for M1 polarisation of microglia*

*(**D**) treated with 100 ng mL^{-1} LPS and fixed 24hrs post treatment. (**E**) Counterstaining nuclear material with Hoechst dye, (**C**) showing merged image obtained using Zeiss fluorescent microscope Axio. A2 and image analysis carried out using Zen Lite software V3.8. Scale bar = 20 µm.*

4.3 Effect of Iloprost on cell surface markers

Microglial markers provide information about the overall pattern or functional state in a microglial population. To determine whether Iloprost treatment would provoke phenotypic switch from M1 to M2 and protect against LPS induced inflammation, resting (M0) and M1 polarized microglial cells were incubated with varying doses of Iloprost (10,100 and 1000 ng mL^{-1}). Thereafter, cells were fixed and labelled with anti-IBA1, anti-CD86 and anti-CD206.

4.3.1 Effect of Iloprost treatment on IBA-1 expression in resting and M1 polarized C8-B4 microglial cells.

To determine if Iloprost induces microglial activation in resting cells and further activation LPS treated cells, IBA-1 expression was determined with the use of fluorescent microscopy. From the results below LPS treatment alone served as positive control for microglial activation (Fig.16 C). The degree of activation following LPS treatment was compared and at a low dosage of 10 ng mL^{-1}, a lower degree of IBA-1 expression was observed compared to LPS treatment. The fluorescence observed was marginally higher than the untreated and DMSO control groups. On the other hand, Fig.16 displays enhanced IBA-1 fluorescence (shown in E and F), indicating microglial activation when exposed to high concentrations (100 or 1000 ng mL^{-1}) of Iloprost. Although immunofluorescence can be observed with both the higher concentrations (100 and 1000 ng mL^{-1}), it appears that at a concentration of 100 ng mL^{-1} the intensity of activation induced by Iloprost was weaker compared to stimulation by LPS alone. This study confirmed the activation of C8-B4 cells upon Iloprost treatment. To explore the impact of Iloprost on inflammatory responses, M1 polarized cells were exposed to varying concentrations of Iloprost (10,100 and 1000 ng mL^{-1}) for 24 hours. Fig. 16 (G-I) demonstrates microglial activation across cultures treated with LPS and varying doses of Iloprost (10, 100 and 1000 ng mL^{-1}), IBA-1 expression was not further increased in LPS treated groups with high concentrations of Iloprost.

However, the type of activation would have to be characterised by specific markers for M1 and M2 polarization. Secondary markers, CD86 and CD206, were then used to determine the type of activation present in each group.

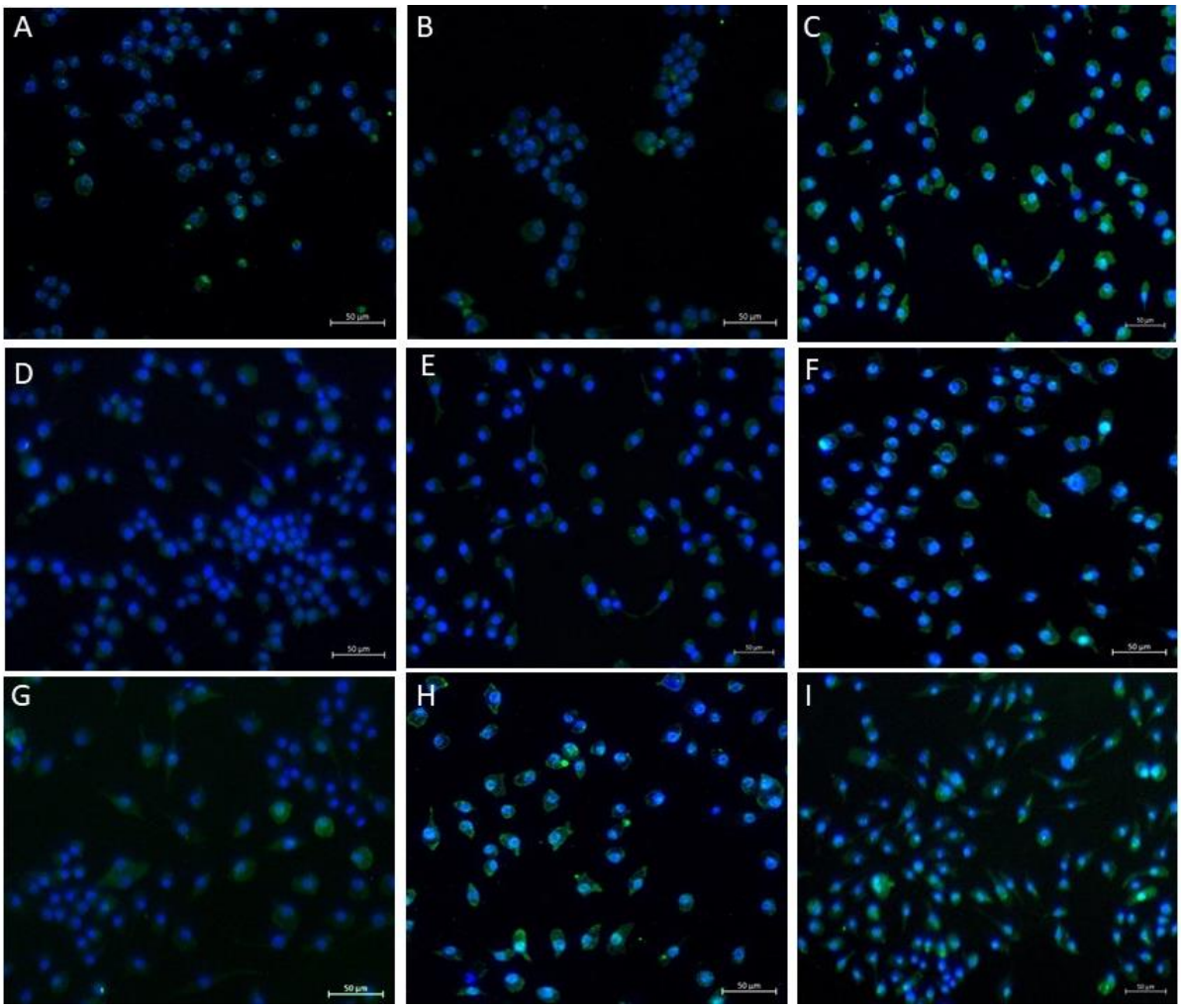

Fig. 16: *IBA-1 localisation in resting C8-B4 microglial cells treated with culture medium alone (**A**), DMSO control (**B**) and M1 polarization with 100ng mL^{-1} LPS for 24 hrs (**C**). To determine if Iloprost induces IBA-1 expression cells were cultured with 10,100 and 1000 ng mL^{-1} Iloprost alone for 24 hrs (**D-F**). Cells were then cultured with LPS for 24 hours to full induce M1 polarization followed by 10, 100 and 1000 ng mL^{-1} Iloprost for 24 hrs (**G-I**). Cells were then fixed 24 hours post treatment and counterstained with Hoechst, Images were obtained using Zeiss fluorescent microscope at 10x objective and image analysis carried out using Zen Lite software V3.8. Scale bar = 50µm.*

4.3.2 Effect of Iloprost on CD86 expression in resting and M1 polarized microglia.

To establish the type of activation present during Iloprost treatment, cells were also labelled with anti-CD86 antibody. This is to determine if Iloprost causes M1

polarization or induces any changes in CD86 expression following LPS and Iloprost treatment.

The cell staining in fig.17 C shows increased CD86 expression in LPS treated cells. LPS treatment was used as the positive control (C) against which the remaining treatment groups were compared. In Fig. 17, untreated and DMSO control groups (A and B) displayed no visible $CD86^+$ cells. There are currently no previous studies which examined the effect of Iloprost on CD86 expression in C8-B4 cells, in the present study no $CD86^+$ cell populations were observed in Iloprost treated cells across the varying doses of 10, 100 and 1000 ng mL^{-1}. To examine if Iloprost reversed M1 polarization of microglia, LPS treated cells were then exposed to varying doses of Iloprost. No visible $CD86^+$ cells were found in the LPS treated cultures followed by Iloprost treatment (Fig. 17).

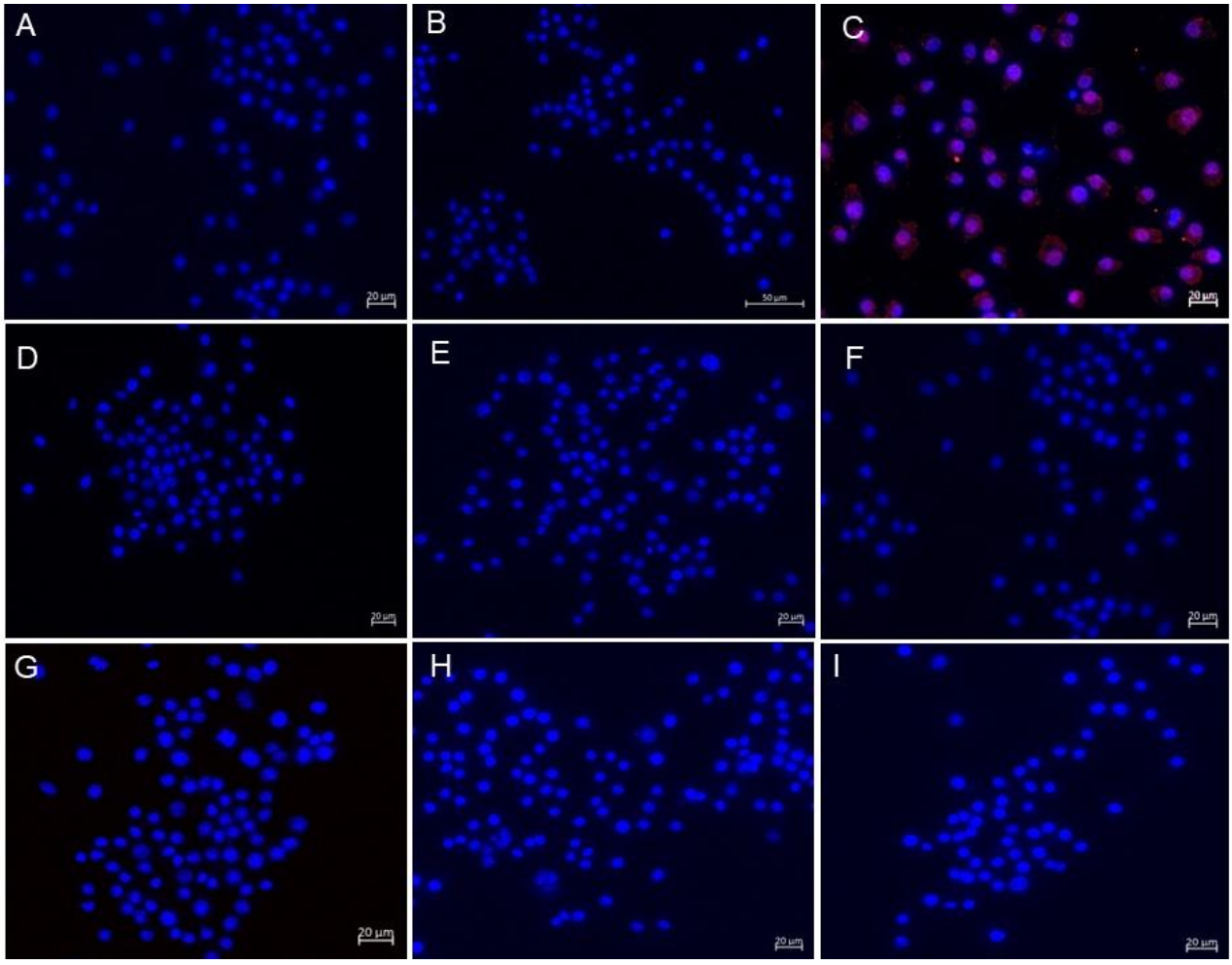

Fig. 17: *CD86 localisation in resting C8-B4 microglial cells treated with culture medium alone (**A**), DMSO control (**B**) and M1 polarization with 100 ng mL^{-1} LPS as a positive control (**C**). Resting C8-B4 cells were treated with 10,100 and 1000 ng mL^{-1} Iloprost for 24 hours (**D, E and F**) and stained with anti-CD86 to determine if the*

*compound induces any M1 polarization. LPS induced M1 polarized cells were then treated with 10,100 and 1000 ng mL^{-1} of Iloprost to determine if the compound would reverse CD86 expression (**G,H and I**). Nuclear staining was carried out with Hoechst and images were obtained using Zeiss fluorescent microscope with image analysis carried out using Zen Lite software V3.8. scale bar = 20 µm.*

4.3.3 Effect of Iloprost treatment on CD206 expression in resting and M1 polarized microglia.

As shown in Fig. 18 C below, no CD206 expression was observed in the LPS-treated cells. There was also no visible fluorescent antibody binding to CD206 in the untreated and DMSO control groups. However, when resting C8-B4 cells were exposed to different dosages of Iloprost, a clear increase in fluorescence of bound CD206 antibody was observed (Fig.18 D-F). This increase in the fluorescence intensity was directly proportional to the varying concentrations of Iloprost. Additionally, the comparison of CD206 expression in M1 polarized microglia treated with different concentrations of Iloprost (G-I) revealed a similar trend, with an increase in CD206^{+} cells as the concentration of Iloprost increased. This suggests that Iloprost had a positive impact on CD206 expression in C8-B4 microglia, indicating a potential role in promoting an anti-inflammatory phenotype.

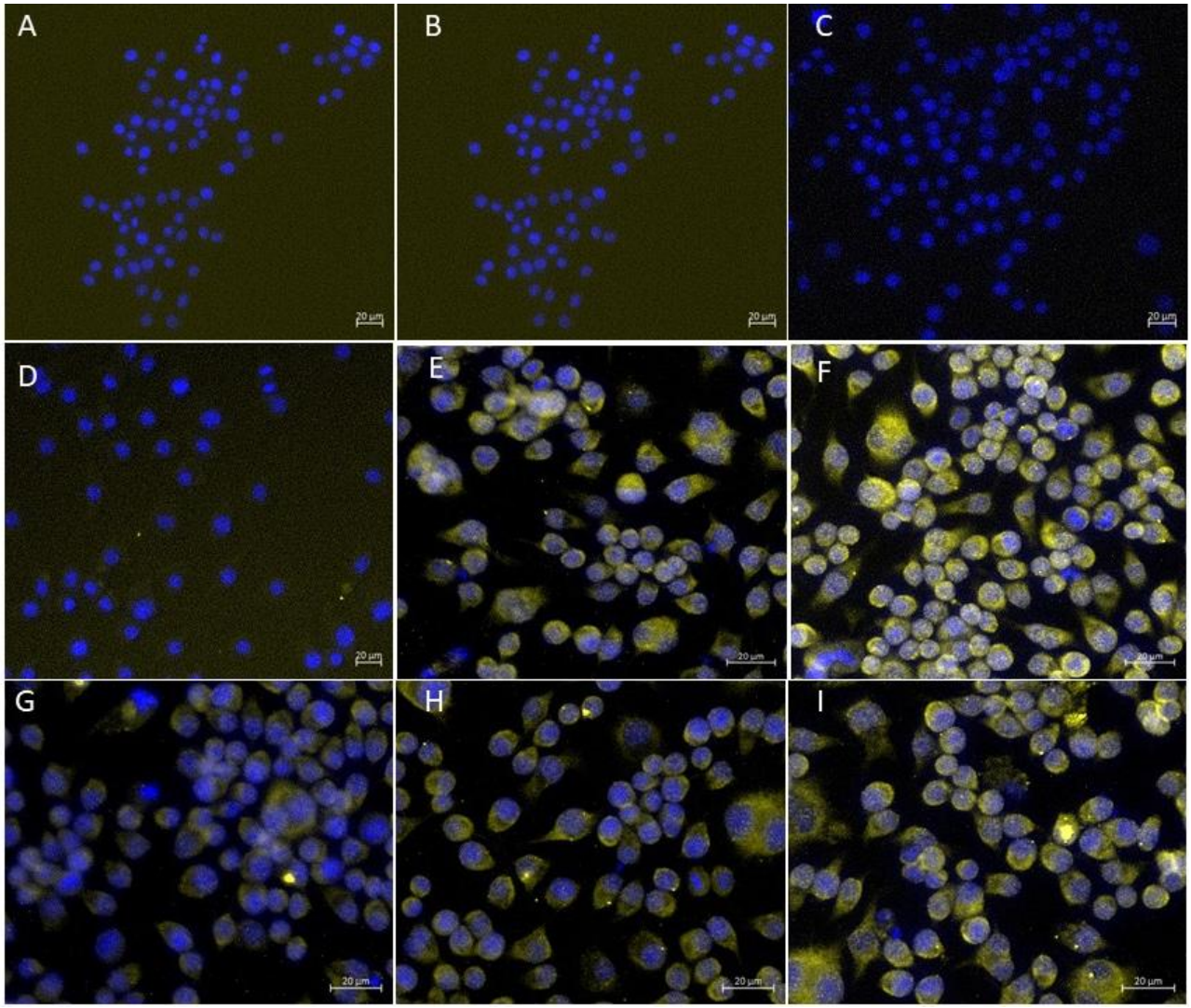

Fig. 18: *CD206 localisation in resting C8-B4 microglial cells treated with culture medium alone (**A**), DMSO control (**B**) and M1 polarization with 100ng mL^{-1} LPS for 24 hrs (**C**). To determine if Iloprost induces CD206 expression resting cells were cultured with 10,100 and 1000 ng mL^{-1} Iloprost alone for 24 hrs (**D-F**). Cells were then cultured with LPS for 24 hours to full induce M1 polarization followed by 10, 100 and 1000 ng mL^{-1} Iloprost for 24 hrs (**G-I**). Cells were then fixed 24 hours post treatment and counterstained with Hoechst, Images were obtained using Zeiss fluorescent microscope with Zen Lite image analysis software V3.8. Scale bar = 20µm*

4.3.4 Fluorescence intensity of cell surface markers.

To distinguish between fluorescence intensities across treatment groups the Zen Lite software was used to obtain the mean arithmetic fluorescence intensity for each image generated from three independent experiments.

A significant increase in IBA-1 antibody fluorescence intensity was observed in LPS treated cells compared to both control cultures ($p<0,0001$). Furthermore, when

comparing the intensity of IBA-1 expression in classically activated microglia, the fluorescence intensity was significantly greater than the level of IBA-1 in resting microglia treated with 10 and 100 ng mL^{-1} Iloprost ($p<0,0001$, Fig.19). This would suggest that Iloprost treatment at these concentrations did not strongly activate microglia as much as LPS treatment with 100 and 1000 ng mL^{-1} Iloprost as well as M1 polarized cells treated with high concentrations of Iloprost, compared to the controls ($p<0,001$, Fig.19 A). In contrast, when comparing LPS-treated microglia to 1000 ng mL^{-1} Iloprost treated cells an equal degree of activation was observed (Fig.19 A). This is also further emphasized by a significant ($p=0,0001$) increase in IBA-1 fluorescence intensity when comparing 10 and 100 ng mL^{-1} to 1000 ng mL^{-1} Iloprost in resting C8-B4 cells (Fig.19 A). Furthermore, IBA-1 fluorescent intensity remained increased in M1 polarized cells treated with 100 and 1000 ng mL^{-1} of Iloprost independently. This indicates that Iloprost did not induce additional activation in already activated cells.

To determine whether M1 or M2 polarization occurred, changes in CD86 fluorescence intensity across treatment groups were obtained. There was a significant ($p<0,0001$) increase in fluorescence intensity in LPS treated cells. However, CD86 fluorescent intensity was reduced to pre-treatment levels in M1 polarized cells treated with varying doses of Iloprost. This would suggest that Iloprost reversed M1 polarization after 24 hours of treatment. There were no significant differences when comparing dosages which suggests that Iloprost is effective in reducing CD86 expression at lower dosages. Furthermore, Iloprost did not cause any significant CD86 expression when administered to resting cells.

To study M2 polarization, we examined CD206 fluorescence detection. Our results show that fluorescence intensity was significantly higher in resting microglial cells treated with 100 and 1000 ng mL^{-1} Iloprost compared to both controls and LPS treated cultures ($p<0,0001$, Fig.19 C). Meanwhile, LPS treated cells that were further treated with 10, 100 and 1000 ng mL^{-1} of Iloprost also exhibited increased CD206 fluorescence intensity compared to LPS-exposed and control cultures ($p=0,0006$, Fig.19 C). Even though CD206 fluorescent intensity was elevated in M1 polarized cells treated with 100 and 1000 ng mL^{-1} Iloprost, we observed that the intensity was significantly higher in resting cells treated with these doses ($p<0,0001$, Fig.19 C).

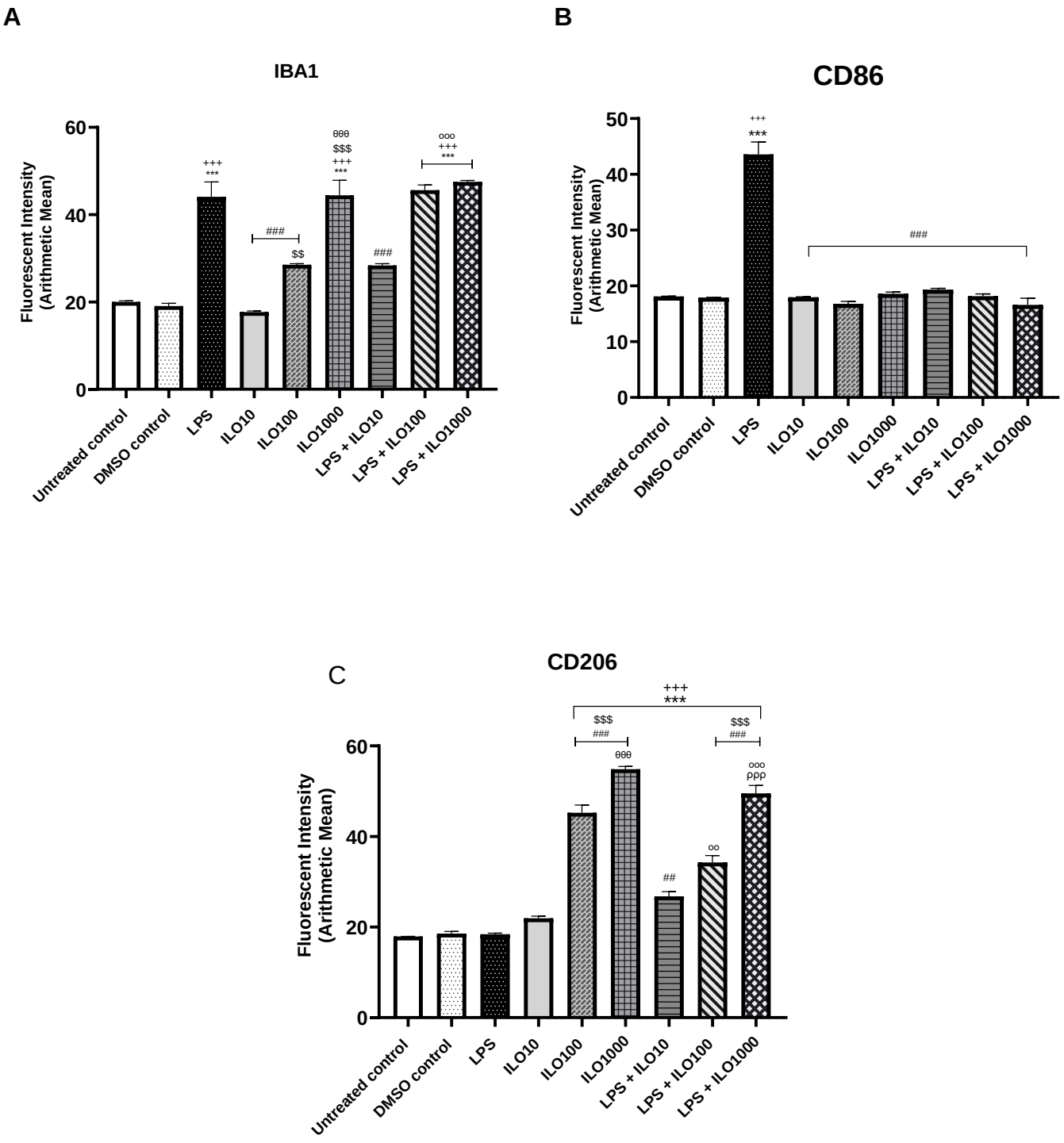

Fig. 19: *Fluorescence intensities of IBA-1 (**A**), CD86 (**B**) and CD206 (**C**) represented as the arithmetic mean of fluorescent signal intensity obtained by ZEN Lite software. Statistical analysis was carried out using One-Way ANOVA with Bonferroni's post hoc analysis. (**A**) $F_{(8,26)} = 54.81$; $p<0,0001$. $^{***}p \leq 0.0001$ compared to untreated control. $^{+}p = 0.03$ and $^{+++}p \leq 0.0001$ compared to DMSO control. $^{\#\#\#}p \leq 0.0001$ compared to LPS treated. $^{\$\$}p = 0.009$ and $^{\$\$\$}p \leq 0.0001$ compared to 10 ng mL^{-1} Iloprost. $^{\theta\theta\theta}p = 0.0001$ compared to 100 ng mL^{-1} Iloprost. $^{ooo}p \leq 0.0001$ compared to LPS + 10 ng mL^{-1} Iloprost. (**B**) $F_{(8,26)} = 96.86$; $p < 0.0001$. . $^{***}p \leq 0.0001$ compared to untreated control. $^{+++}p \leq 0.0001$ compared to DMSO control. $^{\#\#\#}p \leq 0.0001$ compared to LPS treated. (**C**) $F_{(8,26)} = 182.7$; $p < 0.0001$. $^{***}p \leq 0.0006$ compared to untreated control. $^{+++}p \leq 0.0001$ compared to DMSO control.$^{\#\#}p = 0.01$ and $^{\#\#\#}p$*

≤ 0.0001 compared to LPS treated. $$$p ≤ 0.0001 compared to 10 ng mL^{-1} Iloprost. θθθp ≤ 0.0001 compared to 100 ng mL^{-1} . . ººp = 0.004 and ºººp ≤ 0.0001 compared to LPS + 10 ng mL^{-1} Iloprost. ρρρp < 0.0001 compared to LPS + 100 ng mL^{-1} Iloprost.

4.4 Quantification of Pro inflammatory cytokines released 24 hours post treatment.

To further examine the neuroprotective effects of Iloprost on LPS-induced inflammatory changes, pro-inflammatory cytokine TNFα and IL-1β levels were measured in resting cell culture supernatant 24 hours post-treatment with a high dose of LPS or with varying concentrations of Iloprost.

ELISA showed that administration of LPS alone led to a significant increase in TNF-α secretion by C8-B4 cells compared to both untreated and DMSO control cultures (p<0,0001, Fig. 20 A). Moreover, all three cultures pre-exposed to LPS and subsequently treated with varying concentrations of Iloprost exhibited significant reduction in TNF-α and IL-1β secretions compared to cultures exposed only to LPS (p<0,0001, Fig. 20). Specifically, 1000 ng mL^{-1} Iloprost, was observed to be the most effective concentration at decreasing in TNF-α secretion compared to the cultures treated with LPS or 10 and 100 ng mL^{-1} Iloprost (p=0,0014, Fig . 20 A). Interestingly, intracellular production of TNF-α and IL-1β cytokines in resting microglial cells exposed to varying concentrations of Iloprost were undetectable by ELISA. This suggests that Iloprost treatments effectively inhibited LPS-induced secretion of pro-inflammatory cytokines in the microglial cells.

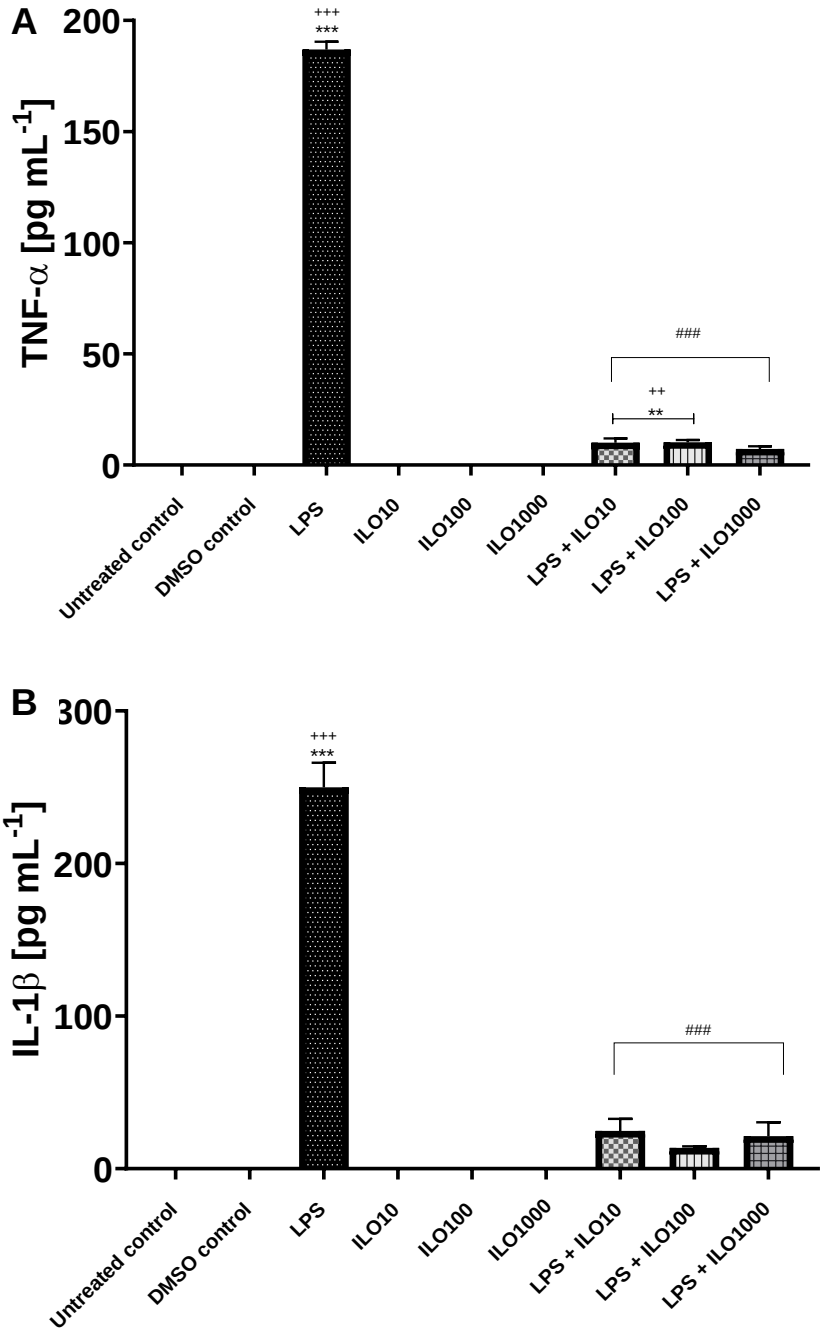

Fig. 20: *TNF-α (**A**) and IL-1β (**B**) secreted 24 hours post LPS and Iloprost treatment. Data are represented as the mean concentration of TNFα in cell culture supernatant ± SEM from three independent experiments. Statistical analysis was carried out using One-Way ANOVA with Bonferroni's post hoc analysis. (**A**) $F_{(8,26)} = 184.8$; p<0,0001. $^{***}p \leq 0.0001$ compared to untreated control. $^{*}p$ 0.0327 compared to untreated and DMSO control. $^{+++}p \leq 0.0001$ compared to DMSO control. $^{###}p \leq 0.0001$ compared to LPS treated. (**B**) $F_{(8,26)} = 56.34$; p<0,0001. $^{***}p \leq 0.0001$ compared to untreated control. $^{+++}p \leq 0.0001$ compared to DMSO control. $^{###}p \leq 0.0001$ compared to LPS treatment.*

4.5 Iloprost treatment activates BDNF signalling in cells.

Previous studies have established that Iloprost exerts its pharmacological effects by binding to prostanoid receptors (Ruan *et al*., 2010, Dorris and Peebles., 2012). To investigate the roles of prostanoid-BDNF signalling in Iloprost-mediated protection against LPS-induced inflammation in cells, endogenous production of BDNF in resting and M1 polarized microglia cells were quantified 24 hours post-treatment using ELISA. As shown in Fig. 21, significant increases in BDNF concentration were observed across all cultures exposed to varying concentrations of Iloprost with or without LPS stimulation, compared to both untreated and DMSO control cultures (P<0,0001). Significantly, Iloprost induced increases in BDNF release at a dose dependent rate. Surprisingly, our data further showed that the culture exposed to LPS treatment only did not exhibit any significant change in BDNF levels compared to control cultures (p>0,05, Fig.21).

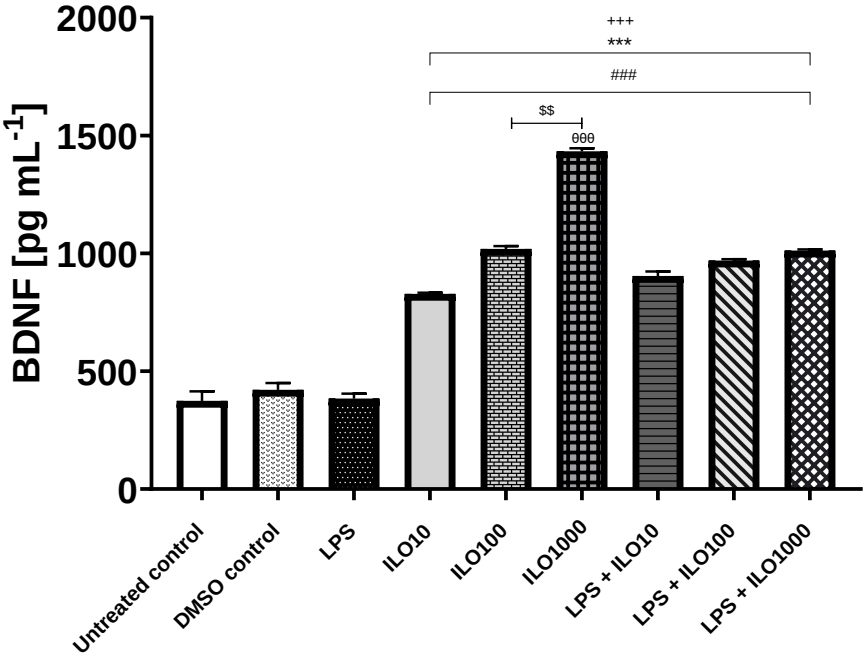

Fig. 21: *Changes in BDNF secreted in response to LPS and Iloprost treatment 24 hours post treatment. Data are represented as the mean concentration of BDNF ± SEM from three independent experiments. Statistical analysis was carried out using One-Way ANOVA with Bonferroni's post hoc analysis.* $F_{(8,26)} = 204.0$ *;* $p<0,0001$. $^{***}p \leq 0.0007$ *compared to untreated control.* $^{+++}p \leq 0.0002$ *compared to DMSO control.* $^{\#\#}p = 0.0065$ *compared to LPS treatment.* $^{\$\$}p = 0.0075$ *compared to Iloprost 10 ng.mL*$^{-1}$ *treatment.* $^{\theta\theta\theta}p \leq 0.0001$ *compared to 100 ng.mL*$^{-1}$ *Iloprost.*

4.6 Gene expression changes in microglial cells.

4.6.1 PCR validation results.

To ensure accuracy in data collection, all steps involved in the PCR protocol were carefully observed and validated. The results of RNA quality and yield are presented in table 7 below. The stability between the two reference genes chosen for this study, GAPDH and β-actin (ACTB), was tested to identify the least variability between treatment groups. The ideal reference gene should be constantly expressed at a moderate level, exhibit minimal variation across treatment groups and yield Ct values between 15-30 (Li *et al*., 2020, Basu *et al*., 2019). This ensures that any changes observed in the expression of the target gene can accurately be attributed to the experimental conditions being investigated and not to variations in reference gene expression. GAPDH was selected as a reference gene as it displayed the least amount of variability between treatment groups (Table 8).

Table 7: *RNA quantity and quality of samples using ThermoFischer Scientific µDrop.*

Sample	260/280 nm ratio	[RNA] (ng μL^{-1})
Untreated	2.1	289.1
Vehicle control	2.1	103
LPS [100 ng mL^{-1}]	2.11	196.3
Iloprost [10 ng mL^{-1}]	2.00	272.6
Iloprost [100 ng mL^{-1}]	2.09	208
Iloprost [1000 ng mL^{-1}]	2.09	204
LPS [100 ng mL^{-1}] + Iloprost [10 ng mL^{-1}]	2.07	190.3
LPS [100 ng mL^{-1}] + Iloprost [100 ng mL^{-1}]	2.07	284.9
LPS [100 ng mL^{-1}] + Iloprost [1000 ng mL^{-1}]	2.08	175.4

Table 8: *Average Ct of reference genes across treatment groups*

Treatment groups	Untreated	DMSO control	LPS	Iloprost [10]	Iloprost [100]	Iloprost [1000]	LPS + [10]	LPS + [100]	LPS + [1000]
GAPDH (Average Ct)	16,15	16,49	16,78	15,72	16,38	17,09	16,60	17,09	17,15
ACTB (Average Ct)	13,77	13,74	19,89	16,57	16,18	20,58	20,54	20,48	26,58

The PCR amplification plots and melting curve analysis are shown in Fig. 22 below. For the PCR amplification cycle, the fluorescence of the amplicon (PCR product) was checked against the background signal and recorded as cycle threshold value (Ct) (Fig. 22 A). Whereas, the melt curve analysis allows for the confirmation of a single PCR product, to determine if no primer dimer formation took place during the reaction and confirms that no PCR products are detected in the “no template control” (NTC). The graph can be interpreted as having a single peak at the correct Tm for the primer pair with no amplification in the NTC (Fig. 22 B).

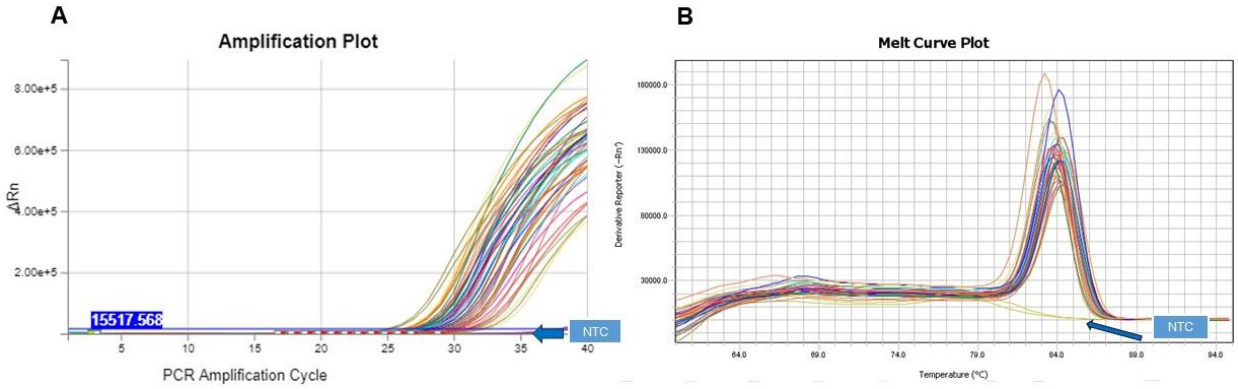

Fig. 22: *Amplification plot (A) and Melt Curve (B) graphs displaying no amplification for the no template control (NTC) and one peak with the absence of primer-dimer formation for the primer pair.*

The PCR amplification efficiency was used as a parameter for monitoring the PCR for potential false-negative results. This is required for accurate data interpretation and calculations of relative fold changes. In general, efficiency determines the rate at which the PCR products accumulate during the exponential phase of amplification, ideally PCR efficiency should be equal to 2 (Karlen *et al*., 2007). However, in practice an

efficiency of 1.8 to 2.1 are considered acceptable (Kuang *et al*., 2018). The PCR efficiency of the reference gene and target genes for each experimental sample was determined from a 6-point standard curve generated for each gene using a 7-fold serial dilution of cDNA cocktail mix. Fig. 23 shows a standard curve generated for the housekeeping gene GAPDH. To validate each qPCR run a cocktail mix was generated from pooled cDNA from experimental samples to determine the PCR efficiency. To employ the $2^{-\Delta\Delta Ct}$ method a PCR efficiency of near 100% is required (Schmittgen and Livak, 2008). The PCR efficiency for all genes was found to be within the accepted range of 90-105% (Fig. 23), indicating the absence of inhibitors in the reaction mix. If inhibitors are present, PCR efficiency above 110% may be expected whereas efficiencies less than 90% indicates poor primer design (Svec *et al*., 2015).

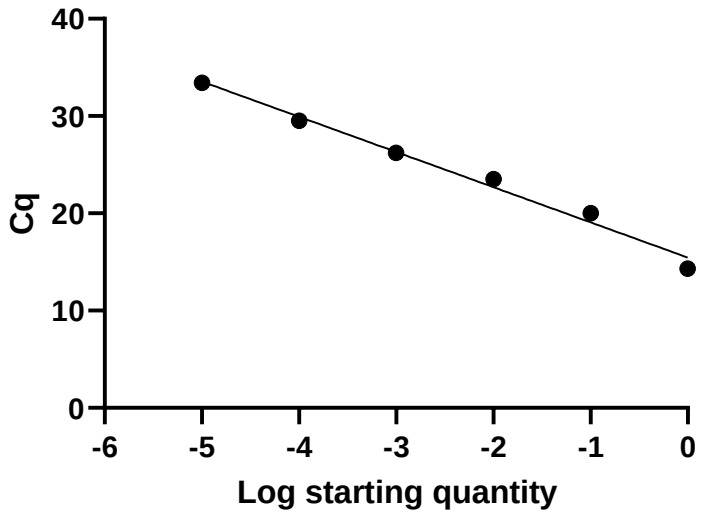

Fig. 23: *Standard curve generated for GAPDH. PCR efficiency was within the acceptable range of 90-105%.*

The correlation coefficient (R^2) results are shown Table 9 below. R^2 provides a measure of the strength and direction of the linear relationship between the Ct values and log-transformed cDNA starting quantities in qPCR. In this study, the R^2 values for both the reference gene and target genes ranged between 0.970 and 0.996 (Table 9), indicating a high degree of linearity. A R^2 0.980 is ideally required for qPCR to ensure a strong linear relationship between Ct values and log-transformed cDNA starting quantities. This further demonstrates that no PCR inhibitors were present in our samples.

Table 9: *qPCR efficiency and regression coefficient obtained from a standard curve of a pooled C8-B4 microglia cDNA cocktail mix.*

Gene Abbreviation	Ta (ºC)	Slope	R^2	qPCR efficiency (%)
GAPDH	60ºC	-3,403	0,970	96,7
TNFα	60ºC	-3,470	0,983	94,1
IL-1β	60ºC	-3,286	0,996	101,5
CREB	60ºC	-3,469	0,984	94,7
BDNF	60ºC	-3,281	0,996	101,7
CD206	60ºC	-3.437	0,986	95,4
ARG-1	60ºC	-3.342	0,998	99.2

To confirm whether the PCR reaction resulted in the formation of a single PCR product, gel electrophoresis was carried out on the housekeeping gene GAPH and at least one target gene. Fig. 24 illustrates single bands for the PCR reaction from amplification of the housekeeping gene GAPDH across treatment groups. This further illustrates the absence of primer dimer formation and any non-specific products. Further confirmation of no amplification in the NTC can be observed in lane 10 with the absence of any band formation.

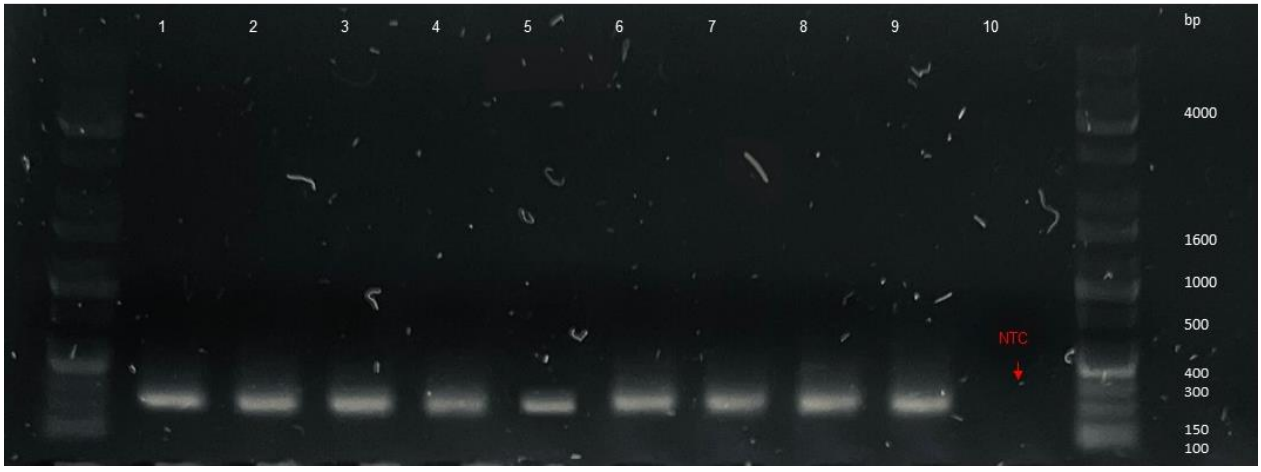

Fig. 24: *Image of gel electrophoresis of qPCR products.*

4.6.2 Effect of Iloprost treatments on LPS-induced transcriptional changes in TNFα and IL-1β gene expression.

To further investigate the effect of Iloprost treatments on LPS-induced inflammatory changes, the levels of TNFα and IL-1β mRNA transcripts expressed in the microglial cells 24 hr post-treatment exposure were quantified. A significant 15-fold increase in TNFα gene expression in cells exposed to LPS only for 24 hr compared to both untreated and DMSO control groups ($p<0,0001$, Fig. 25 A) was observed. The result further demonstrates that TNFα expression was significantly downregulated by Iloprost treatments compared to groups that were exposed to LPS only ($p<0,05$, Fig. 25 A). However, there remained a substantial 10-fold increase in TNFα expression across M1 polarized cells treated with varying concentrations of Iloprost compared to the controls and groups exposed to only Iloprost treatments ($p<0,0001$, Fig. 25 A). Resting microglia exposed to Iloprost treatments did not exhibit any significant changes in gene expression profile of TNF-α compared to untreated and DMSO control groups ($p>0,05$, Fig. 25 A).

Similar to the TNF-α gene expression profile, microglial cells stimulated with LPS for 24 hr evoked approximately 20-fold significant increase in IL-1β expression compared to the controls and other treatment groups ($p<0,0001$, Fig. 25 B). IL-1β gene expression was significantly increased in cells exposed to different concentrations of Iloprost only, compared to the controls ($p<0,05$, Fig. 25 B). Interestingly, M1 polarized cells treated with similar concentrations of Iloprost exhibited significant decreases in IL-1β gene expression compared to cells exposed to LPS only ($p<0,05$, Fig. 25 B). . Iloprost at a dosage of 1000 ng mL^{-1} was the most effective of the three dosages at reducing IL-1β expression in response to LPS induced inflammation (Fig. 25 B).

A

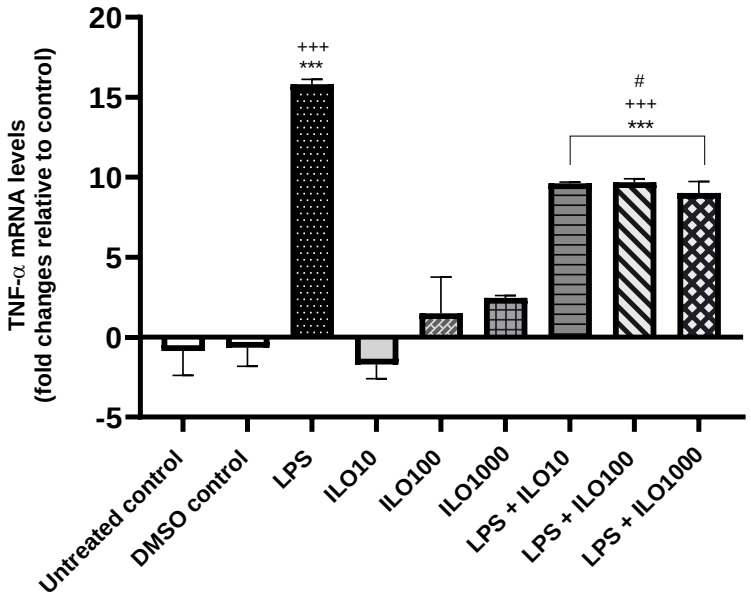

B

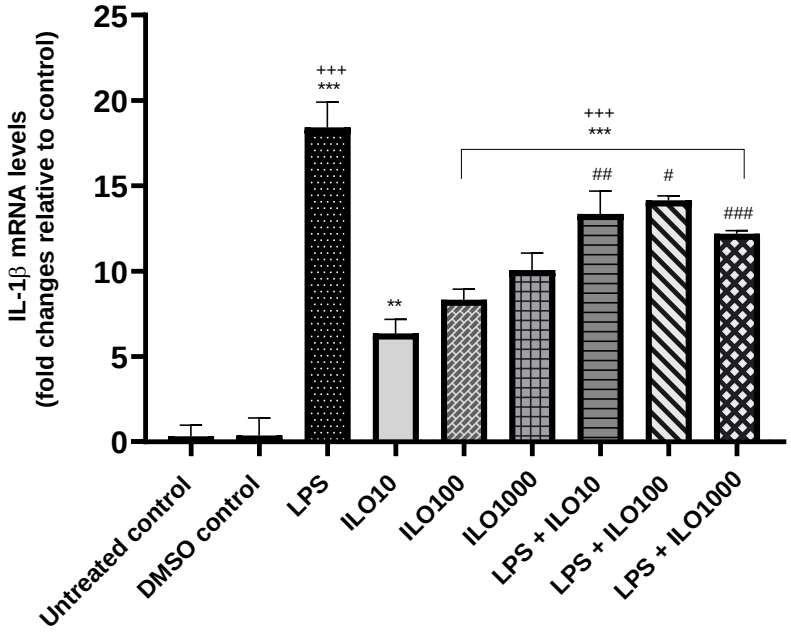

Fig. 25: *Effect of LPS and Iloprost treatment on TNF-α (**A**) and IL-1β (**B**) gene expression 24 hours post treatment in C8-B4 cells. Data are represented as the Log_2 fold change of gene expression relative to GAPDH ± SEM from three independent experiments. Statistical analysis was carried out using One-Way ANOVA with Bonferroni's post hoc analysis. (**A**) $F_{(8,26)} = 33.29$; $p < 0.0001$. $^{***}p < 0.0001$ compared to untreated control. $^{+++}p < 0.0002$ compared to DMSO control. $^{\#\#\#}p < 0.0001$ compared to LPS treatment. $^{\#}p < 0.027$ compared to LPS treatment. (**B**) $F_{(8,26)} = 44.07$; $p < 0.0001$. $^{**}p = 0.007$ and $^{***}p < 0.0001$ compared to untreated control. $^{++}p = 0.0085$ and $^{+++}p < 0.0002$ compared to DMSO control. $^{\#}p = 0.01$, $^{\#\#}p = 0.002$ and $^{\#\#\#}p = 0.0004$ compared to LPS treatment.*

4.6.3 Effect of Iloprost treatments on LPS-induced changes in CD206 and ARG-1 gene expression.

To further investigate the anti-inflammatory potential of Iloprost, CD206 and ARG-1 gene expression changes in both resting and M1 polarized cells were examined. As shown in Fig. 26A, CD206 expression was significantly downregulated in M1 polarized cells compared to both untreated controls ($p<0,001$, Fig. 26A). Contrary to this, there was a significant 4.3 and 5-fold increase in CD206 in M1 polarized cells treated with 100 and 1000 ng mL^{-1} of Iloprost compared to LPS treatment ($p<0,0001$, Fig. 26A). Furthermore, CD206 gene expression was significantly (4.9 and 5.4-fold) upregulated in resting cells exposed to 100 and 1000 ng.mL^{-1} of Iloprost, compared to both untreated and DMSO control cultures ($p\leq0,009$).

Fig. 26B shows the effect of Iloprost treatments on LPS-induced transcriptional changes in ARG-1 gene. There was a 4.6-fold increase in ARG-1 expression in LPS treated cells ($p=0,01$). ARG-1 mRNA levels remained upregulated across LPS cultures treated with varying concentrations of Iloprost compared to both controls ($p\leq0,006$). However, no further upregulation of ARG-1 was detected in M1 polarized cells treated with Iloprost compared to LPS treated microglia. Also, no significant differences were detected between LPS treated microglia combined with varying doses of Iloprost. ARG-1 expression, however, was significantly upregulated (5.4 and 6.4-fold) in resting microglia treated with 100 and 1000 ng.mL^{-1} Iloprost compared to the control cultures ($p\leq0,0002$). Furthermore, ARG-1 mRNA levels were more significantly upregulated in resting cells treated with 1000 ng mL^{-1} of Iloprost compared to a lower concentration of 10 ng mL^{-1} ($p=0,004$).

A

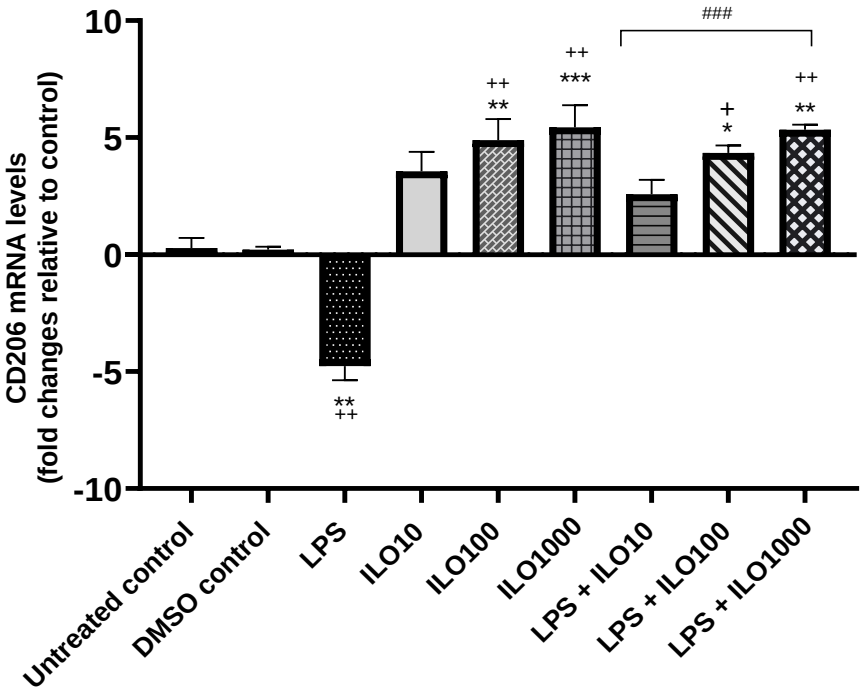

B

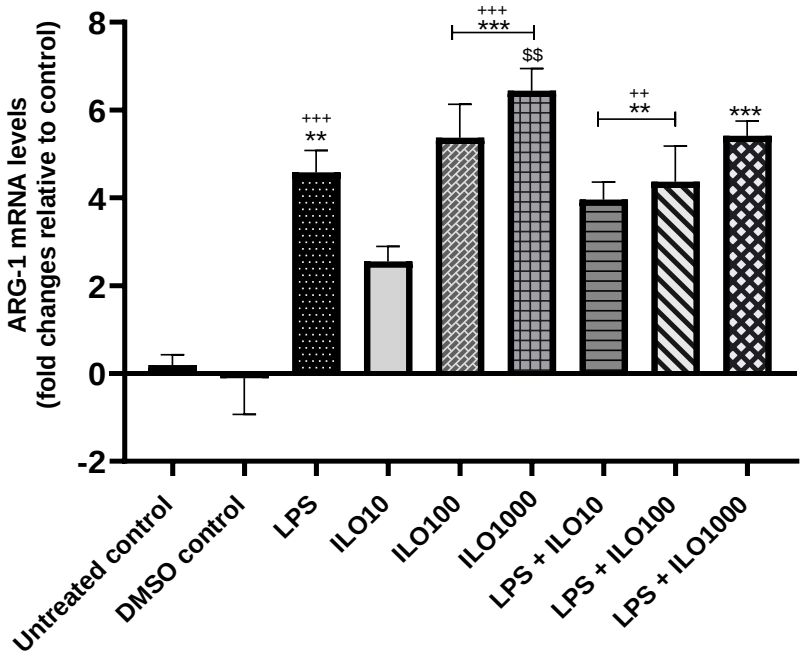

***Fig. 26**: (A) Effect of LPS and Iloprost treatment on CD206 mRNA expression 24 hours post treatment in C8-B4 cells. Data are represented as the Log_2 fold change of gene expression relative to GAPDH ± SEM from three independent experiments.Statistical analysis was carried out using One-Way ANOVA with Bonferroni's post hoc*

*analysis. $F_{(8,26)} = 26.74$; $p < 0.0001$. *p = 0.01 **p = 0.003 and ***p = 0.001 compared to untreated control. ^{++}p = 0.004, ^{+}p = 0.028, ^{++}p = 0.002 and ^{++}p = 0.009 compared to DMSO control. $^{###}p$ <0.0001 compared to LPS treatment. (B) Effect of LPS and Iloprost treatment on ARG-1 mRNA expression 24 hours post treatment in C8-B4 cells. Data are represented as the Log_2 fold change of gene expression relative to GAPDH ± SEM from three independent experiments. Statistical analysis was carried out using One-Way ANOVA with Bonferroni's post hoc analysis. $F_{(8,26)} = 16.54$; $p < 0.0001$. $^{**}p \leq 0.006$, $^{***}p \leq 0.0002$, compared to untreated control. $^{++}p = 0.002$ and $^{+++}p \leq 0.001$ compared to DMSO control. $^{\$\$}p = 0.004$ 10 ng.mL^{-1} Iloprost treatment.*

4.6.4 Effect of Iloprost treatments on LPS-induced changes in CREB and BDNF gene expression.

Both CREB and BDNF have been implicated in various pathological processes in the brain. Activation of CREB may elicit either pro-inflammatory or anti-inflammatory effects depending on the context, whereas BDNF activation is mainly associated with anti-inflammatory response changes. Since CREB is an important regulator of BDNF-induced gene expression, LPS-induced transcriptional changes in CREB/BDNF genes in microglia were examined for implications for Iloprost-driven neuroprotection.

CREB gene expression was upregulated 3-fold in microglia treated with LPS compared to both untreated cultures (p=0,003). This trend was also noted in M1 microglia treated with 100 ng mL^{-1} of Iloprost which showed a 1.8-fold upregulation in CREB expression compared to the untreated and DMSO control (p=0,01, Fig. 27A). Furthermore, CREB expression was most affected by LPS treatment combined with 1000 ng mL^{-1} of Iloprost which resulted in a 5-fold upregulation in the gene (p<0,0001). Surprisingly, CREB gene expression was not significantly altered across resting microglia treated with varying concentrations of Iloprost (p>0,05, Fig. 27A).

As shown in Fig. 27 B, there was a significant 1.7-fold upregulation in BDNF gene expression in LPS treated cells compared to control cultures (p=0,0004). Further, BDNF expression remained upregulated across cell cultures treated with both LPS and varying doses of Iloprost compared to control cultures (p≤0.03). When examining the differences in fold changes of BDNF across cultures treated with LPS and varying concentrations of Iloprost, 1000 ng mL^{-1} of Iloprost strongly upregulated the expression of the neuroprotective cytokine BDNF, compared to cultures that received LPS with 10 ng mL^{-1} of Iloprost (p<0,001, Fig. 27B). Furthermore, BDNF mRNA levels were significantly upregulated in resting cells that were exposed to 1000 ng mL^{-1} of

Iloprost compared to control cultures (p≤0,0008). There was a similar trend between the lower and higher concentrations of Iloprost with 1000 ng mL^{-1} of Iloprost strongly inducing BDNF transcription compared to 10 and 100 ng mL^{-1} in resting microglia (p=0,001, p=0,007).

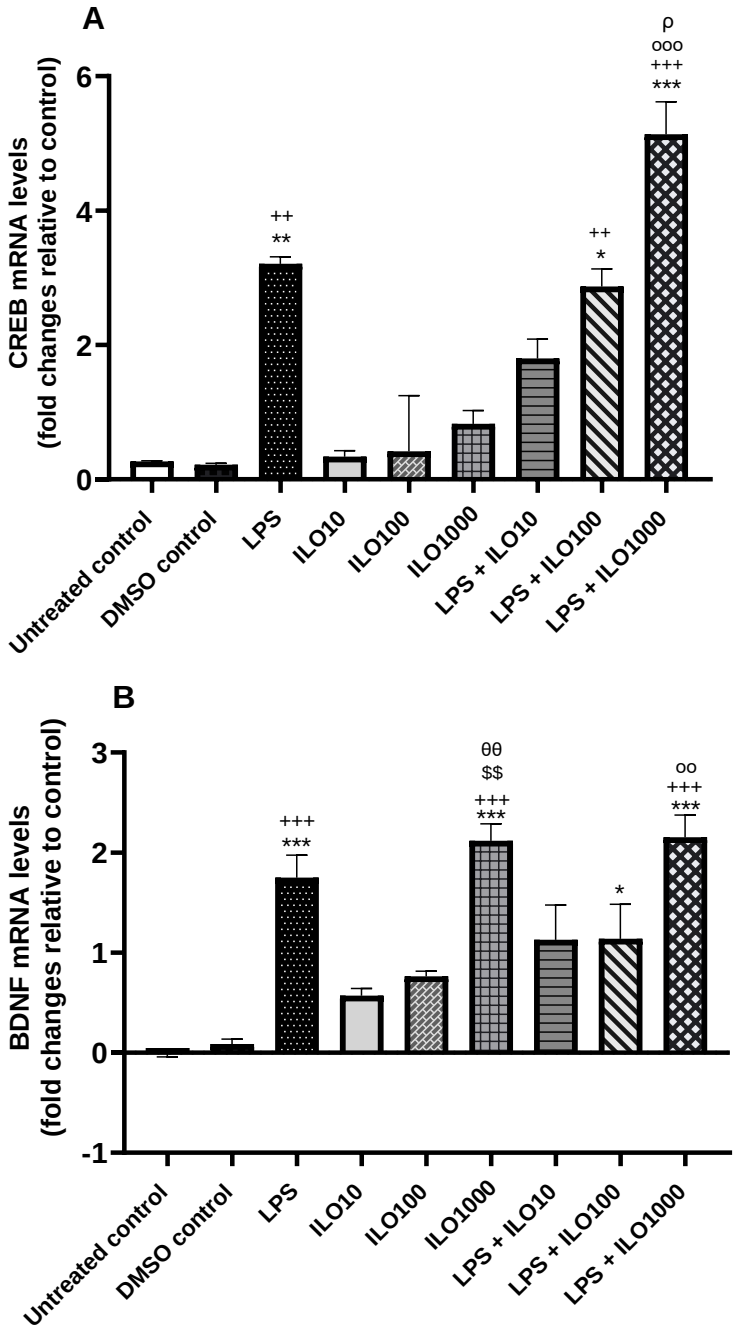

Fig. 27: *Effect of LPS and Iloprost treatment on CREB (**A**) and BDNF (**B**) mRNA expression 24 hours post treatment in C8-B4 cells. Data are represented as the Log_2 fold change of gene expression relative to GAPDH ± SEM from three independent experiments.Statistical analysis was carried out using One-Way ANOVA with Bonferroni's post hoc analysis.(**A**)* $F_{(8,26)} = 6.56$ *; p = 0.0005 .* $^{*}p = 0.01$, $^{**}p=0.003$ *and* $^{***}p<0.0001$ *compared to untreated control.* $^{++}p \leq 0.008$ *and* $^{+++}p<0.0001$ *compared to DMSO control.* $^{ooo}p=0.0007$ *compared to LPS+ILO10.*

*$^{\rho}p$ =0.03 compared to LPS+ILO100 (**B**) $F_{(8,26)} = 12.95$; $p < 0.0001$. $^{*}p = 0.03$ and $^{***}p < 0.0004$ compared to untreated control. $^{+++}p < 0.0008$ compared to DMSO control. $^{\$\$}p = 0.001$ compared to 10 ng.mL^{-1} Iloprost treatment. $^{\theta\theta}p = 0.007$ compared to 100 ng.mL^{-1} Iloprost. $^{oo}p = 0.007$ compared to LPS + ILO10.*

4.6.5 Methylated DNA expression of CREB/BDNF

To investigate the epigenetic changes associated with Iloprost treatment, the DNA methylation status at the CREB and BDNF promoter regions in LPS and Iloprost treated microglia was examined. DNA samples were methylated 24 hr post treatment and the fold change relative to GAPDH was determined in each treatment group. Table 10 below shows the yield and purity of representative DNA samples determined by µDrop plate (ThermoFischer Scientific). Also, successful DNA extraction was further confirmed using agarose gel electrophoresis and the results obtained indicate single bands for all treatment groups with similar molecular weight (Fig. 28).

Table 10: *Extracted DNA quantity and purity across treatment groups using ThermoFischer µDrop.*

Sample	260/280 nm ratio	[RNA] (ng µL^{-1})
Untreated	1.8	269
Vehicle control	1.8	357
LPS [100 ng mL^{-1}]	1.8	162
Iloprost [10 ng mL^{-1}]	1.8	312
Iloprost [100 ng mL^{-1}]	1.8	823
Iloprost [1000 ng mL^{-1}]	1.8	447
LPS [100 ng mL^{-1}] + Iloprost [10 ng mL^{-1}]	1.8	253
LPS [100 ng mL^{-1}] + Iloprost [100 ng mL^{-1}]	1.8	221
LPS [100 ng.mL^{-1}] + Iloprost [1000 ng.mL^{-1}]	1.8	236

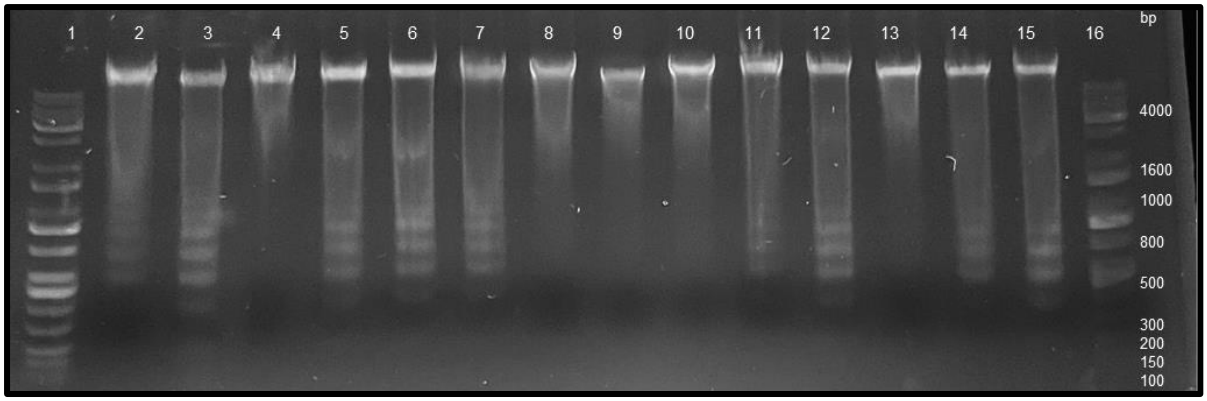

***Fig. 28**: Analysis of extracted DNA samples across treatment groups. Lane 1) DNA ladder, Lanes 2 – 10) n=2 treatment groups, Lanes 11-15) n=3 treatment groups. Lane 16) DNA ladder.*

3.2.3 Gel electrophoresis of PCR products

To confirm whether the PCR reaction resulted in the formation of a single PCR product, gel electrophoresis was carried out on the housekeeping gene GAPH and at least one target gene. Fig. 29 illustrates single bands for the PCR reaction from amplification of the target gene BDNF across treatment groups. This further illustrates the absence of primer dimer formation and any non-specific products. Further confirmation of no amplification in the NTC can be observed in lane 2 with the absence of any band formation.

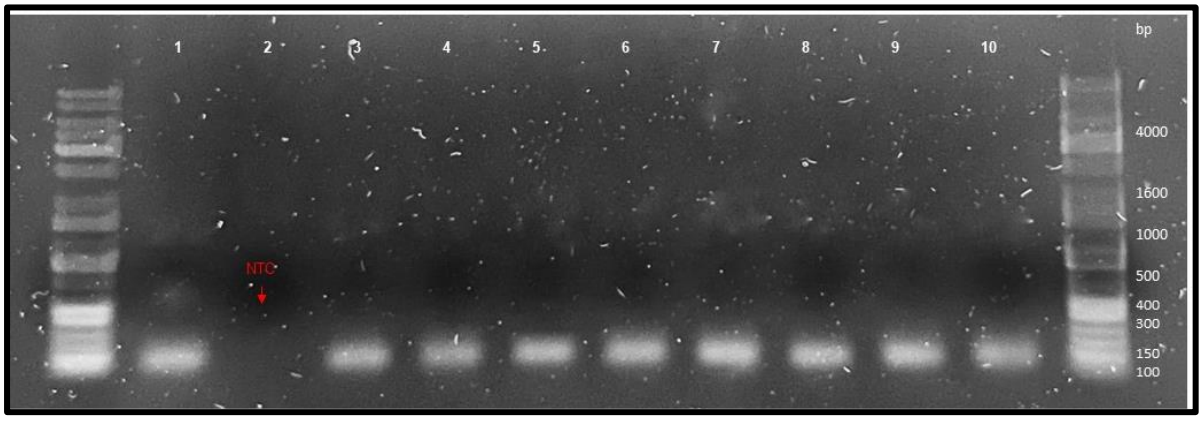

***Fig. 29:** Representative image of Gel electrophoresis on DNA methylated PCR products from BDNF target gene.*

The PCR efficiency of the reference gene and target genes for each experimental sample was determined from a 6-point standard curve generated for each gene using a 7-fold serial dilution of methylated DNA cocktail mix. As shown in table 11 below, the

PCR efficiency for the reference and target genes fell within the acceptable range of 90-100%.

Table 11: *qPCR efficiency and regression coefficient obtained from generating a standard curve of pooled methylated DNA.*

Gene Abbreviation	Ta (ºC)	Slope	R^2	qPCR efficiency (%)
GAPDH	60ºC	-3.286	0.985	101.48
CREB	60ºC	-3.267	0.985	102.3
BDNF	60ºC	-3.219	0.995	104.4

4.6.6 BDNF DNA hypomethylation evoked by LPS-challenge may be reversed by high concentration of Iloprost.

To investigate epigenetic changes associated with the effect of LPS and Iloprost treatments in resting and M1 polarized microglia, DNA methylation changes were assessed in the promoter regions of the CREB and BDNF genes. Significant hypermethylation at the CREB promoter was observed in all treatment groups compared to the untreated and DMSO control cultures ($p<0,01$, $p<0,0001$), thus indicating transcriptional silencing of the CREB gene across the treatment groups (Fig. 30A). No significant differences were observed when comparing LPS-treated microglia to those treated with varying concentrations of Iloprost ($p>0,05$, Fig. 30A).

In contrast to CREB methylation status, LPS treatment evoked significant decrease in DNA methylation at the BDNF promoter region compared to the control cultures ($p<0.05$, Fig. 28B). This implies that LPS stimulation induced transcriptional upregulation in BDNF gene expression in the microglia (Fig. 30 B). Whereas the resting microglia treated with higher concentrations (100 and 1000 ng mL^{-1}) of Iloprost only exhibited significant hypermethylation or transcriptional silencing at the BDNF promoter compared to the control and other treatment cultures ($p<0,05$, $p<0,0001$, Fig.

30 B). There were no changes in DNA methylation status of cell cultures exposed to co-treatments of LPS and higher concentrations of Iloprost (100 and 1000 ng mL^{-1}) when compared to the control (p>0,05) but differ significantly from cultures treated with LPS alone (p<0.05, Fig. 30B).

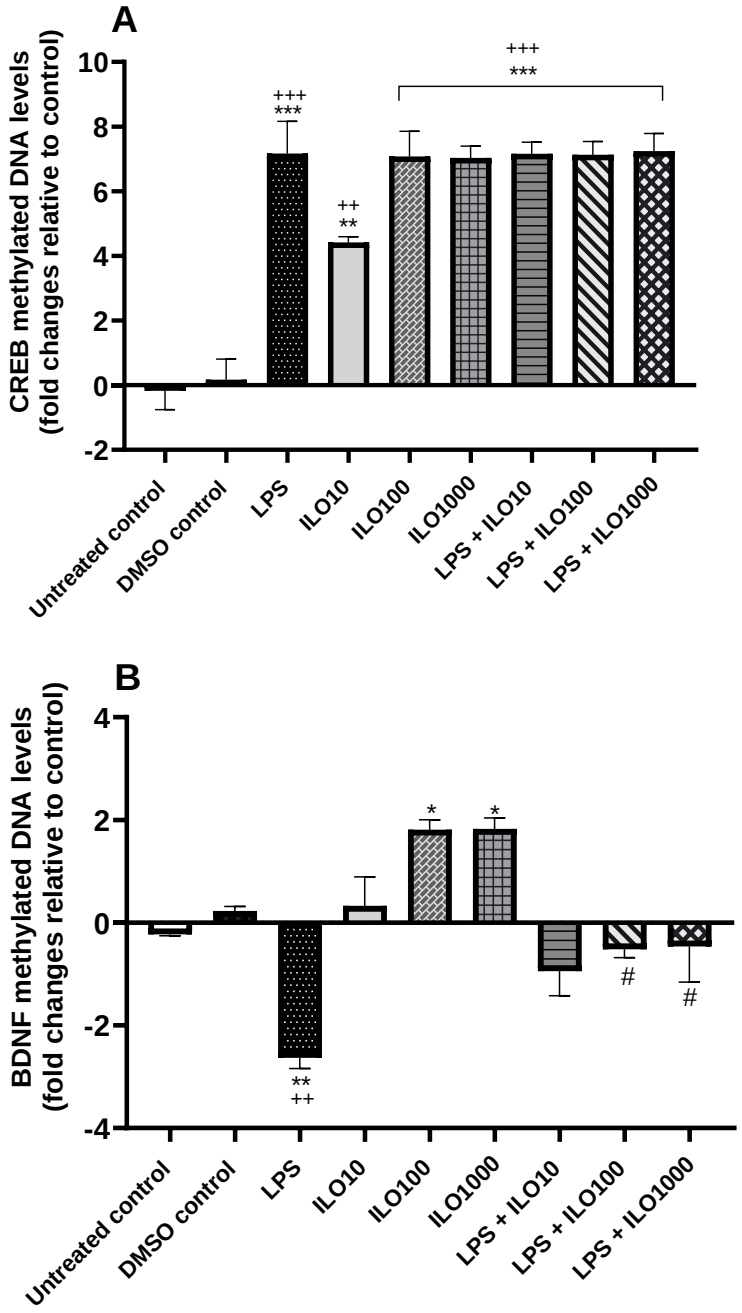

Fig. 30: *Effect of LPS and Iloprost treatment on CREB (**A**) and BDNF (**B**) methylated DNA expression 24 hours post treatment in C8-B4 cells. Data are represented as the Log_2 fold change of gene expression relative to GAPDH ± SEM from three independent experiments.Statistical analysis was carried out using One-Way ANOVA with Bonferroni's post hoc analysis.(**A**)* $F_{(8,26)} = 27.82$ *;* $p<0.0001$. $^{**}p = 0.001$ *and* $^{***}p<0.0001$ *compared to untreated control.* $^{++}p=0.002$ *and* $^{+++}p <0.0001$ *compared to DMSO control (**B**)* $F_{(8,26)} = 14.07$ *;* $p<0.0001$ *.* $^{*}p \leq 0.02$ *and* $^{**}p =$

0.007 compared to untreated control. ^{++}p = 0.001 compared to DMSO control. $^{\#}p \leq 0.002$ compared to LPS treatment.

4.7 Parasite estimation in the blood of trypanosome-infected mice.

To determine if inoculation with *T.b brucei* was successful, visualization of the parasite was carried out by blood-smear on days 3 and 7 (Fig.31). The total number of trypanosomes in each blood smear was obtained within a selected field of view while the average number of *T.b brucei* (Table 12) in all infected groups was determined. It is clear that using an inoculum of 5000 parasites was effective to establish infection in the *T.b brucei* control group. *T.b brucei* parasite counts were significantly higher in the positive control on day 7 compared to day 0 (p=0,003, Fig.32). When comparing treatments, Diminazene aceturate successfully eradicated the parasite by day 7 (p=0,0005, Fig. 32). On the contrary, the infected mice treated with repeated doses of Iloprost still presented with parasite in the blood.

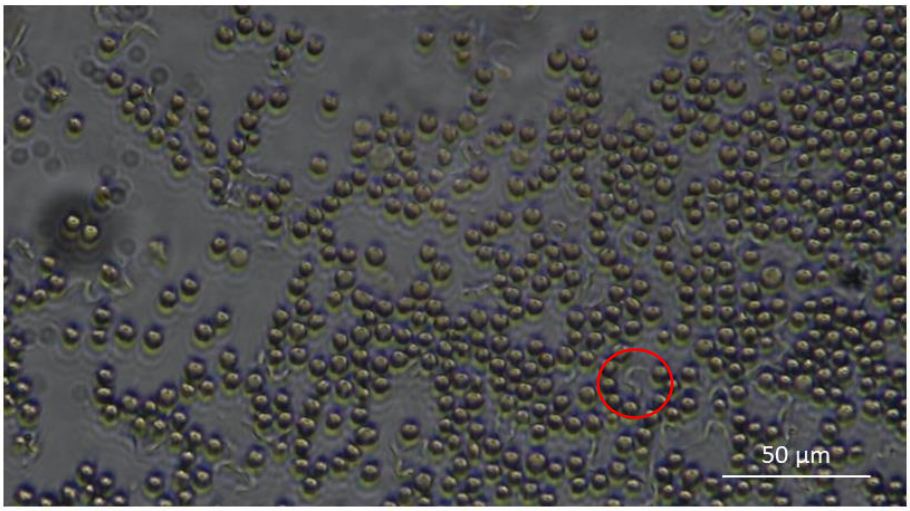

Fig. 31: *Visualization of parasitaemia in blood, obtained at 40x magnification. Scale bar = 50µm. T.b brucei can be observed as slender organism between red blood cells, highlighted in red circle.*

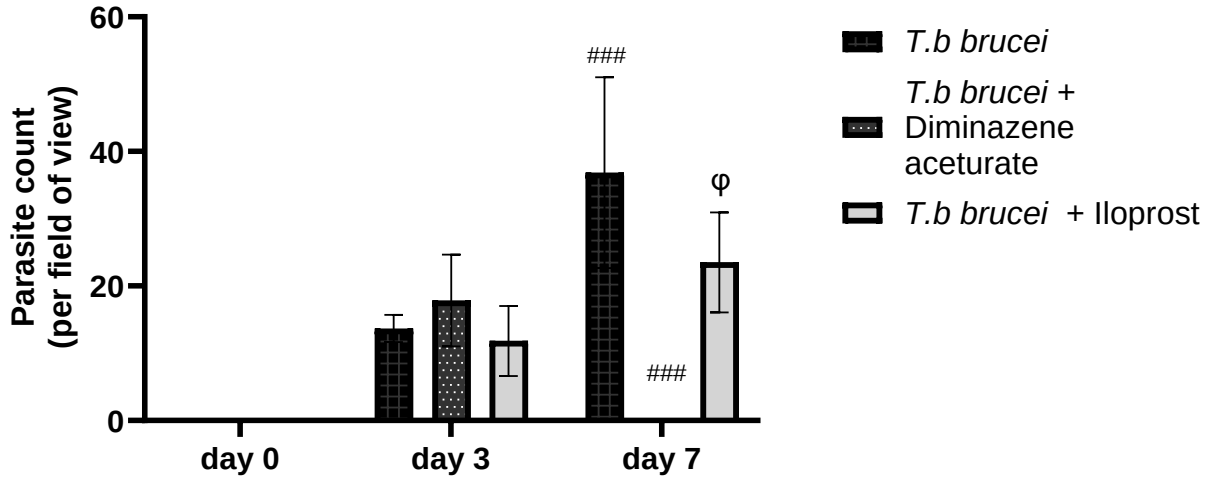

Fig. 32: *Average parasite count per field of view. Data was analysed using a mixed ANOVA with Bonferroni's multiple comparisons post hoc analysis.* $^{###}$*p=0.003 T.b brucei day 7 vs day 0.* $^{###}$*p=0.0005 T.b brucei + Diminazene aceturate day 7 compared to T.b brucei day 7.* $^{\Phi}$*p=0.03 T.b brucei + Iloprost vs T.b brucei + Diminazene aceturate day 7.*

4.8 Effect of Iloprost treatment on hippocampal TNFα/IL-1β gene expression.

To investigate trypanosome-induced inflammatory changes in the brain and possible neuroprotective roles of Iloprost, hippocampal TNF-α and IL-1β gene expression changes were determined in trypanosome infected mice after receiving repeated doses of Iloprost or a single dose of Diminazene aceturate.

A non-significant upregulation in hippocampal TNF-α gene expression was found compared to the control ($p>0.05$), meanwhile Iloprost treatment may likely be associated with downregulation in the expression of this gene (Fig. 33A). No statistically significant difference was observed for *T.b brucei* infection treated with a single dose of Diminazene aceturate.

Further 1.9-fold and 0.8-fold significant increases in hippocampal IL-1β mRNA levels were found following *T.b brucei* infection or co-exposure to *T.b brucei* and Diminazene aceturate treatments, respectively, compared to the wild-type ($p<0.05$, Fig. 32B). The results further showed no statistically significant difference in the hippocampal IL-1β mRNA levels of mice co-exposed to *T.b brucei* infection and Iloprost treatment compared to the wild-type control group ($p>0.05$, Fig. 32B). Interestingly, hippocampal IL-1β mRNA levels was significantly reduced by both Diminazene aceturate and

Iloprost treatments compared to the group of mice infected with *T.b brucei* only ($p<0.05$, Fig. 32B).

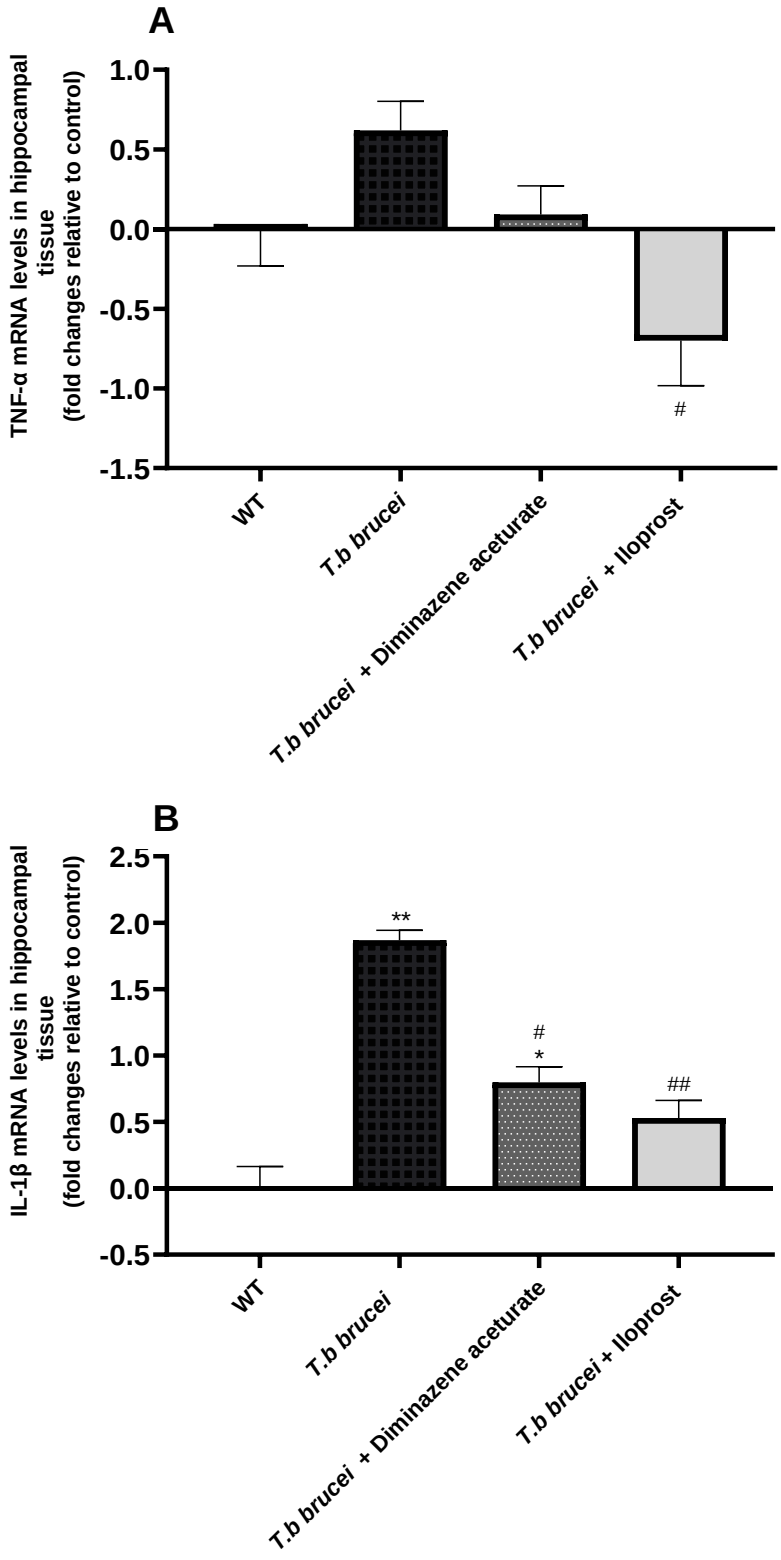

***Fig. 33**: (**A**) Changes in TNF-α mRNA gene expression in Trypanosome infected hippocampal tissue in response to a single dose of Diminazene aceturate and a repeated dose of Iloprost. Data represented as the Log_2 fold change of gene expression relative to GAPDH ± SEM from n=6. Statistical analysis was carried out using One-Way ANOVA*

*followed by Bonferroni's Post hoc analysis. $^{\#}p = 0.01$ compared to T.b infection. (**B**) IL-1 β mRNA gene expression in Trypanosome infected hippocampal tissue in response to a single dose of Diminazene aceturate and a repeated dose of Iloprost. Data represented as the Log_2 fold change of gene expression relative to GAPDH ± SEM from n=6. Statistical analysis was carried out using One-Way ANOVA. $^{*}p$ and $^{**}p$ compared to WT. $^{\#}p$ and $^{\#\#}p$ compared to T.b infection.*

4.9 Effect of Iloprost treatment on hippocampal CREB/BDNF gene expression.

To determine whether Iloprost would induce changes in hippocampal CREB expression in trypanosome infected mouse brain, mRNA expression of the gene was determined after repeated doses of Iloprost or a single dose of Diminazene aceturate. The results from this study (Fig.33) showed that there was no statistical significance when comparing CREB expression in *T.b brucei* infected animals to the control group. However, there was a significant 1.1-fold (p=0.008) upregulation of CREB in *T.b* treated animals with a single dose of Diminazene aceturate compared to *T.b brucei* infected animals alone. CREB expression was also significantly upregulated 1.9-fold with repeated doses of Iloprost compared to *T.b brucei* infected animals alone (p=0.002). However, no significant difference was observed when comparing *T.b brucei* infected animals treated with Diminazene aceturate to *T,b brucei* infected animals treated with Iloprost.

No statistically significant changes in BDNF mRNA levels were found when comparing *T.b brucei* infected animals to the control group (fig.33 B). This trend was also observed with *T.b* infected animals treated with a single dose of Diminazene aceturate. However, when comparing *T.b brucei* infected animals treated with repeated doses of Iloprost to *T.b brucei* infected animals alone, a 3.2-fold increase in BDNF transcription was observed (p=0.017).

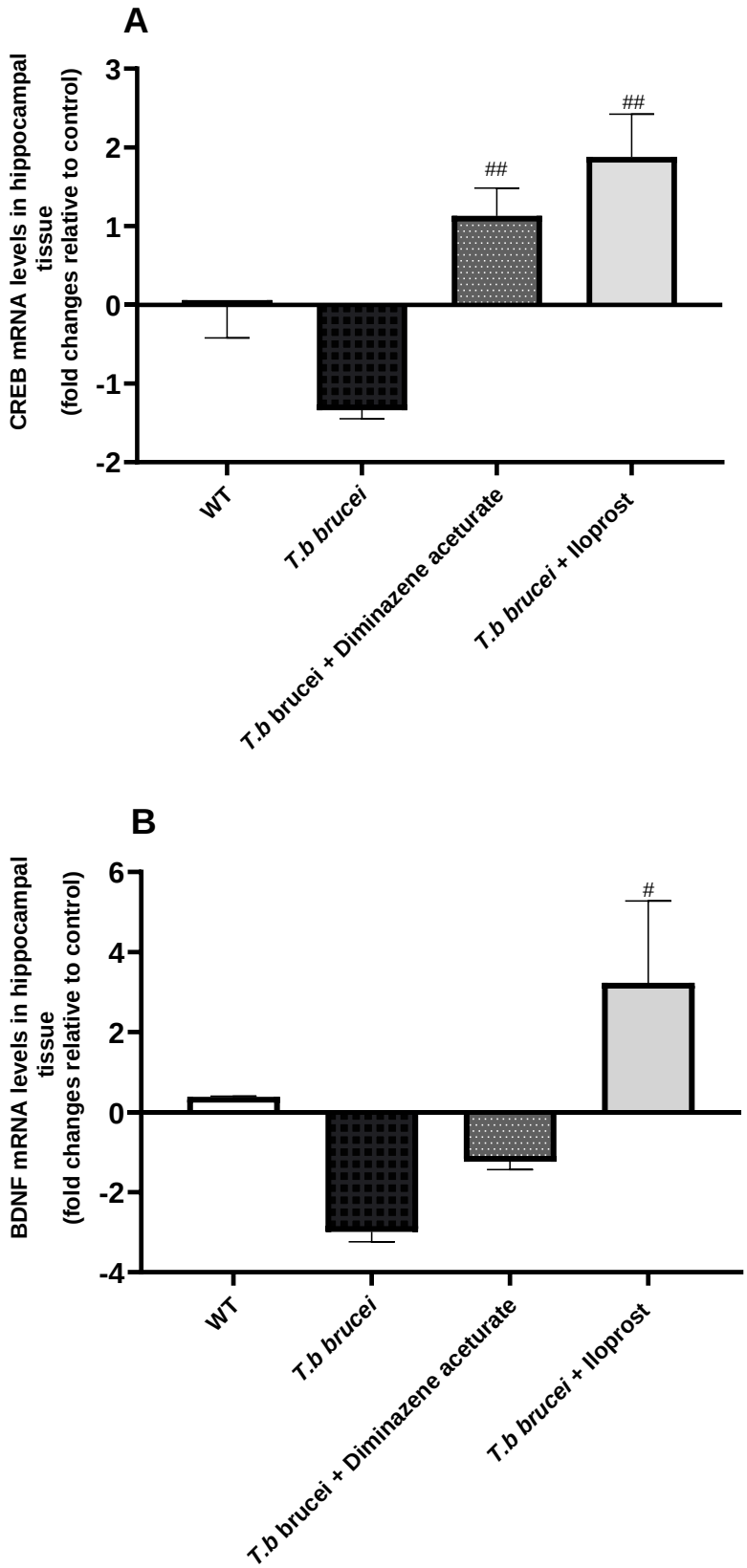

Fig. 34: *Effect of Iloprost and Diminazene aceturate treatment on hippocampal CREB (**A**) and BDNF (**B**) expression in trypanosome infected mouse. Data represented as the Log_2 fold change of gene expression relative to GAPDH ± SEM from n=6. Statistical analysis was carried out using One-Way ANOVA with Bonferroni's post hoc analysis. (**A**) $^{\#}p = 0.016$ and $^{\#\#}p = 0.002$ compared to T.b infection. (B) No statistical significance was observed in BDNF expression.*

CHAPTER FIVE

DISCUSSION

Neurodegeneration is a well-established feature observed in numerous neuroinflammatory diseases (Chen *et al*., 2016, Corallo *et al*., 2022). They often initiate with an immediate immune response to injured neurons or infectious agents as seen in the case of HAT. Neuroinflammation serves as a primary mechanism for safeguarding the brain by eliminating pathogens and preventing their dissemination. Microglia are central to this mechanism where they play key roles in regulating inflammatory responses within the CNS, exhibiting neurotoxic or neuroprotective characteristics based on specific circumstances.

The CNS is a tightly regulated environment and differs from the periphery in cell types and inflammatory responses. In the CNS, microglia constitute the bulk of the immune cells where they function in removing cell debris and damaged neurons and eradicating infectious agents (Wake and Douglas, 2011). Microglial cells play a part in tissue homeostasis by observing the microenvironment, they exhibit a M0 phenotype under healthy conditions and will undergo phenotype switching to either pro or anti-inflammatory states based on changes in the microenvironment (Wei and Li, 2022). In their M0 phenotype, microglia are functionally dormant, have absent expression of activation molecules, and do not display antigen-presenting molecules (Lier *et al*., 2021). Microglia are also not uniformly distributed across the brain and are found in highest numbers in the hippocampal dentate gyrus, substantia nigra, and parts of the basal ganglia (Tan *et al*., 2020, Lawson *et al*., 1990). The number of microglia is also regulated by the microenvironment and changes therein, they can proliferate under conditions that include stress, aging, and infectious disease (Mander *et al*., 2006, Schramm and Waismain, 2022). Proliferative microglia are known to take up M1 or M2 states known as pro-inflammatory and anti-inflammatory respectively.

The hallmark of M1 phenotype microglia is the secretion of pro-inflammatory cytokines, TNF-α and IL-1β, where M1 activation relies on the secretion of these pro-inflammatory cytokines (Orihuela *et al*., 2016). M1 polarization is achieved through stimulation of TLR on the cell surface of microglia by molecules such as PAMP, LPS, and IFN-γ (Guo *et al*., 2022). Contrary to this, M2 microglia can resolve the

inflammatory process by secreting anti-inflammatory cytokines and fostering tissue repair through releasing growth factors, ultimately restoring tissue homeostasis (Uzcategui *et al*., 2023,). Under normal immune responses, once the pathogen is removed via activation of pro-inflammatory pathways, the anti-inflammatory response is favored and characterized by debris clearance and tissue repair (Mantovani *et al*., 2012). However, in the case of *T.b* infection, the persisting pathogen may cause prolonged pro-inflammatory responses and thus leads to further damage to brain tissue. The current study revealed that LPS challenge evoked production of high levels of TNF-α and IL-1β in C8-B4 microglial cells and these changes were comparable to gene expression changes in the single cells. A similar trend was also observed in the *in vivo* experiment, as the results demonstrated an upregulation in IL-1β gene expression in the hippocampi of albino swiss mice infected with *T.b brucei*. These results confirm that both gram-negative bacteria (100 ng mL^{-1} of LPS) and *T.b brucei* infection (5000 inoculum) can sufficiently induce inflammatory changes in single cells or CNS parenchyma, respectively.

Prostacyclin and its analogues have recently become a therapy of interest in various neurogenerative diseases and most importantly for its anti-inflammatory properties (Eisenhut *et al*, 1993; Ipseiz *et al*., 2020). This study first investigated the neuroprotective roles of Iloprost against toxic and inflammatory changes induced by LPS in microglial cells. Similar to previous findings by Zhao *et al*.,(2019), the current study established that 100 ng mL^{-1} of LPS is cytotoxic to neuronal cells (Zhao *et al*., 2019) evidenced by decreased cell viability. Whereas subsequent treatment with Iloprost improved the cell viability with 100 and 1000 ng mL^{-1} concentrations exhibiting the highest efficacy. This suggests that higher concentrations of Iloprost are beneficial for microglia functions which may possibly be attributed to the neuroprotective roles of this compound against cytotoxic effects of LPS. These results are further reinforced with the identification of microglial activation with IBA-1 positive immunofluorescence for LPS and Iloprost treated cultures. IBA-1 is a calcium-binding adapter molecule that has a significant role in the functional change of microglia. It serves as a reliable marker for various forms of microglia not only in the central nervous system but also in other organs. Previous studies have found an increase in IBA-1 expression when microglia become activated during immune responses within the CNS (Lee *et* al.,

2017, Ton *et al*., 2013, Norden *et al*., 2016). We, therefore, used IBA-1 as a primary marker for microglial activation.

To further analyze microglia phenotypes, CD86 was used as a secondary marker. CD86 is a microglial cell surface marker indicative of M1 polarization associated with the pro-inflammatory response (Zhang *et al*., 2023). The activation states showed CD86 positive cell populations in LPS treated cultures. Subsequent treatment of the M1 polarized cultures with Iloprost showed CD86 negative cell populations 24 hours after treatment. This finding shows that there is a shift from M1 polarization with Iloprost treatment across all tested concentrations of 10,100 and 1000 ng mL^{-1}. M1 polarized microglia secrete pro-inflammatory cytokines TNF-α and IL-1β (Orihuela *et al*., 2016). The levels of pro-inflammatory cytokines were quantified using ELISA to determine the concentration of secreted cytokines in response to Iloprost treatment. An increase in the concentration of both TNF-α and IL-1β in response to LPS treatment were measured, which is consistent with previous report by Mizobuchi *et al*. (2020). Therefore, it is possible that LPS exposure successfully induced inflammatory changes in the microglia. Further, TNF-α and IL-1β secretion by microglia were reduced by Iloprost treatments. This result is in line with previous studies, confirming that Iloprost has the potential to exert its anti-inflammatory effects by inhibiting endogenous production of pro-inflammatory cytokines (Eisenhut *et al*, 1993, Ipseiz *et al*., 2020).

Yang and colleagues (2019) have previously reported that inhibiting M1 microglial activation alone is not enough to combat the negative effects of neurodegenerative disease, treating these diseases also relies on promoting M2 microglial activation simultaneously. To examine if Iloprost is also capable of promoting M2 microglial activation, CD206 was used as a secondary marker for M2 polarization. CD206 is a commonly used marker for M2 polarized microglia, the results from our study revealed CD206 negative cell populations in microglia exposed to LPS challenge whereas CD206 positive cells were associated with microglia co-treated with LPS and varying doses of Iloprost. To quantify the changes in CD206 expression, fluorescence intensity was measured across treatment cultures. It was observed that resting cells undergo M2 polarization in the presence of varying doses of Iloprost. This is the first study to confirm successful M2 polarization in microglial with Iloprost treatments. The Iloprost-

induced phenotypic swich from M1 to M2 emphasizes the importance of Iloprost in cellular reparative processes and may serve as a potent therapeutic agent that may help combat oxidative damage and neurodegeneration (Cherry *et al*.,2014). To further characterize the anti-inflammatory potential of Iloprost, gene expression changes in CD206 and ARG-1 was determined. LPS treatment significantly down-regulated CD206 transcription in C8-B4 cells, this was consistent with immunofluorescent data. Furthermore, it was determined that CD206 transcription was significantly upregulated in both resting and LPS treated microglia exposed to varying doses of Iloprost. LPS treatment induced a 4.5-fold increase in ARG-1 gene transcription, this is consistent with a study demonstrating that LPS is capable of inducing ARG-1 transcription 24 hours later (Menzies *et al*., 2010). They further determined that ARG-1 transcripts were significantly increased 24 hr post LPS treatment and continued to increase up to 48 hr post treatment. To determine if Iloprost had any effect on mRNA transcription of ARG-1 gene, resting and LPS-treated microglia were exposed to various doses of Iloprost. Resting microglia treated with high doses (100 and 1000 ng mL^{-1}) of Iloprost showed a 5 and 6-fold increase in ARG-1 mRNA levels compared to the control cultures. Interestingly, ARG-1 transcription was not further increased in the presence of both LPS and Iloprost treatment possibly indicating that Iloprost does not cause over-expression of ARG-1 post inflammatory response. Currently no studies have reported on the expression of ARG-1 in response to Iloprost treatment on LPS induced inflammation. Therefore, determining the exact mechanism of action and pathways affected could form part of future studies.

Since BDNF plays important roles in neuronal growth and survival (Yamada *et al*., 2002), the contribution of BDNF to the neuroprotective effects of Iloprost was examined. BDNF secretion was not increased in LPS treated microglia after 24 hr of exposure. This is contrary to findings in a recent study that reported increased BDNF after 24 hr of LPS treatment (Charlton *et al*., 2023). Differences in the result observed could be attributed to differences in the maintenance of the C8-B4 culture or the laboratory environment prior to LPS treatment. However, the observed changes in BDNF secretion are consistent with findings in a recent study conducted in our laboratory, as the authors also reported a significant increase in BDNF secreted by microglia within 12 hr of LPS exposure. This was followed by a decrease in BDNF after 24 hr of LPS treatment (unpublished data). When examining BDNF secretion in

resting microglia significant increases in BDNF concentration were observed across all cultures exposed to varying concentrations of Iloprost without LPS stimulation. The same trend was also observed for LPS treated microglia exposed to varying doses of Iloprost. Significantly, Iloprost induced increases in BDNF release at a dose dependent rate. This data indicates that Iloprost could promote the survival or neurons and support neurogenesis through increasing BDNF secretion from resting and activated microglia.

In vitro studies form the basis of medical research for the confirmation of therapeutic potential before progressing to *in vivo* studies. *In vitro* models have been one of the key methods used by researchers to find ways to treat human diseases and disorders (Saeidnia et al., 2015). Where animal models carry ethical considerations as well as high costs, *in vitro* studies allow for more feasible, systematic, repetitive, and quantitative investigation of potential therapeutic agents (Elliot, Yuan. 2010). This enables the potential effects of the agents on cellular function and viability to be determined before carrying out research in an animal model. However, murine models are ideal for use in studying disease as they are physiologically similar to humans and their genomes easily manipulated to create murine models of various human diseases to study the efficacy and toxicity of drugs (Bedell *et al*., 2016). Murine models also allow for highly infectious diseases to be studied. The present study sought to combine these two models of research to identify and compare gene expression changes associated with microglial exposure to LPS and trypanosome infected mouse hippocampal brain tissue. mRNA transcriptional changes were quantified for pro-inflammatory genes, TNF-α and IL-1β, post inflammatory insult and subsequent treatment with Iloprost. Previously, TNF-α and IL-1β have been associated with a negative impact on cognitive function (Derecki *et al*., 2009). In our *in vitro* study TNF-α mRNA levels were increased 15-fold in resting cells exposed to LPS, which agrees with previous report that binding of LPS to the LPS-binding protein starts the pro-inflammatory cascade (Guo *et al*., 2022). Surprisingly, *T.b brucei* infection did not statistically alter TNF-α gene expression in the mice but evoked significant transcriptional upregulation in IL-1β gene expression. In general, *T.b brucei* infection is expected to activate antigen-presenting cells and resident microglia to stimulate the pro-inflammatory processes in an attempt to eradicate or alleviate the parasite burden (Kennedy and Rodgers, 2019). Hence most previous studies that investigated the

pathology of trypanosome have reported parasite-induced increases in the expression of pro-inflammatory genes which are often associated with moderate to severe neuroinflammatory reactions (Kennedy and Rodgers, 2019, Amin *et al*., 2012). Therefore, increased gene expression of IL-1β post *T.b* infection confirms activation of pro-inflammatory molecules that may help restore cellular homeostasis. However, a lack in the expected up-regulation in TNF-α transcription would need to be further investigated, as the data trended towards an increase. A possible reason for not observing a statistically significant result could be due to RNA degradation during the extraction process and a larger sample size could be employed to investigate this in future studies.

A key challenge to treating *T.b* infection is antigenic shifting coupled with toxicity of trypanolytic drugs. Also trafficking of curative drugs across the BBB as the trypanosome is shielded from most drugs once it has reached the CNS stage of the disease. Studies have shown that prostacyclin and its synthetic analogues, such as Iloprost, have the potential to suppress inflammatory changes elicited by the parasitic infection (Eisenhut *et al*, 1993; Ipseiz *et al*., 2020). To then determine whether Iloprost could protect against the inflammatory response, cells exposed to LPS were treated with 10, 100 and 1000 $ng.mL^{-1}$ of Iloprost. Microglial cells initially exposed to LPS challenge and later treated with varying concentrations of Iloprost exhibited significant decreases in TNF-α and IL-1β mRNA levels. When comparing these results to the animal model of *T.b brucei* infection, a similar trend was observed with both TNF-α and IL-1β transcriptionally downregulated in *T.b brucei* infected mice treated with repeated dosages of Iloprost.

Dysregulation or excessive production of IL-1β among other pro-inflammatory cytokines has been identified as one of the main causes of death in mice models of trypanosomiasis (Shi *et al*., 2002) and often associated with chronic inflammation and destruction of functional tissues (Uzonna *et al*., 1998, Shi *et al*., 2003). The findings from both *in vitro* and *in vivo* experiments confirm that Iloprost not only inhibits pro-inflammatory cytokines but also plays an immunomodulatory role by shifting microglial activation from pro to anti-inflammatory. Therefore, Iloprost could be a more promising therapeutic agent for treating *T.b brucei* infection as opposed to Diminazene aceturate as it showed to be a more potent inhibitor of pro-inflammatory gene expression.

However, a key parameter to also take into consideration is parasite clearance. Since the *T.b* is able to undergo antigenic shifting to avoid the host immune response (Levison, 2016). The present study showed that Diminazene aceturate successfully cleared the parasite from the blood by day 7 compared to Iloprost treatment and the *T.b brucei* infected control. More data is needed to draw a conclusion from this as the investigative drug could take more time to present its anti-trypanolytic effects. Using Iloprost as an alternative therapy would not only address issues such as cost of Diminazene aceturate but also drug toxicity and drug resistance (Jennings and Gray, 1983, Anene *et al*., 2005, Assefa and Shibeshi, 2018).

To determine if Iloprost enhances secretion of neuroprotective molecules CREB and BDNF, mRNA transcription levels were determined both *in vitro* and *in vivo*. LPS challenge induced a significant increase in CREB transcription in C8-B4 microglial cells, which agrees with previous findings by Avni *et al*. (2010) who demonstrated that CREB activity was increased in macrophages exposed to LPS stimulation. Based on the understanding gained from extensive research this is the first study to examine the effects of LPS challenge on CREB transcription in C8-B4 microglial cells. A high concentration of Iloprost (1000 ng mL^{-1}) induced a further 2-fold upregulation of CREB transcription in LPS treated microglia. CREB is linked to BDNF which modulates the growth and complexity of dendrites, facilitates long-term potentiation, regulation of neuronal development and survival of neuronal cells (Yamada *et al*., 2002, Ibrahim *et al*., 2022). Phosphorylation of CREB ultimately leads to BDNF transcription via Erk (MAPK) pathway to promote neuronal growth, survival, and plasticity (Ibrahim *et al*., 2022). Since BDNF is central to the survival of neuronal cells, the present study sought to investigate if Iloprost induces transcriptional changes in BDNF. Resting and LPS exposed cell cultures were treated with 10,100 and 1000 ng mL^{-1} of Iloprost. BDNF was upregulated 2-fold in LPS treated cultures compared to untreated controls. This is consistent with previous studies showing that LPS stimulates the synthesis of BDNF (Miwa et al., 1997, Gomes *et al*., 2013). Interestingly this did not translate into ELISA data which showed no significant difference in secreted BDNF at 24-hrs. BDNF mRNA was also upregulated 2-fold in resting cells treated with 1000 ng mL^{-1} of Iloprost. This study is the first of its kind to investigate the transcriptional changes associated with BDNF in Iloprost treatment. For cultures exposed to both LPS and 1000 ng mL^{-1} of Iloprost, a 2-fold upregulation in BDNF mRNA was observed, this is similar to the

degree of upregulation seen in LPS treatment alone. The cultures exposed to LPS and either 10 or 100 ng mL^{-1} of Iloprost only, showed a 1-fold increase in BDNF transcription in comparison to control cultures. Interestingly, the combination of LPS and Iloprost treatment did not cause overexpression of BDNF mRNA, suggesting that Iloprost could possibly play a modulatory role in BDNF transcription. When comparing the results in this study to the *in vivo* study, CREB mRNA levels do not seem to be elevated in *T.b* infected hippocampal tissues. However, when comparing the infected groups treated with Diminazene aceturate and the infected groups treated with Iloprost, there was a 1 and 2-fold increase in CREB transcription compared to the *T.b brucei* infected group. When comparing data on BDNF mRNA expression in the *in vitro* study to the *in vivo* study, BDNF transcription was also upregulated 3-fold in the infected group treated with Iloprost while no significant difference was observed in the *T.b* infected group receiving Diminazene aceturate. This further reinforces the evidence that Iloprost could be a more promising therapy for the treatment of *T.b brucei* infection. Currently no studies have been done to investigate Iloprost as a potential therapy or to examine its potential to upregulate transcription of neuroprotective cytokines in an animal model. However, it is known from a study reported by Tesoriero and colleagues (2018) that significant neuronal loss is observed with *T.b* infection. Therefore, treating the infection should not only include eradicating the parasite but also promoting neurogenesis and neuronal survival.

To determine the epigenetic changes associated with microglial response to LPS-insult, CREB and BDNF DNA methylation profiling was carried out. Epigenetic modifications control gene expression patterns. DNA methylation in the brain is a crucial factor in acquiring and retaining memories, as it usually functions to suppress gene expression (Zoghbi and Beaudet, 2016). Changes in the methylation status of genes associated with synaptic plasticity and memory can occur rapidly and be reversible, contrary to the initial belief that methylation served as a stable gene silencing mark (Hwang *et al*., 2017). In the phenotypic transformation of microglia into the M2 state, there is a shift in the activation and expression of particular microglial genes, which is influenced by epigenetic modifications like DNA methylation (Petralla *et al*., 2021). Recent studies have also found DNA methylation to be key in synaptic plasticity and neuronal stem cell differentiation (Juliandi *et al*., 2010, Heyward and Sweatt, 2015). However, the methylation status of genes for the specific proteins,

BDNF and CREB, that are important for memory and synaptic plasticity has yet to be characterized in LPS induced neuroinflammation coupled with Iloprost treatment.

The results from the present study show a 7-fold upregulation in methylation of the CREB promoter region in LPS treated cultures compared to untreated controls. Similar changes were observed across resting cells and LPS treated cultures exposed to high doses of Iloprost however, Iloprost did not induce a further increase in CREB methylation compared to LPS treated cultures. Interestingly transcription levels measured at the same 24 hr time point showed upregulation of the CREB gene in LPS treated cultures. In general, CREB exhibits pleiotropic nature in its response to LPS-induced inflammatory changes (Wen *et al*., 2010). In this study, hypermethylation of CREB agrees with a previous study that demonstrated transcriptional silencing of this gene as means to control inflammatory responses evoked by LPS treatment (Guo *et al*., 2014). Even though the transcriptional efficiency of this gene is expected to decrease within the promoter region, but the observed upregulation in CREB mRNA transcripts may suggest an acute response to LPS-induced inflammatory changes with possibility of reversal in the transcriptional state if examined beyond the initial 24 hours subject to peak period activities. Another reason for the observed increase in methylation at the CREB promoter region could potentially indicate transcriptional regulation through negative-feedback mechanisms resulting in silencing of the CREB gene after 24 hrs. Previous studies have shown that overexpression of CREB is associated with resistance to antiproliferative signals, increased cell metabolism and tumor-promoting inflammation (Xia *et al*., 2018, Zheng *et a*l., 2019). These changes were then also investigated in the BDNF promoter region. The findings of the current study show that LPS treatment induced hypomethylation of BDNF in microglial cells. These results corroborate the upregulation of BDNF transcription in LPS treated cultures, as BDNF is known to promote the survival and growth of neurons (Ibrahim *et al*., 2022). Hypomethylation of BDNF however is reversed in the presence of high concentrations of Iloprost. Furthermore, high concentrations of Iloprost also induced hypermethylation of the BDNF promoter region in comparison to the control cultures. Since this study is the first to present the effects of Iloprost treatment on BDNF methylation levels, the closest comparison in literature was a study by Martinowich *et al*., (2003). They explored the involvement of DNA methylation in controlling BDNF expression in cortical cultures. The results from their *in vitro* study demonstrated that

neuronal activity plays a role in regulating the activation of BDNF transcription and BDNF transcription is increased with an increase in neuronal activity (Martinowich *et al*., 2003, Bathina and Das, 2015). Furthermore, hypermethylation at specific promoter regions can suppress activity-dependent transcription of BDNF. Since Iloprost promotes the phenotypic switching of M1 to M2 microglia, mediating wound healing, inhibiting proliferation, and stimulating anti-inflammatory cytokine secretion, methylation of BDNF could be in response to reduced microglial M1 activity as the inflammatory state has been resolved.

CHAPTER SIX.

CONCLUSION AND FUTURE RESEARCH

6.1 Conclusion

This study aimed to investigate the neuroprotective roles of Iloprost by comparing neuroinflammatory changes in microglial cells and trypanosome infected mouse brain. The study further intended to determine whether Iloprost treatment would induce phenotypic switching in activated microglia, while examining the therapeutic potential of Iloprost against trypanosome induced inflammation, as well as the epigenetic changes associated with LPS-induced inflammation in microglial cells.

This study is the first to confirm M2 microglial polarization in the presence of Iloprost treatment and to examine the epigenetic changes associated with Iloprost treatment in LPS-induced inflammation. Previous studies have shown that prostacyclin and its synthetic analogues can decrease the production of inflammatory cytokines such as TNF-α and induce the production of anti-inflammatory cytokines which further plays a role in regulating and inhibiting the production of pro-inflammatory cytokines (Eisenhut *et al*, 1993; Luttmann *et al*, 1999, Ipseiz *et al*., 2020). This, however, was investigated in peripheral blood mononuclear blood cells, this study is the first to investigate these effects in a neuronal cell line.

Microglia-mediated neurotoxicity is a result of activation through pattern recognition receptors when there is an excessive immune response, this activation leads to the production of pro-inflammatory cytokines that can damage neuronal tissue (Block *et al*., 2007). Previous studies link dysregulation of the cytokine network, excessive production of inflammatory cytokines, and the release of inflammatory mediators as the major cause of death in infected humans and animals (Uzonna *et al*., 1998, Shi *et al*., 2003). This further supported the need to investigate methods of alleviating neuroinflammatory and parasite-elicited pathology through attenuating the production of pro-inflammatory cytokines. This study produced results which demonstrated that Iloprost does in fact down-regulate pro-inflammatory cytokine production in response to both LPS induced inflammation and *T.b brucei* infection. Moreover, the *in vitro* model established transcriptional upregulation in anti-inflammatory genes; ARG-1, CD206, BDNF and CREB in response to Iloprost treatment on LPS-induced

inflammation. These results were confirmed with *in vivo* studies also presenting upregulation of BDNF transcription in *T.b brucei* infected animals treated with repeated Iloprost dosages. A limitation of the study is that inhibitory concentrations of Iloprost on *T.b brucei* was not carried out and also parasite clearance rate could not be determined.

6.2 Future directions.

Future studies are required to understand the exact implications of the methylation status at CREB and BDNF promoter regions. Furthermore, to employ a loss-of function approach to gain a better understanding into the exact molecular pathways used by Iloprost in exerting its anti-inflammatory and anti-*Tb* effects in single cells or whole organisms. It is also desirous to establish if high doses of Iloprost can halt the replication of trypanosomes in blood before gaining access into the CNS parenchyma or sufficiently elicit parasite clearance in the brain, while also investigating the rate of parasite clearance in *T.b* infected mice treated with Iloprost.

REFERENCES

Adeyemi, O. and Sulaiman, F., 2012. Biochemical and morphological changes in Trypanosoma brucei brucei- infected rats treated with homidium chloride and Diminazene aceturate. J Basic Clin Physiol Pharmacol, 23(4).

Afridi, R., Kim, J., Rahman, H., Suk, K., 2020 'Metabolic regulation of glial phenotypes: Implications in neuron–glia interactions and neurological disorders', Front Cell Neurosci, 14.

Agarwal, N., Taberner, F. J., Rangel Rojas, D., Moroni, M., Omberbasic, D., Njoo, C., … Kuner, R. 2020. Sumoylation of enzymes and ion channels in sensory neurons protects against metabolic dysfunction, neuropathy, and sensory loss in diabetes. Neuron, 107(6). doi:10.1016/j.neuron.2020.06.037

Aid, T., Kazantseva, A., Piirsoo, M., Palm, K., & Timmusk, T. 2006. Mouse and rat bdnf gene structure and expression revisited. Journal of Neuroscience Research, 85(3), 525–535. doi:10.1002/jnr.21139

Aitcheson, N., Talbot, S., Shapiro, J., Hughes, K., Adkin, C., Butt, T., … Rudenko, G. 2005. VSG switching in trypanosoma brucei: Antigenic variation analysed using rnai in the absence of immune selection. Mol Micro, 57(6), pp.1608–1622.

Ajonijebu, D., Abboussi, O., Mabandla, M. and Daniels, W., 2017. Differential epigenetic changes in the hippocampus and prefrontal cortex of female mice that had free access to cocaine. Metab Brain Dis, 33(2), pp.411-420.

Alhajj M, Farhana A. Enzyme Linked Immunosorbent Assay, 2021 In: StatPearls [Internet]. Treasure Island (FL): StatPearls Publishing; 2021 Jan-. Available from: https://www.ncbi.nlm.nih.gov/books/NBK555922/

Amin, D., Rottenberg, M., Thomsen, A., Mumba, D., Fenger, C., Kristensson, K., Büscher, P., Finsen, B. and Masocha, W., 2009. Expression and Role of CXCL10 during the Encephalitic Stage of Experimental and Clinical African Trypanosomiasis. J Infect Dis, 200(10), pp.1556-1565.

Amor S, Puentes F, Baker D, van der Valk P, 2010.Inflammation in neurodegenerative diseases. J Immunol, 129:154–169.

Arya, M., Shergill, I., Williamson, M., Gommersall, L., Arya, N. and Patel, H., 2005. Basic principles of real-time quantitative PCR. Expert Rev Mol Diagn, 5(2), pp.209-219.

Baglio, F., Saresella, M., Preti, MG., Cabinio, M., Griffanti, L., Marventano, I., Piancone, F., Calabrese, E., Nemni, F., Clerici, M., 2013. 'Neuroinflammation and brain functional disconnection in alzheimer's disease', Front Aging Neurosci, 5. doi:10.3389/fnagi.2013.00081.

Baral, T., 2010. Immunobiology of African Trypanosomes: Need of Alternative Interventions. J Biomed Biotech, pp.1-24.

Barton, C. H., Ajioka, J. W., Roach, T. I. A., & Blackwell, J. M. 1992. Mapping CREB-1 to chromosome 1 in the mouse. Genomics, 14(3), pp.790–792.

Bathina, S. and Das, U., 2015. Brain-derived neurotrophic factor and its clinical implications. Arch Med Sci, 6, pp.1164-1178.

Batista, P., & Pereira, A. 2016. Biomarkers in neurodegenerative diseases: cortisol. J Mol Biomark Diagn, 7(2), 1000277

Bhattacharjee, A., Shukla, M., Yakubenko, V., Mulya, A., Kundu, S. and Cathcart, M., 2013. IL-4 and IL-13 employ discrete signaling pathways for target gene expression in alternatively activated monocytes/macrophages. Free Radc Biol Med, 54, pp.1-16.

Block, M. L., Zecca, L., & Hong, J. S. 2007. Microglia-mediated neurotoxicity: uncovering the molecular mechanisms. Nat rev. Neurosci, 8(1), 57–69.

Bottieau, E. and Clerinx, J., 2019. Human African Trypanosomiasis. Infect Dis Clin North Am, 33(1), pp.61-77.

Bouteille, B. and Buguet, A., 2012. The detection and treatment of human African trypanosomiasis. Res Rep Trop Med, 3, pp.35-45.

Braakman, H. M., van de Molengraft, F. J., Hubert, W. W., & Boerman, D. H., 2006. Lethal African trypanosomiasis in a traveler: MRI and neuropath. Neurol, 66(7), pp. 1094–1096.

Brombacher, T., Nono, J., De Gouveia, K., Makena, N., Darby, M., Womersley, J., Tamgue, O. and Brombacher, F., 2017. IL-13–Mediated Regulation of Learning and Memory.J Immunol, 198(7), pp.2681-2688.

Bryant, A., Spencer-Harty, S., Owens, S., Jones, R. and Thornton, C., 2017. Interleukin 4 and interleukin 13 downregulate the lipopolysaccharide-mediated inflammatory response by human gestation-associated tissues†. Biol Reprod, 96(3), pp.576-586.

Büscher, P. et al., 2018. 'Do cryptic reservoirs threaten gambiense-sleeping sickness elimination?', Trends in Parasitology, 34(3), pp. 197–207.

Centers for Disease Control and Prevention, C., 2020. CDC - African Trypanosomiasis - Biology. [online] Cdc.gov. Available at: <https://www.cdc.gov/parasites/sleepingsickness/biology.html> [Accessed 25 March 2021].

Chen, W. W., Zhang, X., & Huang, W. J. 2016. Role of neuroinflammation in neurodegenerative diseases (Review). Mol med rep, 13(4), pp.3391–3396.

Chiaramonte, M., Mentink-Kane, M., Jacobson, B., Cheever, A., Whitters, M., Goad, M., Wong, A., Collins, M., Donaldson, D., Grusby, M. and Wynn, T., 2003. Regulation and Function of the Interleukin 13 Receptor α 2 During a T Helper Cell Type 2–dominant Immune Response. J Exp Med, 197(6), pp.687-701.

Corona, A., 2020. 'Disease Eradication: What Does It Take to Wipe out a Disease?', American society for microbiology, 6 March.

Crowther J.R.,1995. Basic Principles of ELISA. Methods Mol Biol, Humana Press, 42.

Cuypers, B., Lecordier, L., Meehan, C. J., Van den Broeck, F., Imamura, H., Büscher, P., Dujardin, J. C., Laukens, K., Schnaufer, A., Dewar, C., Lewis, M., Balmer, O., Azurago, T., Kyei-Faried, S., Ohene, S. A., Duah, B., Homiah, P., Mensah, E. K., Anleah, F., Franco, J. R., … Deborggraeve, S. 2016. Apolipoprotein L1 Variant Associated with Increased Susceptibility to Trypanosome Infection. M Bio, 7(2).

Daneman, R. and Prat, A., 2015. The Blood–Brain Barrier. Cold Spring Harb Perspect Biol, 7(1).

De Chiara, G., Marcocci, M. E., Sgarbanti, R., Civitelli, L., Ripoli, C., Piacentini, R., Garaci, E., Grassi, C., & Palamara, A. T. 2012. Infectious agents and neurodegeneration. Mol neurobiol, 46(3), pp.614–638.

Derecki NC, Cardani AN, Yang CH, Quinnies KM, Crihfield A, Lynch KR, Kipnis J, 2010. Regulation of learning and memory by meningeal immunity: a key role for IL-4. J Exp Med, pp.1067– 1080.

Dhikav, V., & Anand, K. 2012. Hippocampus in health and disease: An overview. Ann Indian Acad Neurol, 15(4), pp.239.

Drennan, M., Stijlemans, B., Van Den Abbeele, J., Quesniaux, V., Barkhuizen, M., Brombacher, F., De Baetselier, P., Ryffel, B. and Magez, S., 2005. The Induction of a Type 1 Immune Response following a Trypanosoma brucei Infection Is MyD88 Dependent. J Immunol, 175(4), pp.2501-2509.

Dunn, N., Wang, S. and Adigun, R., 2020. African Trypanosomiasis. [online] Ncbi.nlm.nih.gov. Available at: <https://www.ncbi.nlm.nih.gov/books/NBK519580/> [Accessed 25 March 2021].

Ernfors P, Lee K-F, Jaenisch R. Mice lacking brain-derived neurotrophic factor develop with sensory deficits. Nature 1994; 368: 147–50.

Franco JR, Cecchi G, Paone M, Diarra A, Grout L, Kadima Ebeja A, Simarro PP, Zhao W, Argaw D., 2022 The elimination of human African trypanosomiasis: Achievements in relation to WHO road map targets for 2020. PLoS Negl Trop Dis. 16(1):e0010047.

Frevert, U., Movila, A., Nikolskaia, O., Raper, J., Mackey, Z., Abdulla, M., McKerrow, J., and Grab, D., 2012. Early Invasion of Brain Parenchyma by African Trypanosomes. PLoS ONE, 7(8), p.e43913.

Gadani, S., Cronk, J., Norris, G. and Kipnis, J., 2012. IL-4 in the Brain: A Cytokine To Remember. The Journal of Immunology, 189(9), pp.4213-4219.

Gemechu, J. and Bentivoglio, M. T Cell Recruitment in the Brain during Normal Aging. Front Cell Neurosci, 6.

Gichuki, C., 1994. THE ROLE OF ASTROCYTES IN THE NEUROPATHOGENESIS OF AFRICAN TRYPANOSOMIASIS. Ph.D. University of Glasgow.

Giordano, A., De Panfilis, L., Perin, M., Servidio, L., Cascioli, M., Grasso, M. G., Lugaresi, A., Pucci, E., Veronese, S., & Solari, A., 2022. Advance Care Planning in Neurodegenerative Disorders: A Scoping Review. Int j environ res pub health, 19(2), 803.

Giovannoni, F. and Quintana, F., 2020. The Role of Astrocytes in CNS Inflammation. Trends Immunol, 41(9), pp.805-819.

Giovannoni, F. and Quintana, F., 2020. The Role of Astrocytes in CNS Inflammation. Trends Immunol, 41(9), pp.805-819.

Giunti D, Parodi B, Cordano C, Uccelli A, Kerlero de Rosbo N., 2014. Can we switch microglia's phenotype to foster neuroprotection? Focus on multiple sclerosis. Immunol. 141(3), pp.328-39.

Gordon, S. and Plüddemann, A., 2017. Tissue macrophages: heterogeneity and functions. BMC Biology, 15(1).

Guo, J. et al. 2014. ‘Etazolate abrogates the lipopolysaccharide (LPS)-induced downregulation of the camp/pcreb/BDNF signaling, neuroinflammatory response and depressive-like behavior in mice’, Neurosci, 263, pp. 1–14.

Hein AM, O’Banion MK, 2009. Neuroinflammation and memory: the role of prostaglandins. Mol Neurobiol, 40:15–32.

Hirayama, D., Iida, T. and Nakase, H., 2017. The Phagocytic Function of Macrophage-Enforcing Innate Immunity and Tissue Homeostasis. International J Mol Sci, 19(1), p.92.

Horiuchi, T., Mitoma, H., Harashima, S. -i., Tsukamoto, H., & Shimoda, T. 2010. Transmembrane TNF-α: Structure, function and interaction with anti-TNF Agents. Rheumatology, 49(7), pp.1215–1228.

Hou, Y., Dan, X., Babbar, M., Wei, Y., Hasselbalch, S. G., Croteau, D. L., & Bohr, V. A. 2019. Ageing as a risk factor for neurodegenerative disease. Nat rev. Neurol, 15(10), pp.565–581.

Hwang, J., Aromolaran, K. and Zukin, R., 2017. The emerging field of epigenetics in neurodegeneration and neuroprotection. Nat Rev Neurosci, 18(6), pp.347-361.

InformedHealth.org, 2006. The innate and adaptive immune systems. [online] Ncbi.nlm.nih.gov. Available at: <https://www.ncbi.nlm.nih.gov/books/NBK279396/?report=classic> [Accessed 29 March 2021].

Ipseiz, N., Pickering, R., Rosas, M., Tyrrell, V., Davies, L., Orr, S., Czubala, M., Fathalla, D., Robertson, A., Bryant, C., O'Donnell, V. and Taylor, P., 2020. Tissue-resident macrophages actively suppress IL-1beta release via a reactive prostanoid/IL-10 pathway. EMBO J, 39(14).

Isik, S., Yeman Kiyak, B., Akbayir, R., Seyhali, R., & Arpaci, T. 2023. Microglia mediated neuroinflammation in parkinson’s disease. Cells, 12(7), pp.1012

Joubert KE, Kettner F, Lobetti RG, Miller DM. 2003. The effects of diminazene aceturate on systemic blood pressure in clinically healthy adult dogs. J S Afr Vet Assoc 74: 69–71.

Jovanovic NJ, Czernik AJ, Fienberg AA, Greengard P, Sihra TS, 2000. Synapsins as mediators of BDNF-enhanced neurotransmitter release. Nat Neurosci 3: 323–329.

Kaneko, N., Kurata, M., Yamamoto, T., Morikawa, S. and Masumoto, J., 2019. The role of interleukin-1 in general pathology. Inflamm Regen, 39(1).

Kato, C., Matovu, E., Mugasa, C., Nanteza, A. and Alibu, V., 2016. The role of cytokines in the pathogenesis and staging of Trypanosoma brucei rhodesiense sleeping sickness. Allergy, Asthma Clin Immunol, 12(1).

Kennedy, P., 2019. Update on human African trypanosomiasis (sleeping sickness). J Neurol, 266(9), pp.2334-2337.

Kettenmann, H., Hanisch, U. K., Noda, M., and Verkhratsky, A., 2011. Physiology of microglia. J Physiol. Rev. 91, 461–553

Kohman RA, Rhodes JS, 2013.Neurogenesis, inflammation, and behavior. Brain Behav Immun, 27:22–32

Kristensson, K. and Bentivoglio, M., 1999. Pathology of African trypanosomiasis. Progress in Human African Trypanosomiasis, Sleeping Sickness, pp.157-181.

Kumar, A., 2018. 'Editorial: Neuroinflammation and Cognition', Front Aging Neurosci, 10. doi:10.3389/fnagi.2018.00413.

Kuriakose, S., Singh, R. and Uzonna, J., 2016. Host Intracellular Signalling Events and Pro-inflammatory Cytokine Production in African Trypanosomiasis. Front Immunol, 7, pp.181-184.

Kurien, Biji T, and R Hal Scofield, 2015. "Western blotting: an introduction." Methods in molec biol. 1312, pp17-30.

Kwon, H.S., Koh, SH., 2020. Neuroinflammation in neurodegenerative disorders: the roles of microglia and astrocytes Transl Neurodegener 9, 42.

Levinson, W., 2016. Review of medical microbiology and immunology. 14th ed. McGraw-Hill, pp.423-450.

Louis, C. A., Mody, V., Henry, W. L., Reichner, J. S., & Albina, J. E. 1999. Regulation of arginase isoforms I and II by il-4 in cultured murine peritoneal macrophages. Am J Physiol-Regul, Integr Comp Physiol, 276(1). doi:10.1152/ajpregu.1999.276.1.r237

Low JA, Ho E., 2012. Managing Ethical Dilemmas in End-Stage Neurodegenerative Diseases. Geriatrics (Basel). Jan 20;2(1):8.

Lucena-Aguilar, G., Sánchez-López, A. M., Barberán-Aceituno, C., Carrillo-Ávila, J. A., López-Guerrero, J. A., & Aguilar-Quesada, R. 2016. DNA source selection for downstream applications based on DNA Quality Indicators Analysis. Biopreservation and Biobanking, 14(4), pp.264–270.

Lucey, D., Clerici, M. and Shearer, G., 1996. Type 1 and type 2 cytokine dysregulation in human infectious, neoplastic, and inflammatory diseases. Clin microbiol rev, 9(4), pp.532-562.

Lynch, G. and Baudry, M., 1984. The biochemistry of memory: a new and specific hypothesis. Science, 224(4653), pp.1057-1063.

Magez, S., Radwanska, M., Beschin, A., Sekikawa, K. and De Baetselier, P., 1999. Tumor Necrosis Factor Alpha Is a Key Mediator in the Regulation of Experimental Trypanosoma brucei Infections. Infect Immun, 67(6), pp.3128-3132.

Mahmood, T., & Yang, P. C. (2012). Western blot: technique, theory, and trouble shooting. North Am j med sci, 4(9), 429–434.

Mansfield, J. and Paulnock, D., 2005. Regulation of innate and acquired immunity in African trypanosomiasis. Parasite Immunol, 27(10-11), pp.361-371.

Martinowich K, Hattori D, Wu H, Fouse S, He F, Hu Y, Fan G, Sun YE., 2015. DNA methylation-related chromatin remodeling in activity-dependent BDNF gene regulation. Sci. 302(5646), pp.890-893.

Masocha, W., Amin, D., Kristensson, K. and Rottenberg, M., 2008. Differential Invasion of Trypanosoma brucei brucei and Lymphocytes into the Brain of C57BL/6 and 129Sv/Ev Mice. Scandinavian J Immunol, 68(5), pp.484-491.

Masocha, W., Rottenberg, M. and Kristensson, K., 2007. Migration of African trypanosomes across the blood–brain barrier. Physiol Behav, 92(1-2), pp.110-114.

Mbaya, A., Kumshe, H. and Okwudiri, C., 2012. The Mechanisms of Anaemia in Trypanosomosis: A Review. Research gate. [available online]

McAllister, A., Lo, D. and Katz, L., 1995. Neurotrophins regulate dendritic growth in developing visual cortex. Neuron, 15(4), pp.791-803.

Minns, M. S., Liboro, K., Lima, T. S., Abbondante, S., Miller, B. A., Marshall, M. E., … Pearlman, E. 2023. NLRP3 selectively drives il-1β secretion by pseudomonas aeruginosa infected neutrophils and regulates corneal disease severity. Nat Comm, 14(1). doi:10.1038/s41467-023-41391-7

Miranda, M., Morici, J., Zanoni, M. and Bekinschtein, P., 2019. Brain-Derived Neurotrophic Factor: A Key Molecule for Memory in the Healthy and the Pathological Brain. Front Cell Neurosci, 13.

Miwa, T., Furukawa, S., Nakajima, K., Furukawa, Y., & Kohsaka, S. 1997. Lipopolysaccharide enhances synthesis of brain-derived neurotrophic factor in cultured rat microglia. J Neurosci Res, 50(6), pp.1023–1029.

Moreno, C., Temporão, A., Torres, T., & Sousa Silva, M. 2019. Trypanosoma brucei Interaction with Host: Mechanism of VSG Release as Target for Drug Discovery for African Trypanosomiasis. Int J mol sci, 20(6), p1484.

Morimoto, K. and Nakajima, K., 2019. Role of the Immune System in the Development of the Central Nervous System. Front Neurosci, 13.

Morris, S. M. 2007. Arginine metabolism: Boundaries of our knowledge. J Nutr. 137(6).

Morrison, L., 2011. Parasite-driven pathogenesis in Trypanosoma brucei infections. Parasite Immunol, 33(8), pp.448-455.

Mudji, J., Blum, A., Grize, L., Wampfler, R., Ruf, M., Cnops, L., Nickel, B., Burri, C. and Blum, J., 2020. Gambiense Human African Trypanosomiasis Sequelae after Treatment: A Follow-Up Study 12 Years after Treatment. Trop Med Infect Dis, 5(1), p.10.

Mulenga, G. M., Namangala, B., Chilongo, K., Mubamba, C., Hayashida, K., Henning, L., & Gummow, B., 2021. Challenges in the Diagnostic Performance of Parasitological and Molecular Tests in the Surveillance of African Trypanosomiasis in Eastern Zambia. Trop med infect dis, 6(2), 68.

Mwiinde AM, Simuunza M, Namangala B, Chama-Chiliba CM, Machila N, Anderson NE, Atkinson PM, Welburn SC., 2022. Healthcare Management of Human African Trypanosomiasis Cases in the Eastern, Muchinga and Lusaka Provinces of Zambia. Trop Med Infect Dis. 7(10):270.

Nazem, A., Sankowski, R., Bacher, M., & Al-Abed, Y., 2015. Rodent models of neuroinflammation for Alzheimer's disease. J neuroinflam, 12, 74.

Nunez J. 2008. Morris Water Maze Experiment. Journal of visualized experiments : JoVE, (19), 897.

Ofen, N., Kao, Y., Sokol-Hessner, P., Kim, H., Whitfield-Gabrieli, S. and Gabrieli, J., 2007. Development of the declarative memory system in the human brain. Nat Neurosci, 10(9), pp.1198-1205.

Okwor, I., Muleme, H., Jia, P. and Uzonna, J., 2009. Altered Proinflammatory Cytokine Production and Enhanced Resistance to Trypanosoma congolense Infection in Lymphotoxin β–Deficient Mice. J Infect Dis, 200(3), pp.361-369.

Onyilagha, C. and Uzonna, J., 2019. Host Immune Responses and Immune Evasion Strategies in African Trypanosomiasis. Frontiers in Immunology, 10.

Orihuela, R., McPherson, C. A., & Harry, G. J. 2015. Microglial M1/m2 polarization and metabolic states. Brit J Pharmacol, 173(4), pp.649–665.

O'Toole, J. F., Bruggeman, L. A., Madhavan, S., & Sedor, J. R. (2017). The Cell Biology of APOL1. Semin nephrol, 37(6), 538–545.

P. De Koning, H., 2020. The Drugs of Sleeping Sickness: Their Mechanisms of Action and Resistance, and a Brief History. Trop Med Infect Dis, 5(1), p.14.

Parameswaran, N, & Patial S (2010) Tumor Necrosis Factor α Signaling in Macrophages. NIH 20 (2), 87-103.

Paulnock, D., Freeman, B. And Mansfield, J., 2010. Modulation of innate immunity by African Trypanosomes. Parasitol, 137(14), pp.2051-2063.

Pearce, E.J., A. Cheever, S. Leonard, M. Covalensky, R. Fernandez-Botran, G. Kohler, and M. Kopf. 1996. Schistosoma mansoni in IL-4-deficient mice. Int Immunol. 8: 435-444

Pearson, R., 2020. African Trypanosomiasis - Infectious Diseases - MSD Manual Professional Edition. [online] MSD Manual Professional Edition. Available at: <https://www.msdmanuals.com/professional/infectious-diseases/extraintestinal-protozoa/african-trypanosomiasis> [Accessed 30 March 2021].

Pentreath, V., 1995. Trypanosomiasis and the nervous system. Transactions of the Royal Society of Trop Med Hyg, 89(1), pp.9-15.

Philip, K., Dascombe, M., Fraser, P. and Pentreath, V., 1994. Blood-brain barrier damage in experimental African trypanosomiasis. Ann Trop Med Parasitol, 88(6), pp.607-616.

Priego, N. and Valiente, M., 2019. The Potential of Astrocytes as Immune Modulators in Brain Tumors. Front Immunol, 10.

Rao JS, Kellom M, Kim HW, Rapoport SI, Reese EA: Neuroinflammation and synaptic loss. Neurochem Res 2012, 37:903–910.

Rauluseviciute, I., Drabløs, F. and Rye, M., 2019. DNA methylation data by sequencing: experimental approaches and recommendations for tools and pipelines for data analysis. Clin Epigenet, 11(1).

Risau, W., Engelhardt, B. and Wekerle, H., 1990. Immune function of the blood-brain barrier: incomplete presentation of protein (auto-)antigens by rat brain microvascular endothelium in vitro. J Cell Biol, 110(5), pp.1757-1766.

Rock, R. B., Gekker, G., Hu, S., Sheng, W. S., Cheeran, M., Lokensgard, J. R., & Peterson, P. K. (2004). Role of microglia in central nervous system infections. Clin microbiol rev, 17(4), 942–964. https://doi.org/10.1128/CMR.17.4.942-964.2004

Rodgers, J., Bradley, B. and Kennedy, P., 2017. Delineating neuroinflammation, parasite CNS invasion, and blood-brain barrier dysfunction in an experimental murine model of human African trypanosomiasis. Methods, 127, pp.79-87.

Rodgers, J., Steiner, I. and Kennedy, P., 2019. Generation of neuroinflammation in human African trypanosomiasis. Neurology – Neuroimmunol Neuroinflamm, 6(6), p.e610.

Shi, M., Pan, W. and Tabel, H., 2003. Experimental African trypanosomiasis: IFN-γ mediates early mortality. Europ J Immunol, 33(1), pp.108-118.

Siret, C., van Lessen, M., Bavais, J., Jeong, H. W., Reddy Samawar, S. K., Kapupara, K., … van de Pavert, S. A. 2022. Deciphering the heterogeneity of the lyve1+ perivascular macrophages in the Mouse Brain. Nat Comm, 13(1). doi:10.1038/s41467-022-35166-9

Soung, A. and S. Klein, R., 2020. Astrocytes: Initiators of and Responders to Inflammation. Glia in Health and Disease.

Steverding D. 2010. The development of drugs for treatment of sleeping sickness: a historical review. Parasites & vectors, 3(1), 15. https://doi.org/10.1186/1756-3305-3-15

Stich, A., Abel, P. and Krishna, S., 2002. Human African trypanosomiasis. BMJ, 325(7357), pp.203-206.

Stijlemans, B., De Baetselier, P., Magez, S., Van Ginderachter, J. and De Trez, C., 2018. African Trypanosomiasis-Associated Anemia: The Contribution of the Interplay between Parasites and the Mononuclear Phagocyte System. Front Immunol, 9.

Stitham, J., Midgett, C., Martin, K. and Hwa, J., 2011. Prostacyclin: An Inflammatory Paradox. Front Pharmacol, 2.

Tesoriero, C., Xu, Y., Mumba Ngoyi, D. and Bentivoglio, M., 2018. Neural Damage in Experimental Trypanosoma brucei gambiense Infection: The Suprachiasmatic Nucleus. Front Neuroanat, 12.

Ton, B.-H. T., Chen, Q., Gaina, G., Tucureanu, C., Georgescu, A., Strungaru, C., … Ristoiu, V. 2013. Activation profile of dorsal root ganglia IBA-1 (+) macrophages varies with the type of lesion in rats. Acta Histochem, 115(8).

Uchiyama-Tsuyuki, Y. et al. 1995. 'Prostacyclin analogue TTC-909 reduces memory impairment in rats with cerebral embolism', Pharmacol Biochem Behav, 52(3), pp. 555–559.

Vanwalleghem, G., Morias, Y., Beschin, A., Szymkowski, D. and Pays, E., 2017. Trypanosoma brucei growth control by TNF in mammalian host is independent of the soluble form of the cytokine. Sci Rep, 7(1).

Varin A, Gordon S: Alternative activation of macrophages: immune function and cellular biology. Immunobiol 2009, 214:630–641

Vincendeau, P. and Bouteille, B., 2006. Immunology and immunopathology of African trypanosomiasis. An Acad Bras Ciênc, 78(4), pp.645-665.

Vorhees, C. and Williams, M., 2006. Morris water maze: procedures for assessing spatial and related forms of learning and memory. Nat Protoc, 1(2), pp.848-858.

Wake, H. and Fields, R., 2011. Physiological function of microglia. Neuron Glia Biology, 7(1), pp.1-3.

Wei, Y., Li, X. 2022 Different phenotypes of microglia in animal models of Alzheimer disease. Immun Ageing 19, 44 .

Wen A.Y., Sakamoto K.M., Miller L.S. 2010. The role of the transcription factor CREB in immune function. J. Immunol. 185, pp. 6413–6419.

Wible, C. 2013. Hippocampal physiology, structure and function and the neuroscience of schizophrenia: A unified account of declarative memory deficits, working

memory deficits and schizophrenic symptoms. Behav Sci, 3(2), 298–315. doi:10.3390/bs3020298

Wong, M. and Medrano, J., 2005. Real-time PCR for mRNA quantitation. BioTechniques, 39(1), pp.75-85.

Xia, Y., Zhan, C., Feng, M., Leblanc, M., Ke, E., Yeddula, N., & Verma, I. M. 2018. Targeting CREB pathway suppresses small cell lung cancer. Mol Cancer, 16(5), 825–832.

Yamada, K., Mizuno, M. and Nabeshima, T., 2002. Role for brain-derived neurotrophic factor in learning and memory. Life Sci, 70(7), pp.735-744.

Yamada, K., Mizuno, M. and Nabeshima, T., 2002. Role for brain-derived neurotrophic factor in learning and memory. Life Sci, 70(7), pp.735-744.

Zheng, K. B., Xie, J., Li, Y. T., Yuan, Y., Wang, Y., Li, Ch., & Shi, Y. F. 2019. Knockdown of CERB expression inhibits proliferation and migration of glioma cells line U251. Bratisl Med J, 120(04), pp.309–315.

Zhou, W., Hashimoto, K., Goleniewska, K., O’Neal, J., Ji, S., Blackwell, T., FitzGerald, G., Egan, K., Geraci, M. and Peebles, R., 2007. Prostaglandin I2Analogs Inhibit Proinflammatory Cytokine Production and T Cell Stimulatory Function of Dendritic Cells. J Immunol, 178(2), pp.702-710.